This microfiche was produced according to ANSI / AIIM Standards and meets the quality specifications contained therein. A poor blowback image is the result of the characteristics of the original document.

(NASA-TP-3288) TENSILE PROPERTIES OF CAST TITANIUM ALLOYS: TITANIUM-6Al-4V ELI AND TITANIUM-5Al-2.5Sn ELI (NASA) 16 p

N93-10072

Unclas

H1/26 0122417

NASA
Technical
Paper
3288

1992

Tensile Properties of Cast Titanium Alloys

Titanium-6Al-4V *ELI and* *Titanium*-5Al-2.5Sn *ELI*

E. E. Billinghurst, Jr.
George C. Marshall Space Flight Center
Marshall Space Flight Center, Alabama

National Aeronautics and
Space Administration
Office of Management
Scientific and Technical
Information Program

ACKNOWLEDGMENT

The author wishes to thank the IIT Research Institute/Metallurgy Research Facilities personnel, particularly Mr. Robert W. Bond, for their help in running the tests and providing the data contained in this report.

TABLE OF CONTENTS

Page

INTRODUCTION/BACKGROUND 1

MATERIALS/PROCESSING 1

TEST PROCEDURE 1

RESULTS/DISCUSSION 2

CONCLUSIONS 2

LIST OF ILLUSTRATIONS

Figure Title Page

1. Cast, hot isostatic pressed (HIP'ed), annealed ingots 2

2. Photomacrograph of as-cast Ti-6Al-4V ELI taken from areas of the casting where tensile samples were removed (× 10, Kallings etch) 3

3. Photomicrographs of as-cast Ti-5Al-2.5Sn ELI (× 50 and × 400, Kallings etch) 4

4. Photomacrograph of as-cast Ti-5Al-2.5Sn ELI taken from areas of the casting where tensile samples were removed (× 10, Kroll's etch) 5

5. Photomicrographs of as-cast Ti-6Al-4V ELI (× 50 and × 400, Kallings etch) 6

6. Drawing No. MRF-126, EDM cutting template for 0.505 bars 7

7. Drawing No. MRF-1030, standard 0.505 smooth tensile specimen 8

LIST OF TABLES

Table Title Page

1. Summary of cast ELI grade analytic results 9

2. Tensile properties of cast ELI grade titanium alloys 9

3. Summary test results/average of tensile mechanical properties 10

4. Ultimate tensile strength (ksi)/percent reduction in area 10

TECHNICAL PAPER

TENSILE PROPERTIES OF CAST TITANIUM ALLOYS (TITANIUM-6AL-4V ELI AND TITANIUM-5AL-2.5SN ELI)

INTRODUCTION/BACKGROUND

The liquid hydrogen turbopump for the space transportation main engine (STME) is under development. The turbopump impeller is proposed to be cast from titanium alloys in order to lower the cost and improve reliability. To help with the alloy selection, it was necessary to obtain reliable mechanical property data for the two candidate titanium alloys—Ti-6Al-4V ELI and Ti-5Al-2.5Sn ELI. Because available data for these alloys were from different sources, a fair comparison of properties could not be made. It is important to keep the process variables—such as casting source, casting size, hot isostatic pressing (HIP'ing), annealing, etc.—constant. Therefore, Marshall Space Flight Center (MSFC) Materials and Processes Laboratory conducted a test program to determine the tensile properties of cast Ti-6Al-4V and Ti-5Al-2.5Sn alloys in-house. Process variables were kept constant to minimize variability. This report describes the test procedure, then presents and discusses the results.

MATERIALS/PROCESSING

Ti-6Al-4V ELI and Ti-5Al-2.5Sn ELI alloys were cast—in 4-in diameter by 20-in long ingots in 1-in thick machined carbon molds—by the Duriron Company, Inc., Dayton, OH. The material was heated to 200 °F above the melting temperature and held for 15 min after all visible solids had melted. The cast ingots were HIP'ed at 1,650 °F, 15 ksi pressure, for 2 h; then annealed at 1,350 °F for 2 h. Photographs of the ingots are shown in figure 1. The microstructures were obtained from samples taken from several places—from the center to the outside of the ingot. These pictures of the structure are included as figures 2, 3, 4, and 5. The grain size was determined to be ASTM No. 1. The chemical compositions of the extra low interstitial grade titanium alloys were certified by the supplier and verified on the material adjacent to the tensile test specimens. Duriron's certification and MSFC's analytic results are summarized in table 1.

TEST PROCEDURE

Eight bars (0.505-in diameter by 5.0-in long) were electrical discharge machined (EDM'ed) from each ingot. The drawing of the EDM cutting template is shown in figure 6. The bars were machined into tensile specimens (fig. 7). The surface finish of the specimens was examined and visually compared to a standard, and was determined to be acceptable. Three samples from each ingot were tensile tested in air at ambient temperature (70 °F). Five samples from each ingot were tensile tested in liquid hydrogen at –423 °F. The tensile test data are reported in table 2 and summarized in table 3.

RESULTS/DISCUSSION

As expected, the Ti-6Al-4V ELI alloy has higher strength, but lower ductility, than the Ti-5Al-2.5Sn ELI alloy (table 3). The Ti-6Al-4V is 19.0-percent stronger at 70 °F and 19.7-percent stronger at –423 °F. Percentage of elongation was not used in the analysis because the samples frequently broke at or outside the gauge marks; hence, the numbers were not reliable. For this reason, the reduction of area was used as a measure of ductility, and the results are summarized in table 4. As expected, the Ti-5Al-2.5Sn has higher ductility than the Ti-6Al-4V at both test temperatures (61.8 percent at 70 °F and 34.5 percent at –423 °F). The present work does not support the reported extremely low ductility of Ti-6Al-4V ELI in the literature. As expected, both alloys are stronger and their ductilities are lower at cryogenic temperature (–423 °F) than at room temperature (70 °F).

It appears that either alloy could be used as an investment cast impeller for the STME fuel turbopump. The lower ductility of Ti-6Al-4V reported here is considered acceptable for the intended application. Because of its higher strength, Ti-6Al-4V alloy should be a preferred material choice for the impeller. This recommendation, however, does not take into account the possible differences in castability of the two alloys. Furthermore, minimum web thickness requirements of the investment casting process might render the strength difference of no consequence. It is suggested that castability of both alloys be investigated before the final selection is made.

CONCLUSION

Either Ti-6Al-4V ELI or Ti-5Al-2.5Sn ELI alloy has adequate strength/ductility for use for the STME fuel turbopump impeller application; however, Ti-6Al-4V ELI does have an edge over Ti-5Al-2.5Sn ELI in tensile strength.

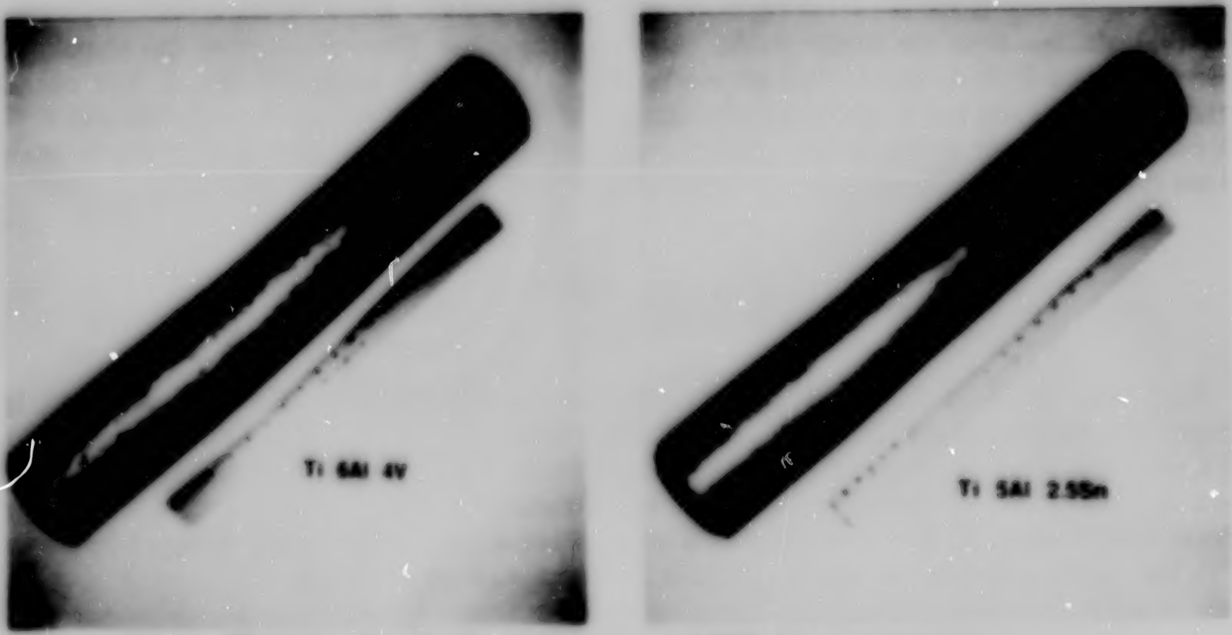

Figure 1. Cast, hot isostatic pressed (HIP'ed), annealed ingots.

ORIGINAL PAGE
BLACK AND WHITE PHOTOGRAPH

ORIGINAL PAGE
BLACK AND WHITE PHOTOGRAPH

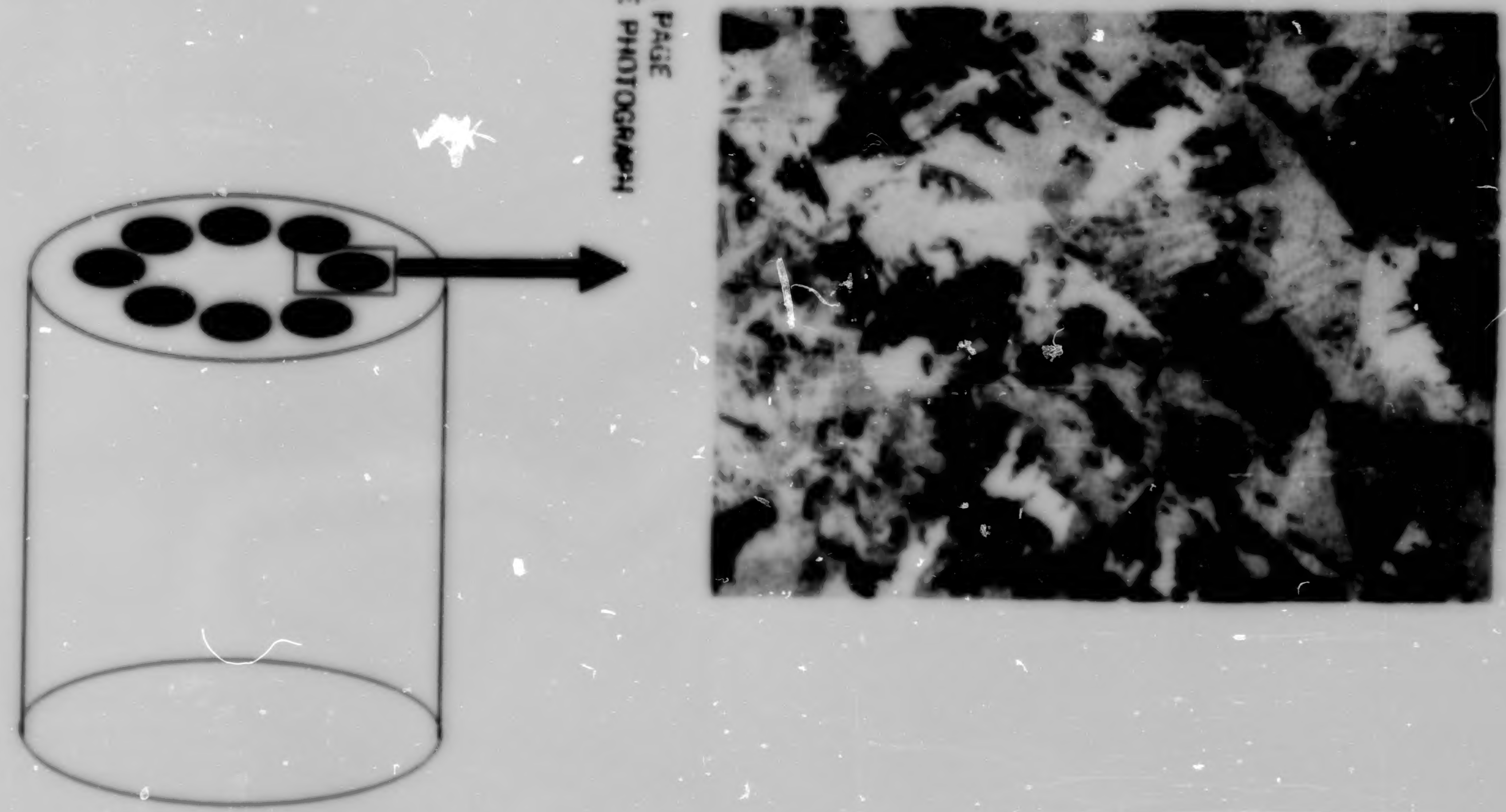

Figure 2. Photomacrograph of as-cast Ti-6Al-4V ELI taken from areas of the casting where tensile samples were removed (× 10, Kallings etch)

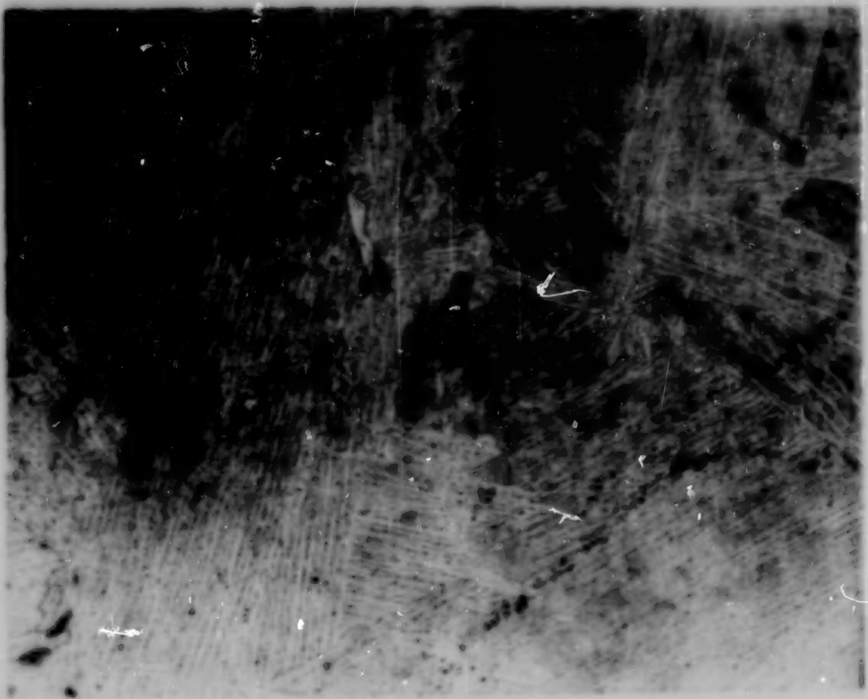

50X

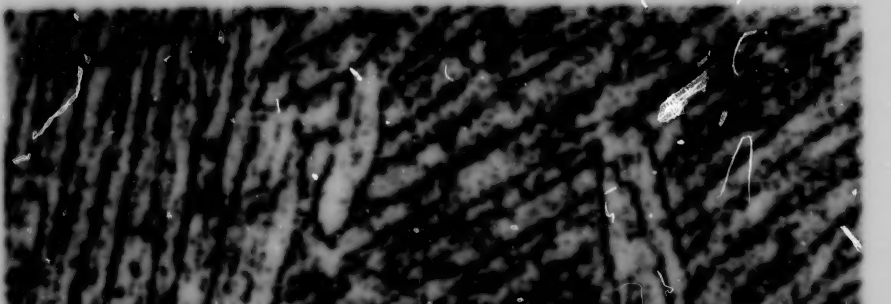

400X

Figure 3. Photomicrographs of as-cast Ti-5Al-2.5Sn ELI (× 50 and × 400, Kallings etch).

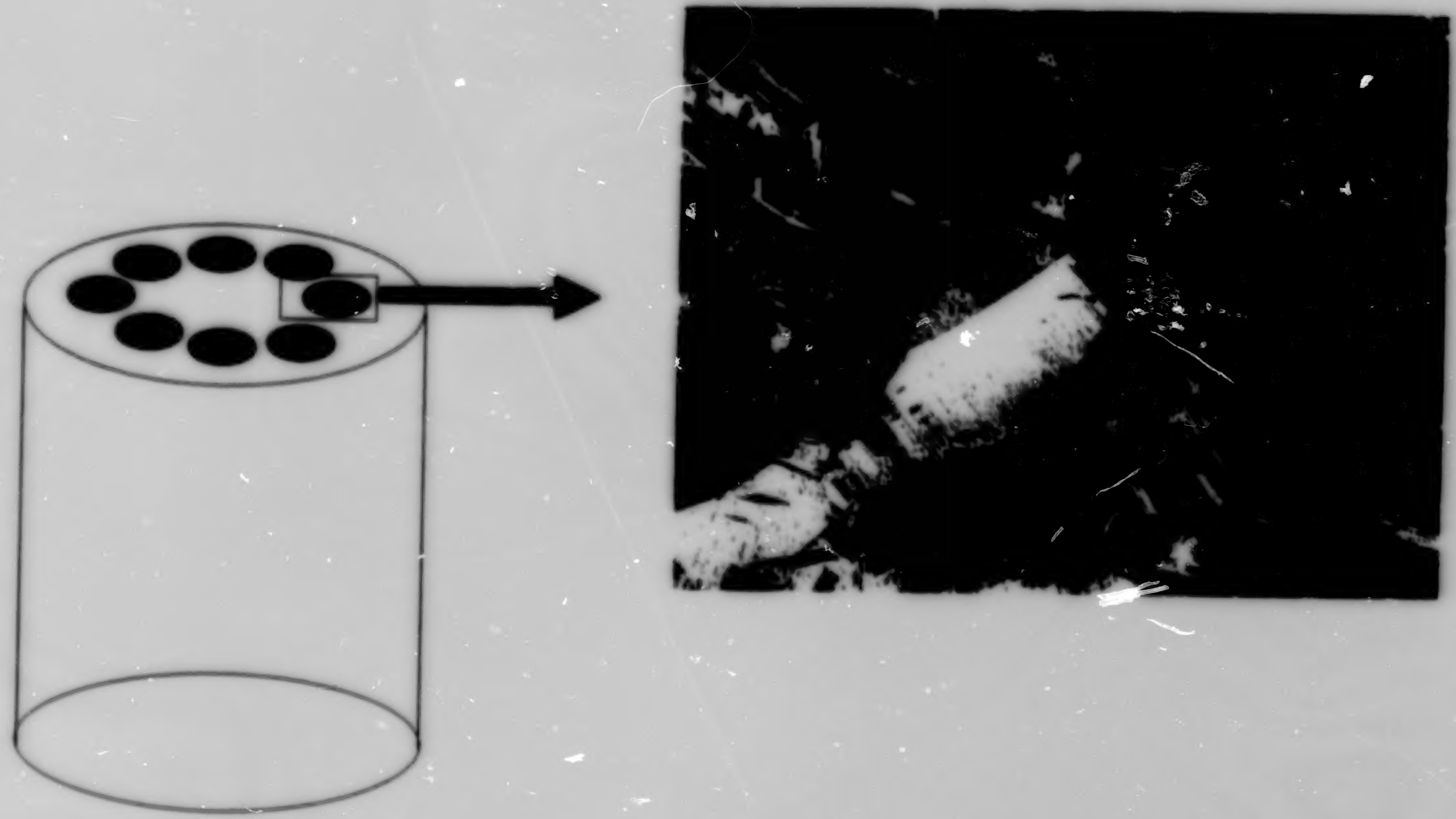

Figure 4. Photomacrograph of as-cast Ti-5Al-2.5Sn ELI taken from areas of the casting where tensile samples were removed (× 10, Kroll's etch).

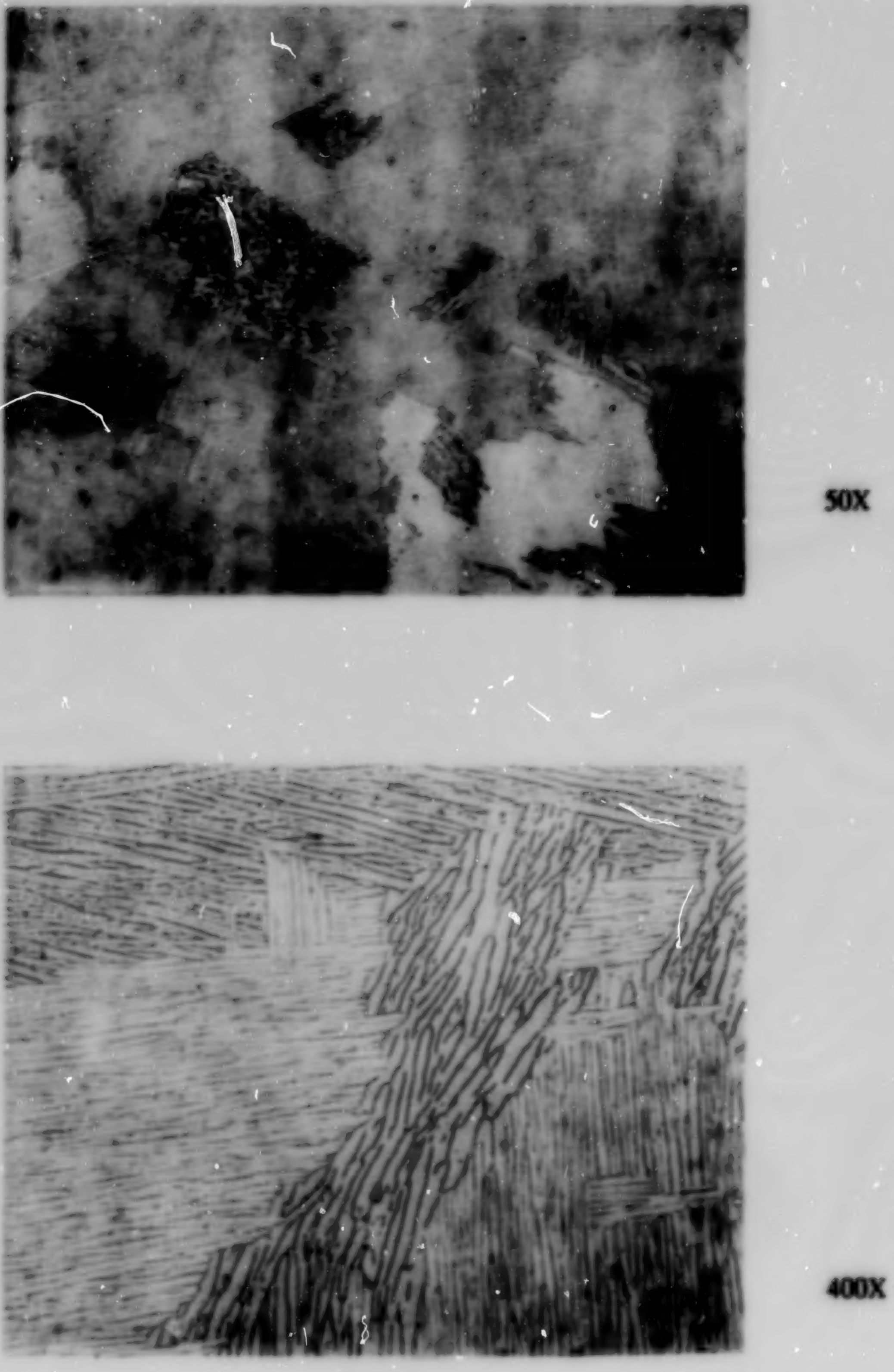

Figure 5. Photomicrographs of as-cast Ti-6Al-4V ELI (× 50 and × 400, Kallings etch).

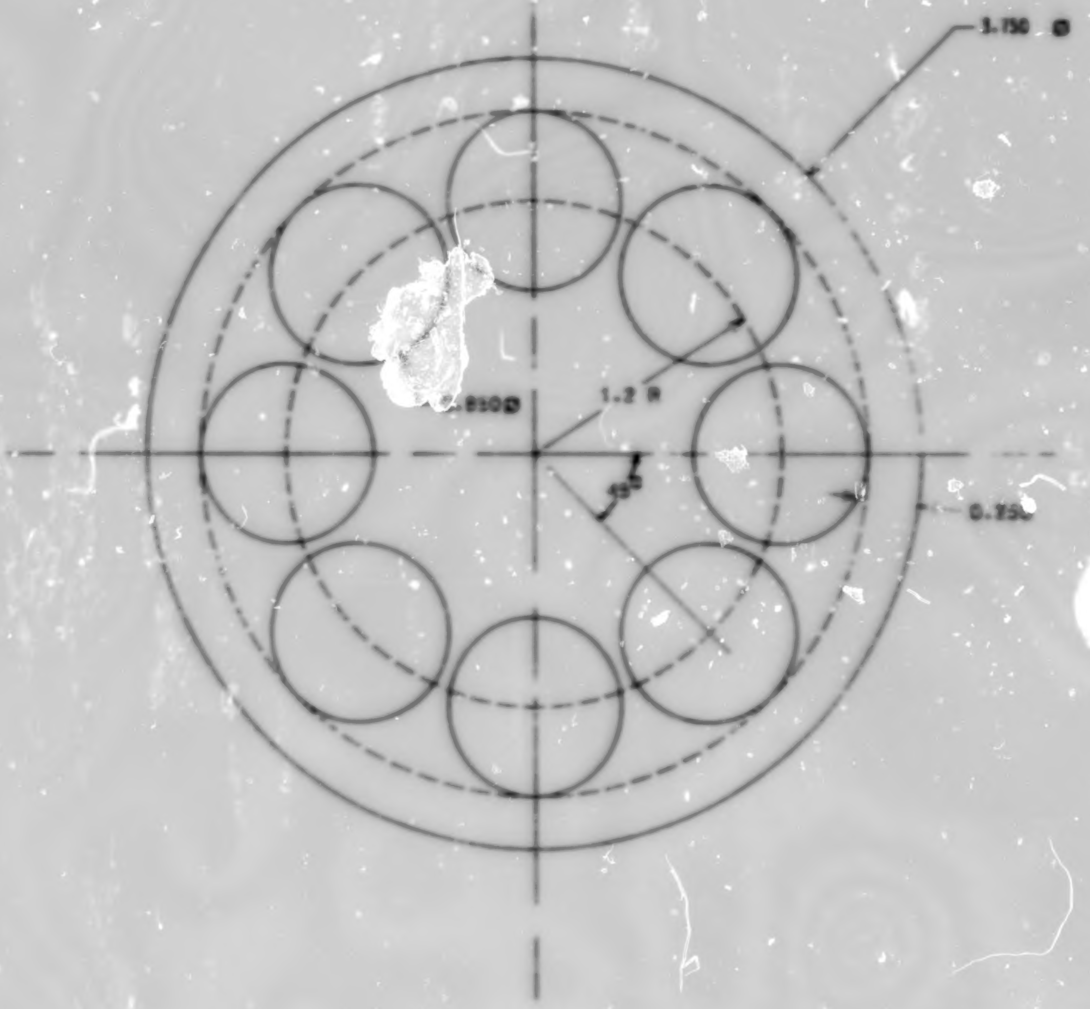

1. ALL DIMENSIONS IN INCHES
2. NOT TO SCALE. WORK TO DIMENSIONS GIVEN

REV. DATE: 10/30/90	DRAWN: REJ	EDM CUTTING TEMPLATE FOR .505 BARS
REV. DATE:	INSPECTED: SJM	
REV. DATE:	APPROVED: EJV	DRAWING NO. MRF-126

Figure 6. Drawing No. MRF-126, EDM cutting template for 0.505 bars.

FROM ASTM E 8

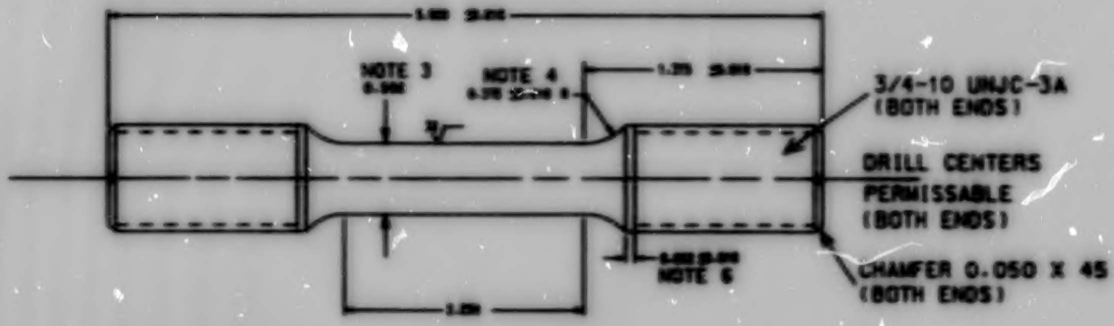
NOTE 3
NOTE 4
3/4-10 UNJC-3A
(BOTH ENDS)
DRILL CENTERS
PERMISSABLE
(BOTH ENDS)
NOTE 6
CHAMFER 0.050 X 45
(BOTH ENDS)

1. NOT TO SCALE. WORK TO DIMENSIONS GIVEN
2. ALL DIMENSIONS IN INCHES
3. SLIGHT TAPER TO CENTER REQUIRED (0.005 MAX)
4. DO NOT UNDERCUT RADII
5. UNSPECIFIED TOLERANCES ± 0.005
6. THREADS ARE NOT TO EXTEND TO RADIUS

REV. DATE: 11/8/90	DRAWN: RKJ	STANDARD .505 SMOOTH TENSILE SPECIMEN
REV. DATE:	INSPECTED: SJM	
REV. DATE:	APPROVED: EJV	DRAWING NO. MRF-1030

Figure 7. Drawing No. MRF-1030, standard 0.505 smooth tensile specimen.

Table 1. Summary of cast ELI grade analytic results.

	Composition					
	Ti-6Al-4V ELI			Ti-5Al-2.5Sn ELI		
	Specification Percentage	Duriron Cert.	MSFC Anal.	Specification Percentage	Duriron Cert.	MSFC Anal.
Ti	REM	89.54	91.24	REM	92.00	93.27
Al	5.5–6.75	6.20	5.28	4.5–5.1	5.04	4.59
V	3.5–4.5	4.09	3.27	—	—	0.08
Sn	—	—	0.03	1.9–2.5	2.50	1.96
C	0.08 max.	0.013	0.015	0.05 max.	0.017	0.01221
	0.05 max.	0.0148	0.00073	0.05 max.	0.0122	0.00043
H	0.015 max.	0.0059	0.00593	0.015 max.	0.045	0.003586
O	0.13 max.	0.151	0.0093	0.10 max.	0.077	0.0161
Fe	0.25 max.	—	0.15	0.25 max.	—	0.01

Table 2. Tensile properties of cast ELI grade titanium alloys.

Sample I.D.	Material	Media	Test Temp. (°F)	UTS (ksi)	YS (ksi)	Percent RA	Percent EL 1 in	Percent EL 2 in
2332	Ti-5Al-2.5Sn	Air	70	107.5	99.4	22.7	15.4	10.4
2333	Ti-5Al-2.5Sn	Air	70	108.0	100.0	24.4	5.5	9.1*
2334	Ti-5Al-2.5Sn	Air	70	108.9	101.3	26.7	6.7	7.5*
			Averages:	108.5	100.2	24.6	9.2	9.0
2335	Ti-5Al-2.5Sn	LH_2	-423	186.9	NA	13.6	10.0	6.3
2336	Ti-5Al-2.5Sn	LH_2	-423	187.7	NA	10.7	7.4	7.1*
2337	Ti-5Al-2.5Sn	LH_2	-423	188.5	NA	12.1	7.0	7.3*
2338	Ti-5Al-2.5Sn	LH_2	-423	174.8	NA	12.6	2.5	4.1*
2331	Ti-5Al-2.5Sn	LH_2	-423	187.1	156.9	9.5	10.9	7.0
			Averages:	185.0		11.7	7.6	6.4
2344	Ti-6Al-4V	Air	70	128.8	118.4	12.9	10.5	7.5
2345	Ti-6Al-4V	Air	70	130.0	119.6	14.3	9.4	7.4
2346	Ti-6Al-4V	Air	70	128.4	117.8	18.5	12.5	8.5
			Averages:	129.1	118.6	15.2	17.4	7.8
2339	Ti-6Al-4V	LH_2	-423	214.1	NA	10.7	2.8	2.8*
2340	Ti-6Al-4V	LH_2	-423	219.1	NA	8.2	4.4	3.4
2341	Ti-6Al-4V	LH_2	-423	211.3	NA	8.2	5.5	2.9
2342	Ti-6Al-4V	LH_2	-423	203.0	NA	11.6	7.3	4.0
2343	Ti-6Al-4V	LH_2	-423	213.4	199.0	4.9	8.1	3.3
			Averages:	212.2		8.7	5.6	3.3

*Sample broke outside of 1-in gauge marks.

Table 3. Summary of test results/average of tensile mechanical properties.

Material	Test Temp.	UTS (ksi)	YS (ksi)	Percent RA	Percent EL 1 in	 2 in	No. of Samples
Ti-6Al-4V ELI	70 °F	129.1	118.6	15.2	17.4	7.8	3
Ti-5Al-2.5Sn ELI	70 °F	108.5	100.2	24.6	9.2	9.0*	3
Ti-6Al-4V ELI	–423 °F	212.2	199.0†	8.7	5.6	3.3	5
Ti-5Al-2.5Sn ELI	–423 °F	185.0	156.9†	11.7	7.6	6.4*	5

*Samples broke outside 1-in gauge marks.
†YS value for one sample only.

Table 4. Ultimate tensile strength (ksi)/percent reduction in area.

Alloy	Ultimate Tensile Strength (ksi) Tested in Air (70 °F)	 Tested in LH_2 (–423 °F)	Percent Reduction of Area Tested in Air (70 °F)	 Tested in LH_2 (–423 °F)
Ti-5Al-2.5Sn ELI	108.4	185.0	24.6	11.7
Ti-6Al-4V ELI	129.1	212.2	15.2	8.7

REPORT DOCUMENTATION PAGE

Form Approved
OMB No. 0704-0188

Public reporting burden for this collection of information is estimated to average 1 hour per response, including the time for reviewing instructions, searching existing data sources, gathering and maintaining the data needed, and completing and reviewing the collection of information. Send comments regarding this burden estimate or any other aspect of this collection of information, including suggestions for reducing this burden, to Washington Headquarters Services, Directorate for Information Operations and Reports, 1215 Jefferson Davis Highway, Suite 1204, Arlington, VA 22202-4302, and to the Office of Management and Budget, Paperwork Reduction Project (0704-0188), Washington, DC 20503.

1. AGENCY USE ONLY *(Leave blank)*

2. REPORT DATE
October 1992

3. REPORT TYPE AND DATES COVERED
Technical Paper

4. TITLE AND SUBTITLE
Tensile Properties of Cast Titanium Alloys
Titanium-6Al-4V *ELI and Titanium*-5Al-2.5Sn *ELI*

5. FUNDING NUMBERS

6. AUTHOR(S)
E.E. Billinghurst, Jr.

7. PERFORMING ORGANIZATION NAME(S) AND ADDRESS(ES)
George C. Marshall Space Flight Center
Marshall Space Flight Center, Alabama 35812

8. PERFORMING ORGANIZATION REPORT NUMBER
M-699

9. SPONSORING/MONITORING AGENCY NAME(S) AND ADDRESS(ES)
National Aeronautics and Space Administration
Washington, DC 20546

10. SPONSORING/MONITORING AGENCY REPORT NUMBER
NASA TP-3288

11. SUPPLEMENTARY NOTES
Prepared by Materials and Processes Laboratory, Science and Engineering Directorate.

12a. DISTRIBUTION/AVAILABILITY STATEMENT
Unclassified—Unlimited
Subject Category: 26

12b. DISTRIBUTION CODE

13. ABSTRACT *(Maximum 200 words)*

This work was performed to determine the tensile properties of cast, hot isostatic pressed (HIP'ed), and annealed titanium alloys, Ti-6A1-4V ELI and Ti-5A1-2.5Sn ELI, that are candidate materials for the space transportation main engine (STME) liquid hydrogen turbopump impeller. Samples of the cast alloys were HIP'ed, annealed, and machined into tensile specimens. The specimens were tested in air at ambient temperature (70 °F) and also at –423 °F in liquid hydrogen. The Ti-6A1-4V alloy had an average ultimate strength of 129.1 ksi at 70 °F and 212.2 ksi at –423 °F. The Ti-5A1-2.5Sn alloy had an average ultimate strength of 108.4 ksi at 70 °F and 185.0 ksi at –423 °F. The ductility, as measured by reduction of area, for the Ti-6A1-4V averaged 15.2 percent at 70 °F and 8.7 percent at –423 °F, whereas for the Ti-5A1-2.5Sn alloy average reduction of area was 24.6 percent at 70 °F and 11.7 percent at –423 °F.

14. SUBJECT TERMS
Titanium Alloys
Mechanical Properties
Cast Titanium Alloys
Liquid Hydrogen Turbopump Impeller
Cryogenic Properties

15. NUMBER OF PAGES
16

16. PRICE CODE
A03

17. SECURITY CLASSIFICATION OF REPORT
Unclassified

18. SECURITY CLASSIFICATION OF THIS PAGE
Unclassified

19. SECURITY CLASSIFICATION OF ABSTRACT
Unclassified

20. LIMITATION OF ABSTRACT
Unlimited

NSN 7540-01-280-5500

Standard Form 298 (Rev 2-89)
Prescribed by ANSI Std. Z39-18
298-102

NASA-Langley, 1992

END

DATE

FILMED

NOV 13 1992

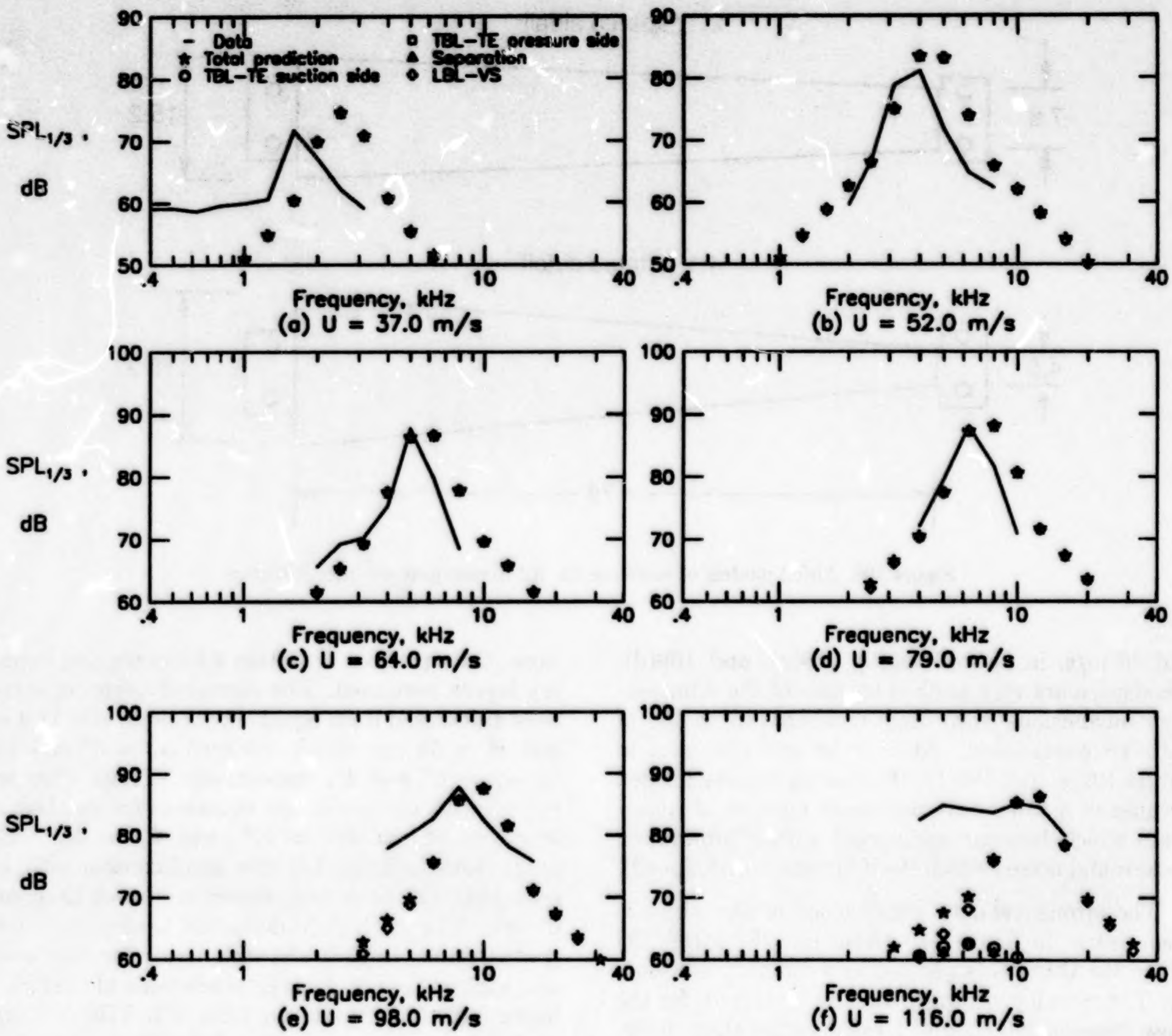

(a) U = 37.0 m/s

(b) U = 52.0 m/s

(c) U = 64.0 m/s

(d) U = 79.0 m/s

(e) U = 98.0 m/s

(f) U = 116.0 m/s

Figure 109. Noise spectra for constant-chord airfoil at $\alpha_t = 4°$ ($\alpha_* = 1.9°$) from reference 27 compared with prediction of present paper.

C-2

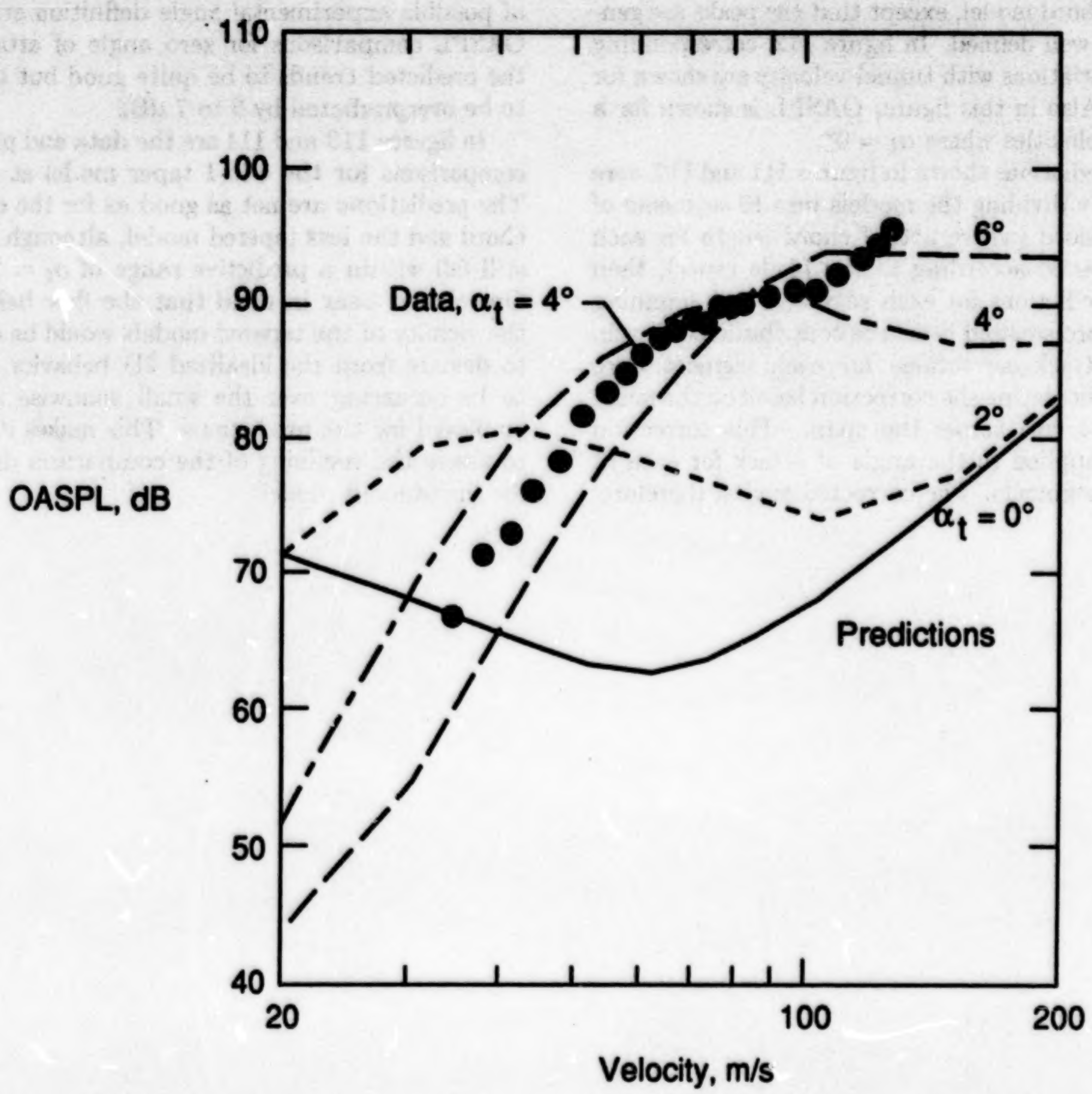

Figure 110. Overall sound pressure level versus velocity for constant-chord airfoil from reference 27 compared with predictions of present paper.

was found not to be continuous; however the tapered models did produce spectra containing a large number of peaks spread over a somewhat wider frequency range than those for the constant-chord airfoil at about the same velocities. In figure 111, 1/3-octave spectra are shown for the 2-to-1 taper airfoil at $\alpha_t = 4°$ for tunnel velocities between $U = 27$ and 107 m/s. The data are similar to those for the constant-chord model, except that the peaks are generally less well defined. In figure 112, corresponding OASPL variations with tunnel velocity are shown for $\alpha_t = 4°$. Also in this figure, OASPL is shown for a range of velocities where $\alpha_t = 0°$.

The predictions shown in figures 111 and 112 were obtained by dividing the models into 10 segments of constant chord (where actual chord length for each segment varied according to the blade taper), then making predictions for each segment, and summing on a pressure-squared basis the contributions of each. Angle-of-attack corrections for each segment were made by calculating the correction based on the mean chord (11.4 cm) across the span. This correction was then applied to the angle of attack for each of the blade segments. The corrected angles, therefore, were the same as for the constant-chord model, that is, $\alpha_* = 0°$ and 1.9° for $\alpha_t = 0°$ and 4°, respectively. The comparisons between predictions and data for the 2-to-1 taper airfoil appear about as good as those for constant-chord comparisons. It appears that the predictions for OASPL at $\alpha_t = 4°$ (fig. 112) would best agree if $\alpha_t \approx 3.5°$ had been used rather than 4°. This again indicates that agreement is on the order of possible experimental angle definition error. The OASPL comparisons for zero angle of attack show the predicted trends to be quite good but the levels to be overpredicted by 5 to 7 dB.

In figures 113 and 114 are the data and prediction comparisons for the 4-to-1 taper model at $\alpha_t = 0°$. The predictions are not as good as for the constant-chord and the less tapered model, although the data still fall within a predictive range of $\alpha_t = 2°$ to 3°. One should bear in mind that the flow behavior in the vicinity of the tapered models would be expected to deviate from the idealized 2D behavior assumed to be occurring over the small spanwise segments employed for the predictions. This makes it difficult to assess the meaning of the comparison deviations for the tapered models.

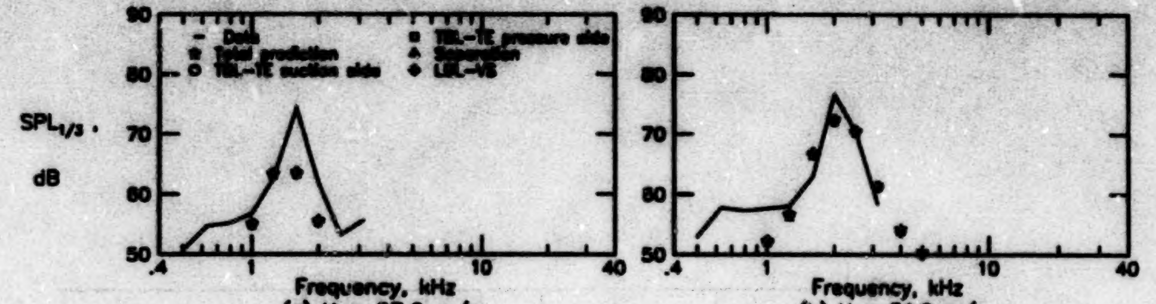

(a) U = 27.0 m/s (b) U = 34.0 m/s

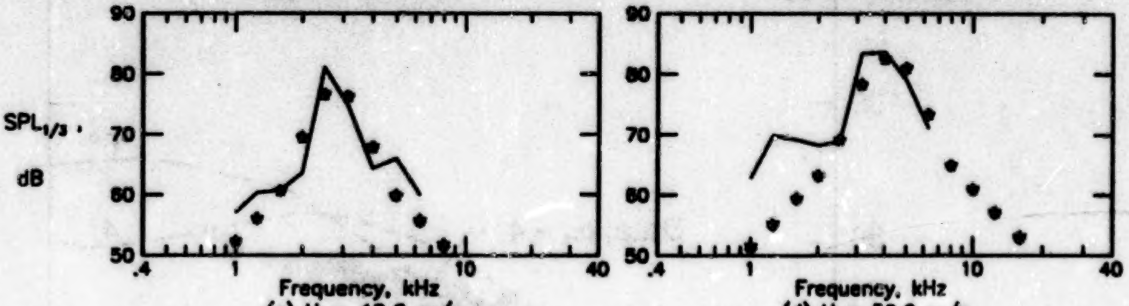

(c) U = 40.0 m/s (d) U = 52.0 m/s

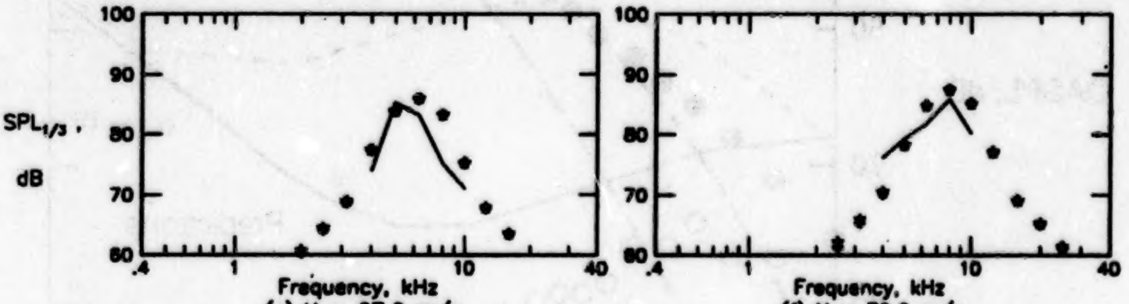

(e) U = 67.0 m/s (f) U = 79.0 m/s

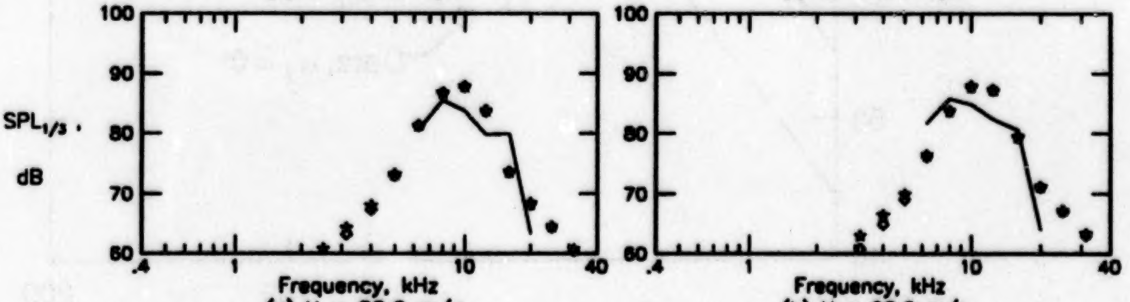

(g) U = 88.0 m/s (h) U = 98.0 m/s

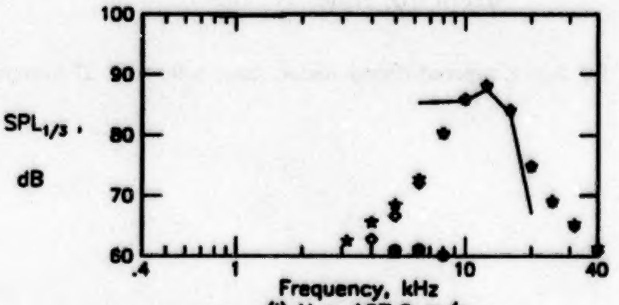

(i) U = 107.0 m/s

Figure 111. Noise spectra for 2-to-1 tapered-chord airfoil at $\alpha_t = 4^\circ$ ($\alpha_* = 1.9^\circ$) from reference 27 compared with prediction of present paper.

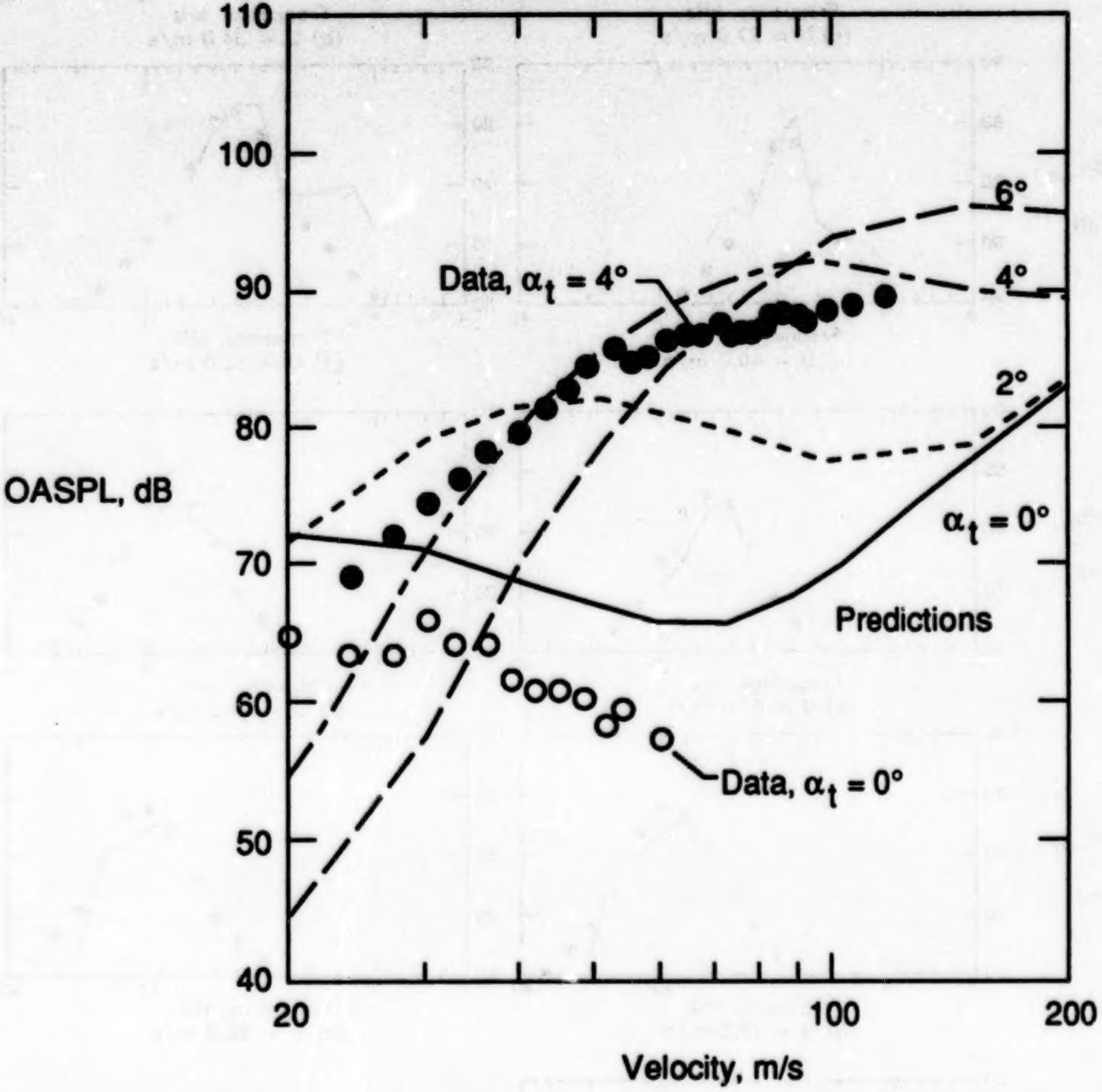

Figure 112. Overall sound pressure level versus velocity for 2-to-1 tapered-chord airfoil from reference 27 compared with predictions of present paper.

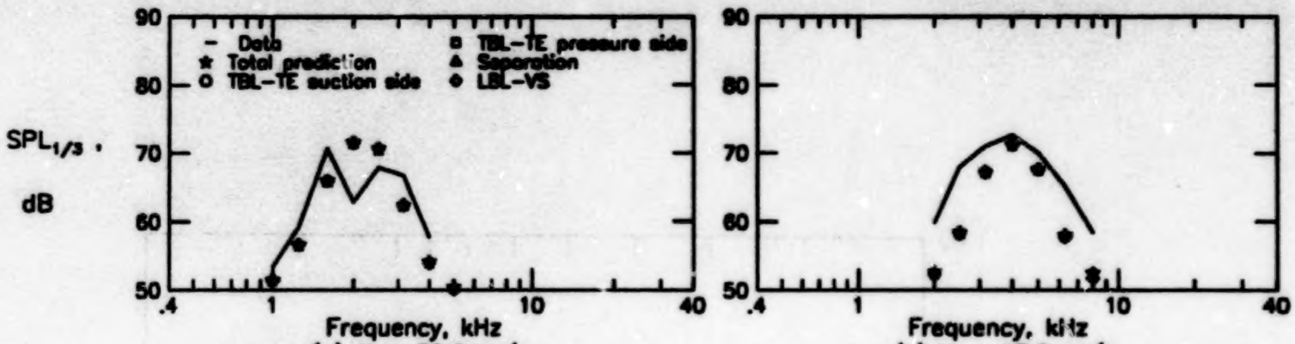

(a) U = 30.0 m/s

(b) U = 43.0 m/s

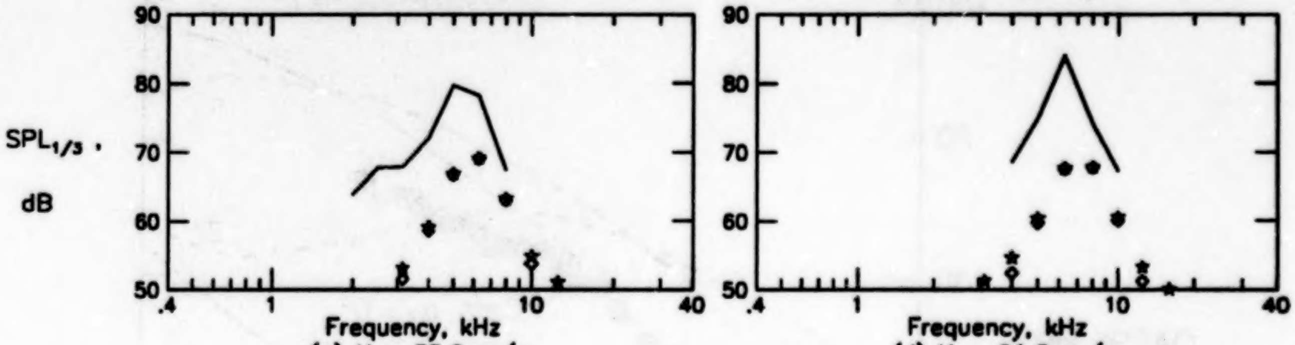

(c) U = 55.0 m/s

(d) U = 61.0 m/s

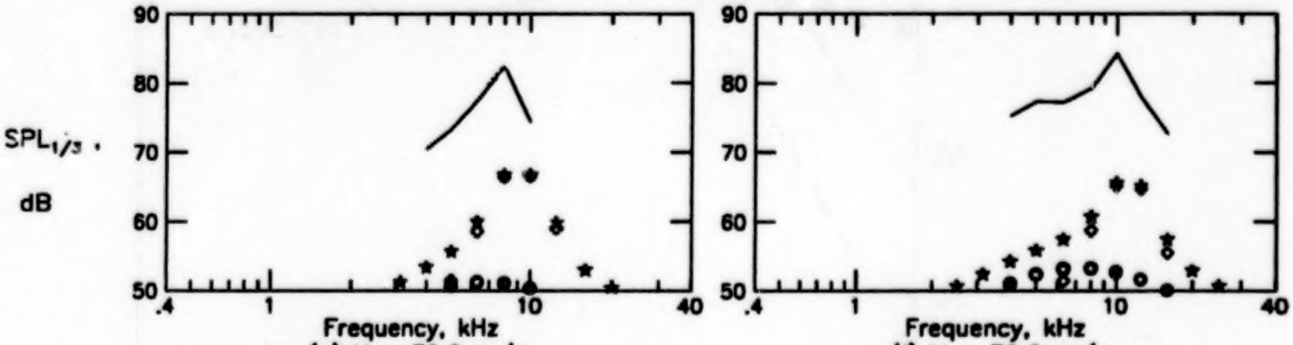

(e) U = 70.0 m/s

(f) U = 79.0 m/s

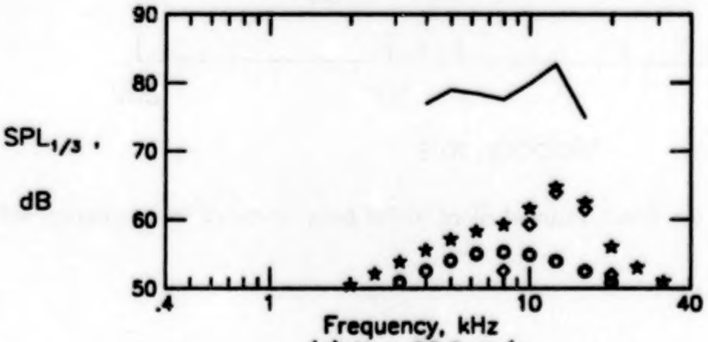

(g) U = 88.0 m/s

Figure 113. Noise spectra for 4-to-1 tapered-chord airfoil at $\alpha_t = 0^\circ$ ($\alpha_* = 0^\circ$) from reference 27 compared with prediction of present paper.

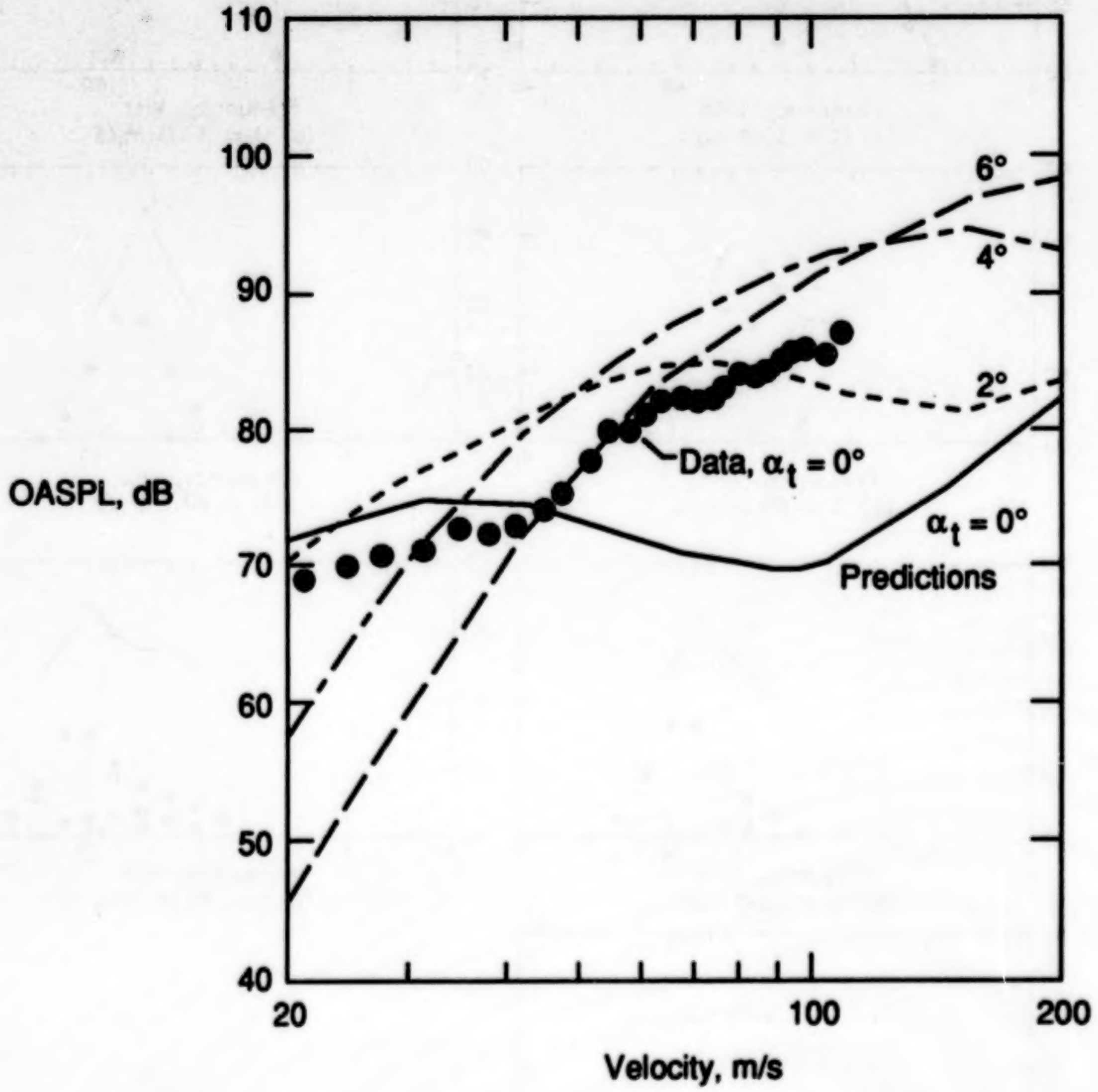

Figure 114. Overall sound pressure level versus velocity for 4-to-1 tapered-chord airfoil from reference 27 compared with predictions of present paper.

7. Conclusions

This paper documents the development of an overall prediction method for airfoil self-noise. The approach is semiempirical and is based on previous theoretical studies and data from a series of aerodynamic and acoustic tests of isolated airfoil sections. The acoustic data processing employed a correlation editing procedure to obtain self-noise spectra uncontaminated by extraneous noise. Five self-noise mechanisms, each related to specific boundary-layer phenomena, are identified in the data and modeled. For each mechanism, the data are first normalized by fundamental techniques using scaled aerodynamic parameters. The spectral shape, level, and frequencies are then examined and modeled for dependences on parameters such as Reynolds number, Mach number, and geometry.

The modeling accuracy of the resulting self-noise prediction methods is established by comparing predictions with the complete data base. The methods are shown to have general applicability by comparing predictions with airfoil self-noise data reported in the literature from three studies. A successful application of the methods is reported for a large-scale-model helicopter rotor broadband noise test.

Conclusions can be drawn regarding the specific self-noise mechanisms. For the turbulent-boundary-layer–trailing-edge noise and separation noise sources, an accurate and generally applicable predictive capability is demonstrated, especially for the important conditions of high Reynolds number and low to moderate angle of attack. The mechanism which can dominate the spectra for low Reynolds number, laminar-boundary-layer–vortex-shedding noise, is also demonstrated to have good predictive capability. For this quasi-tonal noise mechanism, there are some issues, not fully addressed herein, about how to apply the formulations in the most appropriate way to different airfoil geometries. The tip vortex formation noise source appears to be well predicted, although its relative lack of importance compared with the other self-noise sources prevents a full assessment of accuracy. The trailing-edge-bluntness–vortex-shedding noise source is shown to be very important and predictable by the method developed. For this source, there is an associated "flow angle" parameter which is found to be constant for any given trailing-edge geometry, but is difficult to determine a priori. However, for application of the bluntness noise prediction method, reasonable estimates for this parameter can be made based on the examples in this report.

The unique prediction capability presented should prove useful for the determination of broadband noise for helicopter rotors, wind turbines, airframe noise, and other cases where airfoil shapes encounter low- to moderate-speed flow. For modern propeller designs, the present equations should be applied with some caution because the high-speed, high-loading, and skewed-flow conditions existing about propeller blades do not match the low- to moderate-speed and generally 2D flow conditions of the present data base. The computer codes given herein can be readily incorporated into existing or future noise prediction codes. The documentation provided in this report should provide the means to evaluate where and how any needed future refinements can be made in the prediction codes for particular applications.

NASA Langley Research Center
Hampton, VA 23665-5225
April 19, 1989

Appendix A

Data Processing and Spectral Determination

In section 4, the special processing approach used to determine the self-noise spectra for the 2D airfoil models was summarized. Details are given here.

A.1. Data Acquisition and Initial Processing

Signals from the microphones shown in figure 4 were recorded during the test on a 14-channel FM analog tape recorder, operated to provide a flat frequency response up to 40 kHz. Individual amplifiers were used to optimize signal-to-noise ratio for each microphone channel, and pure-tone and white-noise insertions were used to calibrate amplitude and phase response, respectively. These calibrations and signal-conditioning techniques were the same as in reference 2, where additional details are given. The data were reduced from tape on a spectrum analyzer interfaced with a minicomputer. Pairs of microphones were used to obtain 1024-point cross-correlations at an analysis range of ±4.167 milliseconds.

A.2. Correlation Editing

The correlation records are modified to eliminate contributions from extraneous noise sources prior to taking the Fourier transforms to obtain the spectra. The first step is to remove, to the extent possible, the noise from the test hardware by subtracting the correlation $R_{45}(\tau)$ without the airfoil in place (the background noise) from $R_{45}(\tau)$ with the airfoil in place. (See fig. 9.) The resulting record should then be comprised of correlation peaks from the desired TE noise, LE noise, and other extraneous noise related to interaction between the model and test rig not accounted for in the subtraction. The TE and LE noise peaks in the cross-correlation are assumed to represent the autocorrelation of the TE and LE noise, respectively.

To eliminate the LE contribution, the correlation record on the right-hand-side (RHS) of τ_{TE} is discarded and replaced by the mirror image of the left-hand-side (LHS). However, for this folding process, it was found that it is important to preserve the basic shape of the TE peak to more accurately represent the spectra at higher frequencies. Because this is a digital correlation, made up of discrete points which are $\Delta\tau$ apart, it is likely that the true TE noise peak falls somewhere between two discrete values of τ. Folding about a discrete point instead of the actual effective peak center would introduce error by distorting the peak shape. In figure A1, the discrete points of the TE correlation peak are illustrated to show how the folding was accomplished. The discrete center is at τ_{TE}, whereas the effective center is to the left. The correlation values at $\tau_{\mathrm{TE}} + \Delta\tau$ and $\tau_{\mathrm{TE}} + 2\,\Delta\tau$ must not be changed to avoid modifying the shape near the very peak. The correlation value at $\tau_{\mathrm{TE}} + 2\,\Delta\tau$ is projected to the LHS to intercept a line connecting $\tau_{\mathrm{TE}} - 3\,\Delta\tau$ and $\tau_{\mathrm{TE}} - 2\,\Delta\tau$. This defines the constants $\bar{a}$ and $\bar{b}$ which are shown. These constants then are used to interpolate between the points on the LHS to determine values at the points on the RHS, that is

$$R(\tau_{\mathrm{TE}} + N\,\Delta\tau) = \frac{\bar{b}}{\Delta\tau} R(\tau_{\mathrm{TE}} - N\,\Delta\tau) + \frac{\bar{a}}{\Delta\tau} R(\tau_{\mathrm{TE}} - (N+1)\Delta\tau) \quad \text{(A1)}$$

for $N > 2$. The entire LHS of the correlation is folded about the effective peak center using this interpolation scheme.

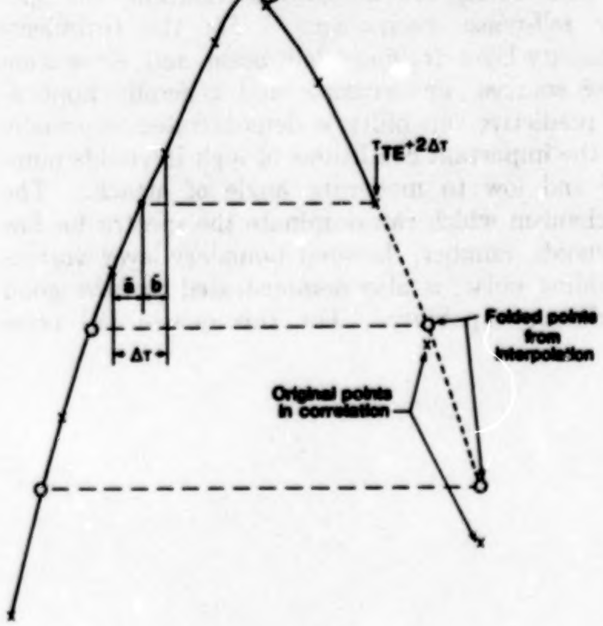
Effective peak center
τ_{TE}
Discrete peak center
$\tau_{\mathrm{TE}}+2\Delta\tau$
$\bar{a}$
$\bar{b}$
$\Delta\tau$
Folded points from interpolation
Original points in correlation

Figure A1. Sample correlation peak.

A.3. Separation of TE and LE Peaks

As indicated in section 4, for some of the correlation data for the three smaller chord lengths, the LE and TE peaks are so close that the LE contribution overlaps and distorts the TE peak shape. For many such cases a procedure was found to successfully remove the distortion prior to implementing the TE peak folding process described above. This procedure is explained by way of example for the 5.08-cm-chord airfoil shown in the bottom trace of figure A2. The predicted locations of the TE and LE noise peaks in the correlations are indicated and agree well with the peaks in the actual trace. Note the proximity of the two peaks.

The procedure to separate these two peaks involves combining the original $R_{45}(\tau)$ at the bottom of figure A2 with time-shifted versions of itself, so that the peaks are separated by larger time delays. The procedure depends on the implied symmetry of the LE and TE peaks, inherent in the assumption that they represent the autocorrelations for the LE and TE noise, respectively. The first step is to invert $R_{45}(\tau)$ in sign, and reverse it in time, by "flipping" the correlation about τ_{LE}. The result of combining these two curves is seen in the second trace from the bottom of figure A2, denoted $R'_{45}(\tau)$. The two peaks seen here are the original TE noise peak, and an inverted TE noise peak at $2\tau_{\mathrm{LE}} - \tau_{\mathrm{TE}}$. There is some increase in level and some distortion in the correlation record away from the peaks, as should be expected. The LE noise peak has been removed, but the inverted TE noise peak still affects the original peak at τ_{TE}. To remove the inverted peak, the initial $R_{45}(\tau)$ must be shifted by $2(\tau_{\mathrm{LE}} - \tau_{\mathrm{TE}})$ and summed with the previous result. This produces the third curve from the bottom in figure A2, denoted $R''_{45}(\tau)$. The TE noise peak has remained at τ_{TE}, while the LE noise peak is now at $3\tau_{\mathrm{LE}} - 2\tau_{\mathrm{TE}}$. The peaks are now separated in time so that details of each peak can be seen. Note that as the peaks no longer affect one another's shape, their basic symmetry is evident. This helps to validate the initial assumption that the peaks represent the autocorrelations of TE and LE noise. If the peaks must be further separated, this procedure can be successively repeated, with the results of the next two iterations seen in the top two traces of figure A2, $R'''_{45}(\tau)$ and $R''''_{45}(\tau)$. It should be noted that only the inner portion of the correlation is shown (the correlation was performed for ±4.067 ms). Because of the data record manipulations, much of the outer portions of the correlations did not overlap and were thus zeroed out.

A.4. Determination of Spectra

Once the correlation records, or their modified forms after the separation processing, are folded about the effective peak center, the resulting TE noise correlations are transformed into spectra of the noise. Because the correlation record lengths are reduced by varying amounts (typically 20 percent) because of the editing described above, the use of fast Fourier transform techniques is not convenient. Instead, regular Fourier transform techniques are used in an approach based on chapter 9 of reference 28. In summary, a data window is applied to the correlation (eq. 9.116, ref. 28) and is used to provide the real and imaginary portions of the spectrum (eqs. 9.167–9.168, ref. 28). The resulting cross-spectra (eqs. 9.172–9.174, ref. 28) are presented in terms of magnitude and phase.

With the cross-spectra produced, amplitude corrections are applied to account for shear layer effects, using the technique of Amiet (ref. 22), as well as self-noise directivity effects, which are described in appendix B. The spectrum for each microphone pair was corrected to an effective position of 90° with respect to the airfoil chord line. The combined effect of both of these corrections tended to be small, with the corrections for many test conditions being less than 1 dB. Since cross-spectra were obtained, the corrections for each of the two microphones involved were averaged to correct the cross-spectral magnitude.

The results obtained from this method are given in figure A3 for the example correlation records of figure A2. Figure A3(a) shows the cross-spectrum obtained from the correlation of the original $R_{45}(\tau)$ record, which is the bottom curve of figure A2, while figure A3(b) shows the cross-spectrum obtained after folding the $R_{45}(\tau)$ record about the TE noise peak. Note that the cross-spectral phase ϕ is a partial indicator of how well the cross-spectrum represents the total TE self-noise. Ideally the phase should vary linearly with frequency, $\phi = 360° f\tau_{\mathrm{TE}}$. The breaks seen in this phase line and the corresponding spectral peculiarities indicate regions adversely affected by contamination, which was not removed by the background subtraction and, in the case of figure A3(b), the folding process. The contamination from the LE is seen to primarily affect the cross-spectrum of figure A3(a) below around 4 kHz. Folding the correlation removes most of this, leaving a dip in the spectrum of figure A3(b) at about 1.5 kHz. Figure A3(c) shows the spectrum for the third curve from the bottom in figure A2, $R''_{45}(\tau)$, which is the modified correlation after two manipulations have separated the TE and LE noise peaks. The phase difficulty and spectral dip at about 1.5 kHz in figure A3(b) are eliminated in figure A3(c). Figure A3(d) shows the spectrum for the top curve of figure A2, $R''''_{45}(\tau)$, which is for four manipulations. This spectrum is similar to that of figure A3(c) except for some apparent increase in contamination at the low- and high-frequency ends. For the airfoil presented here, a choice was made to use the spectrum of figure A3(c), based on two

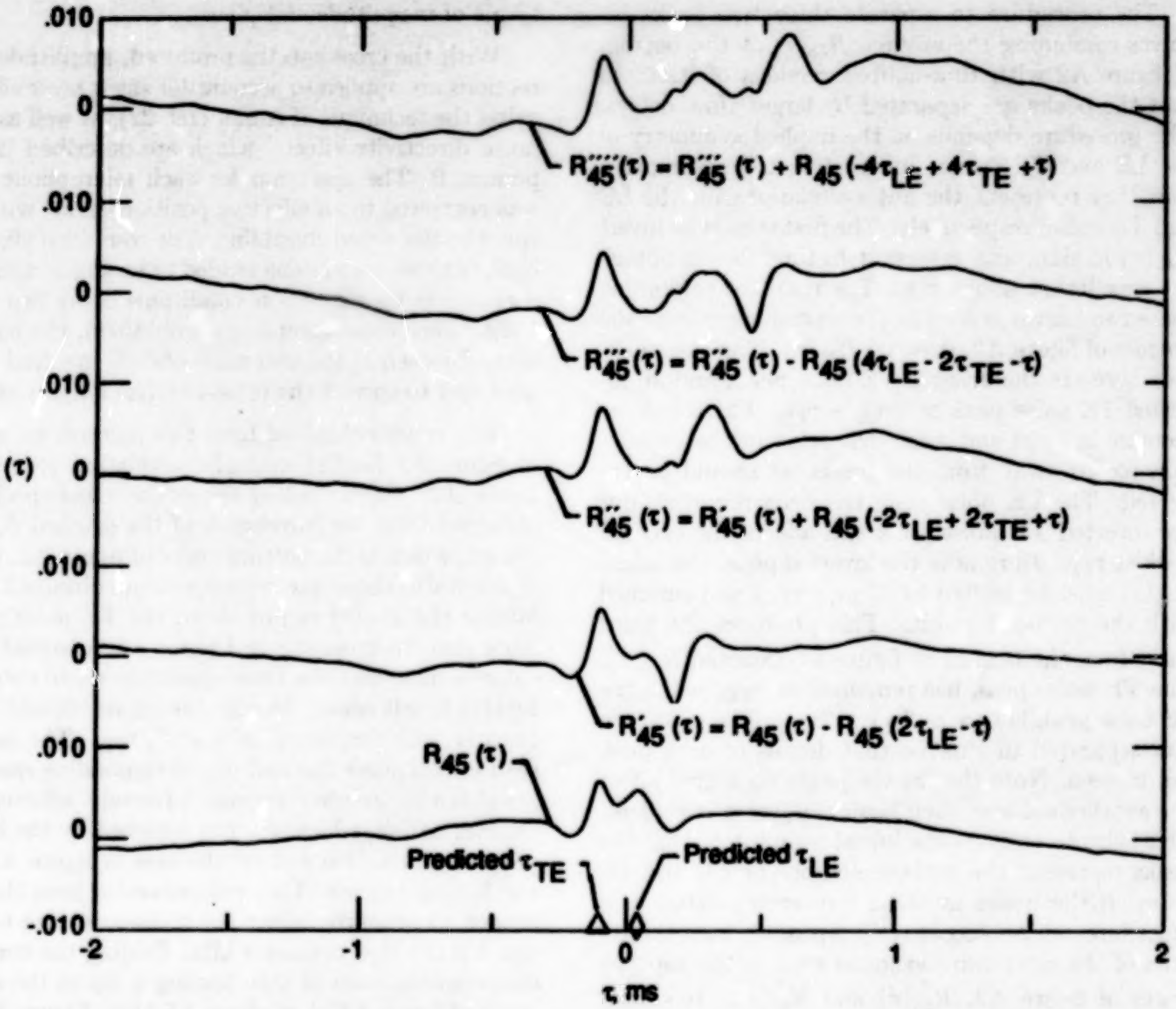

Figure A2. Separation of TE and LE peaks in a cross-correlation. Example is cross-correlation between microphones M4 and M5 for the 5.08-cm-chord airfoil with tripped BL. $\alpha_* = 0°$, $U = 71.3$ m/s.

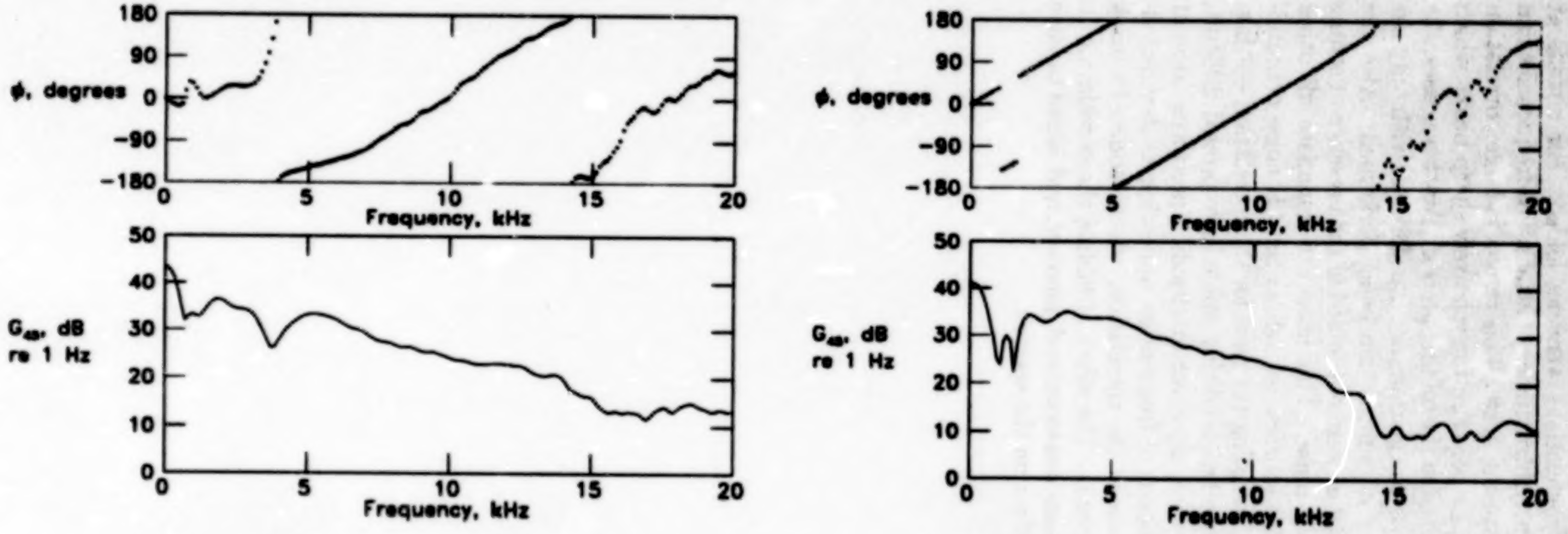

(a) Transform of $R_{45}(\tau)$ with no folding.

(b) Transform of $R_{45}(\tau)$ with folding about TE peak.

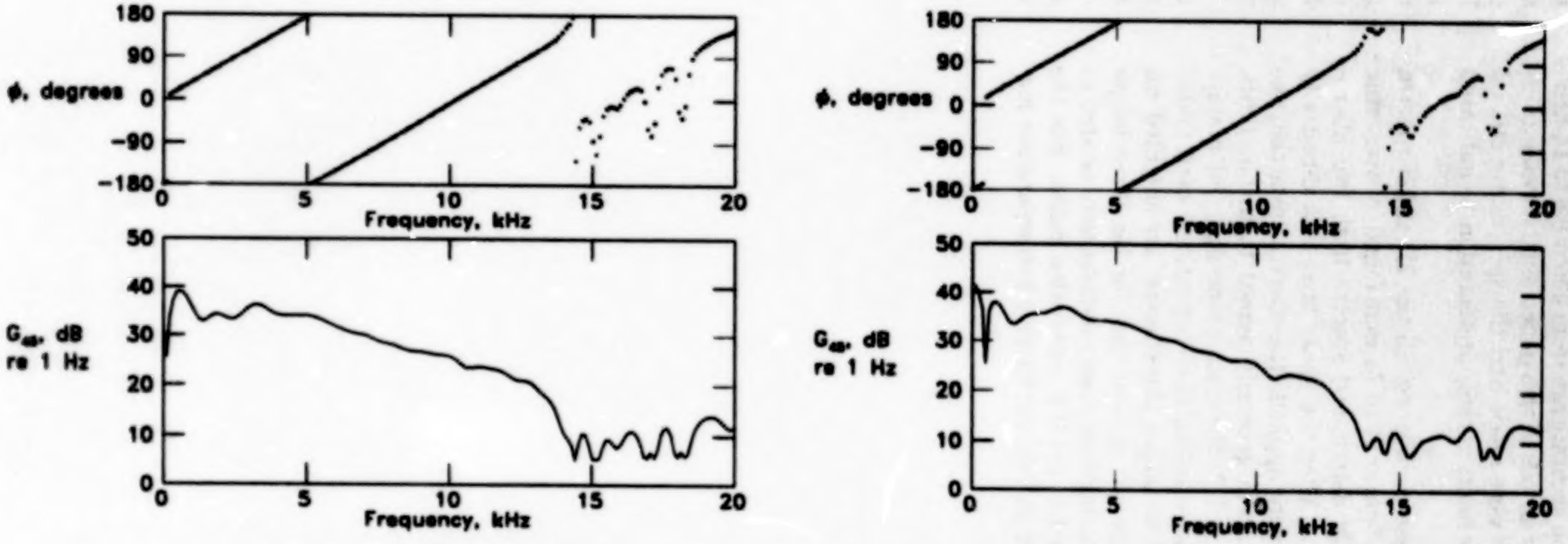

(c) Transform of $R''_{45}(\tau)$ with folding about TE peak.

(d) Transform of $R'''_{45}(\tau)$ with folding about TE peak.

Figure A3. Cross-spectra obtained by transforming correlations of figure A2.

separation manipulations, to represent the self-noise. The lower and upper limits to which the spectrum is believed to be accurate are from about 0.8 to 13 kHz. For the other airfoils of this paper, similar evaluations of the limits were made and the spectra are cut off beyond these limits in their presentation, as indicated in section 4.

To increase confidence, all the 2D airfoil spectra presented in figures 11 to 74 were found by averaging independently determined spectra from two microphone pairs. After the shear layer and directivity corrections were applied, the spectra from the two microphone pairs generally agreed to within 1 dB. In tables 1 and 2, the data processing and manipulations, and whether the correlations were folded or not prior to taking the spectra, are specified for each test case. It is seen that for the three larger airfoils, no correlation manipulations were needed to separate the LE and TE correlation peaks. For the three smaller airfoils, performing two separation manipulations was advantageous for about a quarter of the cases. The table shows that a substantial number of correlations were not folded. For airfoils at sufficiently high angles of attack, low frequencies can dominate the noise. This results in large correlation humps, rather than the relatively sharp peaks which are needed in the folding process. For these cases, the raw cross-correlations are transformed, with only the background subtraction being performed. Also the correlations were not folded in the presence of strong LBL–VS noise. This noise can dominate all other self-noise sources, as well as the LE noise contamination, negating the need for the correlation editing. This correlation editing would have proved difficult, in any case, since vortex shedding produces noise at small bands of frequencies, appearing as damped sinusoidals in the correlation, which tended to mask other peaks. The effect of folding the correlation in such cases was examined, however, and found to have little effect on the spectra.

Appendix B

Noise Directivity

The purpose of this appendix is to define the directivity functions $\overline{D}_h$ and $\overline{D}_\ell$, which are employed in the tunnel noise data processing and proposed for use in the prediction equations for the self-noise sources.

B.1. Retarded Coordinates

The retarded coordinate system is explained by first referring to figure B1 where the airfoil is at zero angle of attack to the tunnel flow. If the velocity were zero everywhere, sound from the model which reaches the microphones (M2 is shown) would follow the ray path defined by the measured distance r_m and angle Θ_m. But with the velocity in the free jet equal to U, the ray which reaches the microphones follows first the radiation angle Θ_c until it encounters the shear layer where it is refracted. It emerges at angle Θ_t with an amplitude change and travels to the microphone. The theoretical treatment employed in this study for the angle and amplitude corrections is that due to Amiet (refs. 22 and 23). A convenient reference for the corrected microphone measurements is a retarded coordinate system where the source and the observer are at corrected positions. The angle Θ_e is referenced to a retarded source position and a corrected observer position where the distance between the positions is $r_e = r_m$. As defined, if there were no shear layer present with flow extending to infinity, the center of the wave front emitted from the source would be at the retarded source position when the wave front reaches the corrected observer position. The retarded coordinates are equivalent to the emission time coordinates employed in the literature, for example, see reference 29, for moving sources and stationary observers. Figure B2 shows a source flyover geometry corresponding to the open jet wind tunnel geometry of figure B1. Physical equivalence between the cases is attained by accounting for the Doppler-related frequency shifts due to the relative motion between the source and observer in one instance and no relative motion in the other. There are no Doppler-related amplitude corrections required between the flyover and wind tunnel cases as the effect of the flow on the source definition is already included in the wind tunnel environment.

B.2. Directivity Functions

In figure B3, a 3D retarded coordinate system is defined where the origin is located at the trailing edge of a thin flat plate, representing an airfoil. The flat plate is in rectilinear motion of velocity U in direction of the negative x_e axis. The observer is stationary. Trailing-edge noise is produced when boundary-layer turbulence and its associated surface pressure pattern convect downstream (with respect to the plate) at a velocity U_c (Mach number M_c) past the trailing edge. If the noise-producing turbulence eddies are sufficiently small and the convection velocities are sufficiently large to produce acoustic wavelengths much shorter than the chord length, the directivity can be shown to be (based on analysis of Schlinker and Amiet, ref. 3)

$$\overline{D}_h(\Theta_e, \Phi_e) \approx \frac{2\sin^2(\Theta_e/2)\sin^2\Phi_e}{(1+M\cos\Theta_e)[1+(M-M_c)\cos\Theta_e]^2} \qquad \text{(B1)}$$

where the h subscript indicates the high-frequency (or large-chord) limit for $\overline{D}$. The overbar on $\overline{D}_h$ indicates that it is normalized by the TE noise radiated in the $\Theta_e = 90°$ and $\Phi_e = 90°$ direction, so $\overline{D}_h(90°, 90°) = 1$. For the flyover plane ($\Phi_e = 90°$), equation (B1) is the same as equation (32a) of reference 3. In reference 3, the equation was compared favorably with measured airfoil TE noise results, for limited M and Θ_e ranges, as well as with previous theoretical results. The directivity expression used in reference 2 was found to give virtually identical results for low Mach numbers.

Although developed for when the velocity U is parallel to the plate along the x_e axis, equation (B1) can be applied when the plate or airfoil is at an angle of attack α to the flow. In application (refer to fig. B3), one should define the angles with respect to a coordinate system that is fixed with respect to the airfoil with the x_e axis fixed along the chord line, rather than one where the x_e axis is fixed along the direction of motion. Note, however, that any analysis of Doppler frequency shifts (not treated in this paper) should reference angles with respect to the direction of motion. Applications of equation (B1) at angles of attack should result in little additional error to that already built into the relation. Because it was derived with the plate assumed to be semi-infinite, $\overline{D}_h$ becomes inaccurate at shallow upstream angles ($\Theta_e \rightarrow 180°$), when applied to finite airfoils even for high frequencies. As frequency is lowered, the wavelengths become larger with respect to the chord and the directivity becomes increasingly in error. However, $\overline{D}_h$ should be of sufficient accuracy to define the directivity of all the self-noise sources discussed because of their high-frequency character. The one exception to this is the stalled-airfoil noise.

When the angle of attack of the airfoil is increased sufficiently, the attached or mildly separated TBL flow on the suction side gives way to large-scale

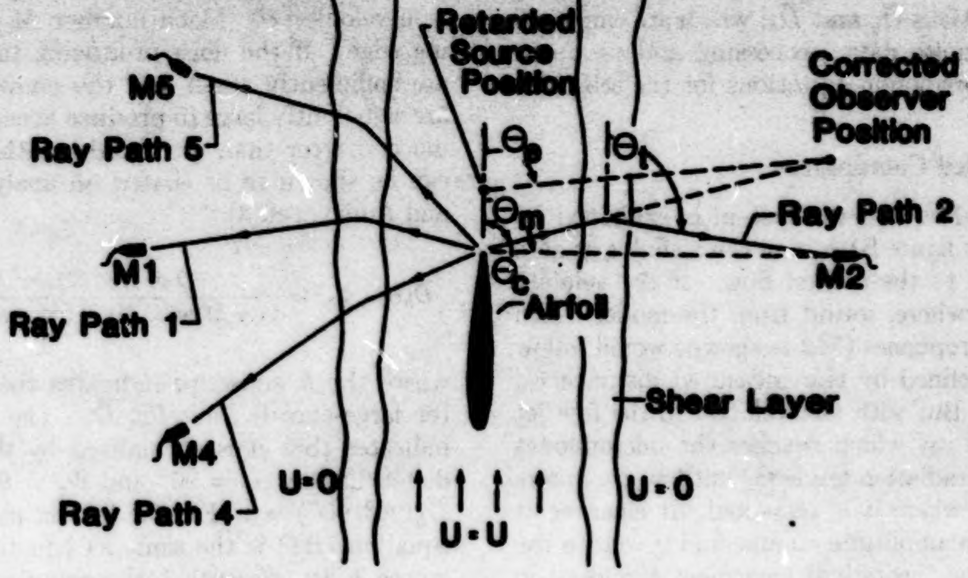
M5
Ray Path 5
Retarded Source Position
Corrected Observer Position
Θ_o
Θ_t
Θ_m
Θ_c
Ray Path 2
M1
M2
Ray Path 1
Airfoil
Shear Layer
M4
Ray Path 4
U = 0
U = U
U = 0

Figure B1. Sketch of shear layer refraction of acoustic transmission paths.

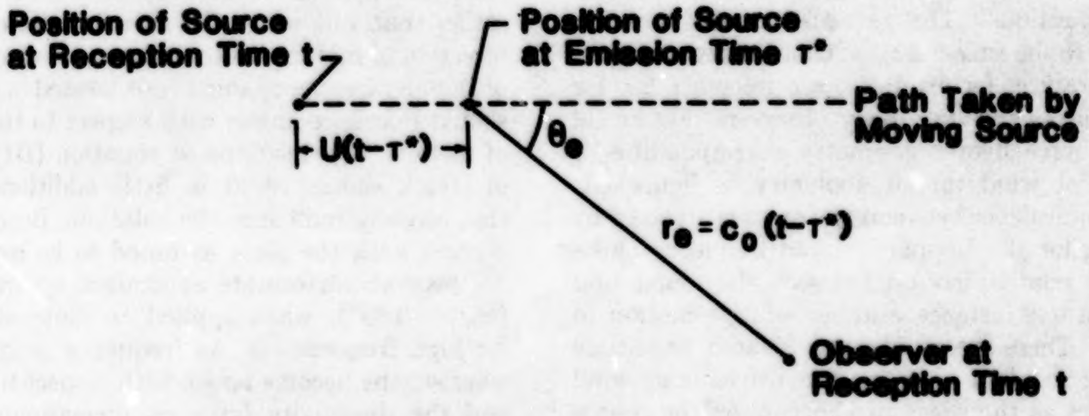
Position of Source at Reception Time t
Position of Source at Emission Time τ^*
Path Taken by Moving Source
$U(t-\tau^*)$
θ_e
$r_e = c_0\,(t-\tau^*)$
Observer at Reception Time t

Figure B2. Emission from a source moving with a constant velocity.

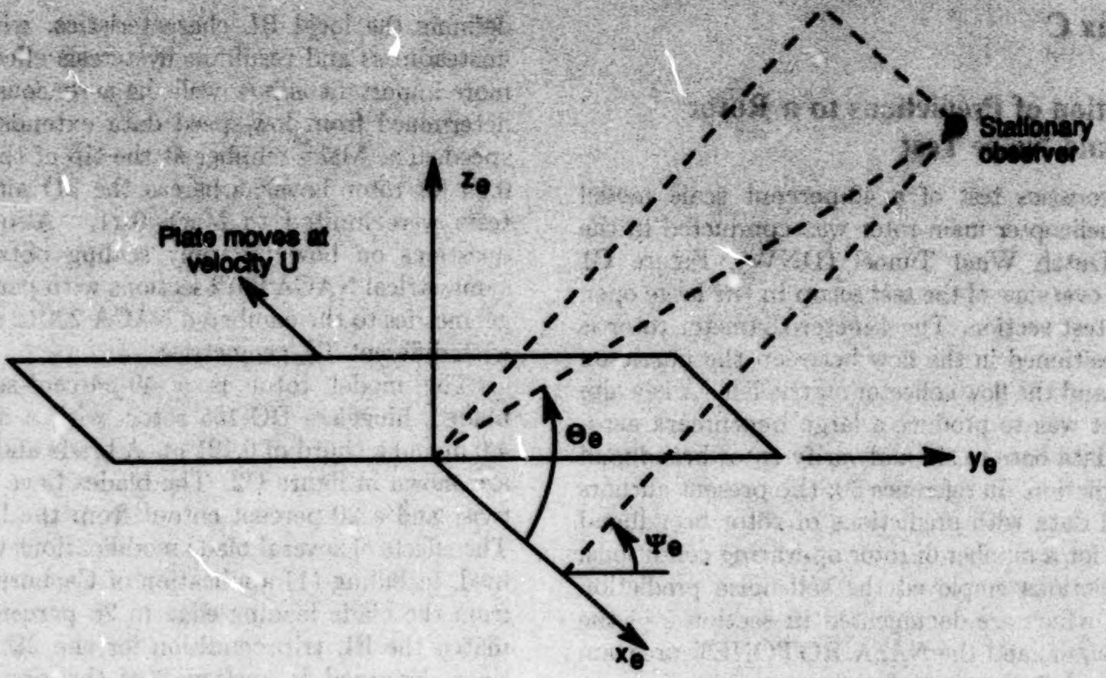

Figure B3. Flat plate in rectilinear motion.

separation. The turbulence eddies are then comparable in size to the airfoil chord length and the eddie convection speeds are low. The directivity for this low-frequency noise is more properly defined as that of a translating dipole, which is

$$\overline{D}_\ell(\Theta_e, \Phi_e) \approx \frac{\sin^2 \Theta_e \sin^2 \Phi_e}{(1 + M \cos \Theta_e)^4} \qquad \text{(B2)}$$

where the ℓ subscript indicates a low-frequency limit. The coordinate system and comments about angle definitions in equation (B1) apply also in equation (B2). Equation (B2) is employed for the directivity in the expression for stalled flow noise (eq. (30)).

For the noise data reduction in the present study, equation (B1) was used in the determination of the self-noise spectral levels for the reference observer position, at $r_e = 122$ cm and $\Theta_e = 90°$. First, shear layer refraction corrections were calculated to determine the spectral level adjustments, to add to measured values, and a resultant source-observer location at r_e and Θ_e. This was done while keeping track of the actual physical coordinates of the trailing edge which varied with airfoil angle of attack. Finally, equation (B1), with $\Phi = 90°$ and an assumed convection Mach number of $M_c \approx 0.8M$, was used to determine final level adjustments required to match results to the $\Theta_e = 90°$ location.

Appendix C

Application of Predictions to a Rotor Broadband Noise Test

An acoustics test of a 40-percent scale model BO-105 helicopter main rotor was conducted in the German-Dutch Wind Tunnel (DNW). Figure C1 shows an overview of the test setup in the large open anechoic test section. The 4-meter-diameter rotor is shown positioned in the flow between the nozzle on the right and the flow collector on the left. A key aim of the test was to produce a large benchmark aeroacoustic data base to aid and verify rotor broadband noise prediction. In reference 30, the present authors compared data with predictions of rotor broadband self-noise for a number of rotor operating conditions. The predictions employed the self-noise prediction methods, which are documented in section 5 of the present paper, and the NASA ROTONET program (ref. 31) to define rotor performance and to sum contributions of noise from individual blade segments.

In this appendix, the experiment is not reviewed in detail nor are data-prediction comparisons presented, as reference 30 is complete in this regard. Rather, reference 30 is complemented by specifying how the self-noise prediction methods of the present paper were applied. Given below is a summary of the rotor prediction method, a definition of the rotor blade geometry and test modifications and a specification of input parameters for the individual source predictions. The degrees of success of data-prediction comparisons in reference 30 are discussed along with recommended refinements to the prediction methods.

To produce a rotor prediction, the rotor geometry definition and flight conditions, specified as thrust, rotor angle, rotor speed, flight velocity, and trim condition, are provided as inputs to the ROTONET rotor performance module. The particular module used assumes a fully articulated rotor with rigid blades and a simple uniform inflow model. The module determines local blade segment velocities and angles of attack for a number of radial and azimuthal positions. Ten radial segments were considered at 16 azimuthal positions. The BL thicknesses and other parameters needed are calculated. The noise due to each source is predicted for each blade segment, and the ROTONET noise radiation module is used to sum contributions from all blade segments to obtain, after accounting for Doppler shifts and the actual number of blades, the noise spectrum at the observer.

As indicated in reference 30, the accuracy of predictions depends on a number of factors including the accuracy of the performance module used. One may question the quasi-steady assumptions used in defining the local BL characteristics, which ignore unsteadiness and resultant hysteresis effects. Likely more important is how well the aeroacoustic scaling determined from low-speed data extends to higher speed. The Mach number at the tip of the blades is 0.64 for rotor hover, whereas the 2D airfoil model tests were limited to Mach 0.21. Also there are questions on how to apply scaling obtained from symmetrical NACA 0012 sections with particular TE geometries to the cambered NACA 23012 rotor blade with different TE geometries.

The model rotor is a 40-percent-scale, four-bladed, hingeless BO-105 rotor, with a diameter of 4.0 m and a chord of 0.121 m. A blade and its details are shown in figure C2. The blades have −8° linear twist and a 20-percent cutout from the hub center. The effects of several blade modifications were examined, including (1) application of Carborundum grit from the blade leading edge to 20 percent chord to match the BL trip condition for the 2D blade sections described in section 2 of the present paper, (2) taping of the TE with 0.064-mm-thick plastic tape to modify the "step tab" geometry, and (3) attachment of a rounded tip to each blade (the standard blades have a squared-off tip).

C.1. Boundary-Layer Definition

With the local blade segment mean velocities and angles of attack determined by the rotor performance module, the equations of section 3 were directly applied to determine the BL thicknesses required in the noise predictions. Most noise comparisons in reference 30 are for the blades with untripped BL. For the tripped BL, the fact that the BL trip conditions for the rotor blades matched the 2D test models assured the appropriateness of using the equations for a heavy trip rather than modifying the equations as required for the UTRC comparisons reported in section 6. For all BL thickness calculations, the aerodynamic angles of attack were used in the equations. The aerodynamic angle is referenced to the zero lift angle, which is −1.4° from the geometric angle for the NACA 23012 airfoil.

C.2. TBL–TE and Separation Noise Prediction

Given the definitions of segment chord length, span width, velocity, aerodynamic angle of attack, and BL thicknesses, the calculation of TBL–TE and separation noise is straightforward as specified in section 5. From the data-prediction comparisons of reference 30, it is concluded that the TBL–TE and separation noise calculations demonstrated a good predictive capability for these mechanisms. The rotor was tested from hover to moderately high flight

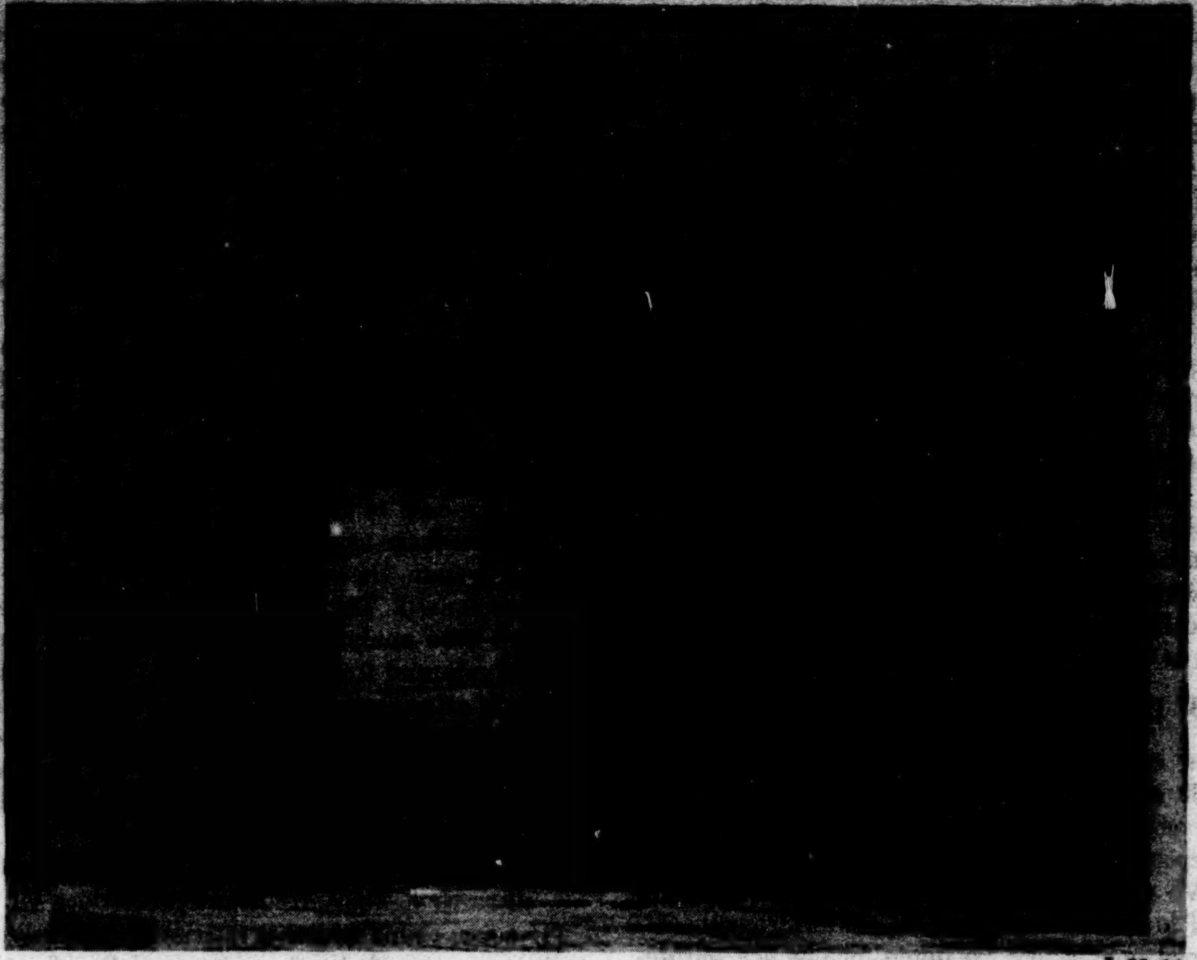

L-89-44

Figure C1. Test setup in DNW for helicopter main rotor broadband noise study reported in reference 30.

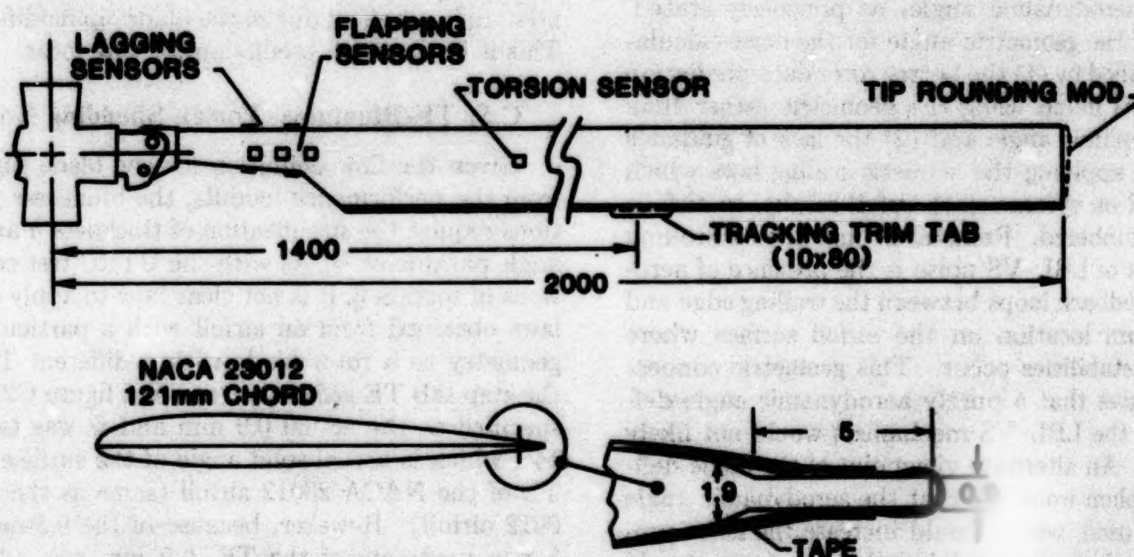
LAGGING SENSORS
FLAPPING SENSORS
TORSION SENSOR
TIP ROUNDING MOD
TRACKING TRIM TAB (10x80)
1400
2000
NACA 23012 121mm CHORD
5
1.9
0.
TAPE
TRAILING EDGE MOD

Figure C2. Model BO-105 blade details. All dimensions in mm.

ORIGINAL PAGE
BLACK AND WHITE PHOTOGRAPH

speeds for various climb and descent rates at different thrust settings. Diagnostics included 1/2 rotor speed tests and the BL tripping tests. It is noted that the TBL–TE and separation noise predictions for a number of rotor conditions fell below contributions of LBL–VS, especially at the 1/2 rotor speed, and of TE bluntness noise. This represents a limitation of the comparisons which prevents sweeping statements regarding predictive accuracy of TBL–TE and separation noise sources. Still the agreements were quite good except when the rotor operated at full speed (tip speed of $M = 0.64$) and the boundary layers were tripped. Then the noise was underpredicted by about 6 dB. It is believed that for this high speed the heavy trip disturbed the flow substantially, made it dissimilar to the 2D model cases, where the speed was limited to $M = 0.21$, and perhaps changed the controlling noise mechanisms. Comparisons for the tripped BL rotor at 1/2 speed and the untripped BL blades at full and 1/2 speed produced good results.

C.3. LBL–VS Noise Prediction

The comparisons for LBL–VS noise in reference 30 showed, for a broad range of rotor conditions, very good predictions. As with the TBL–TE and separation noise predictions, the calculation of LBL–VS noise is straightforward given the specification of local flow conditions at the blade segments. A special note should be made for one key parameter involved in the calculations. The angle of attack α_* employed in the LBL–VS noise prediction (eqs. (53) to (60)) was the geometric angle rather than the aerodynamic angle for the NACA 23012 airfoil section. The BL thickness calculations, however, used the aerodynamic angle, as previously stated. The use of the geometric angle for the noise calculation is justified by (1) the better rotor data-prediction comparisons found using the geometric rather than the aerodynamic angle and (2) the lack of guidance one has in applying the acoustic scaling laws which were based on symmetrical airfoil results, to airfoils that are cambered. Remember that the controlling mechanism of LBL–VS noise is the presence of aeroacoustic feedback loops between the trailing edge and an upstream location on the airfoil surface where laminar instabilities occur. This geometric connection indicates that a purely aerodynamic angle definition for the LBL–VS mechanism would not likely be correct. An alternate viewpoint of the angle definition problem would be that the aerodynamic angle should be used, which would increase the noise predicted over that measured, but that allowance should be made for the fact that the inflow to the rotor blade segments is not the assumed smooth quasi-steady flow. The presence of sufficiently unsteady flow conditions over portions of the rotor would inhibit the establishment of the LBL–VS mechanism and related noise. Limiting LBL–VS noise production to some measure of inflow turbulence offers promise as a refinement to the self-noise prediction method.

C.4. Tip Vortex Formation Noise

The tip noise predictions were made for both the rounded and the squared-off blade tips tested. The performance module was used to determine the local flow velocities and angles for the tips at different azimuth locations. The α_{TIP} used was the NACA 23012 aerodynamic angle. Because the tip loading characteristics for the rotor blades differed from the reference case of the tip noise model, which was an untwisted large-aspect-ratio blade with uniform flow over the span, the sectional lift term of equation (66) was evaluated. The sectional lift slopes for the rotor blades were analyzed by employing a lifting-surface model adapted from reference 18. The velocity and angle of attack were linearly varied over the span near the tip of the lifting surface blade. It was found that the tip loading is increased over the reference case by a small amount. For equation (66), the redefined α'_{TIP} angle was then given by $\alpha'_{\text{TIP}} = 1.1\alpha_{\text{TIP}}$.

The predictions for tip noise in reference 30 were in all cases significantly below predictions for TBL–TE noise. This makes it impossible to truly assess the accuracy of the tip noise modeling for the rotor. However, since the data comparisons with the total levels predicted were good for both low and normal rotor speeds, the tip noise is apparently well predicted. It is noted that a review of data for a number of rotor cases, not all given in reference 30, indicated no significant effect due to the blade tip modification. This is in line with prediction for this rotor.

C.5. TE-Bluntness–Vortex-Shedding Noise

Given the flow definition for the blade segments from the performance module, the bluntness predictions require the specification of thickness h and flow angle parameter Ψ. As with the UTRC test comparisons of section 6, it is not clear how to apply scaling laws obtained from an airfoil with a particular TE geometry to a rotor blade with a different TE. For the step tab TE geometry, shown in figure C2, h was specified as the actual 0.9 mm and Ψ was taken as 14°, which is actual solid angle of the surface at the TE of the NACA 23012 airfoil (same as the NACA 0012 airfoil). However, because of the 0.5-mm step 5 mm upstream of the TE, 0.5 mm was added to the calculated value of δ^*_{avg} to approximately account for the anticipated step-caused BL flow deficit. For the TE tape modification case, δ^*_{avg} was taken as that calculated, because the step was removed, but h was increased by four tape thicknesses. Had the tape remained fully attached to the TE surface (see fig. C2) during the test, two thicknesses would have been added. The flow angle Ψ was taken as 18°. The choice of this specific number was rather arbitrary, but is in line with that used for the UTRC comparisons (section 6) for rounded trailing edges. The tape rounded the TE bluntness which should reduce the persistence of and noise due to the separated flow in the near wake. The larger Ψ angle value (18° compared with 14°) results in less noise predicted.

The comparisons of reference 30 obtained using the above "reasonable" choices for the TE parameters give good results for all 1/2 rotor speed cases. For the full rotor speed cases the levels were consistently overpredicted. This is believed to be due to a speed dependence for the bluntness mechanism that could not have been anticipated from the low speed airfoil data, from which the scaling laws were developed. Subsequent analysis indicates that much better agreement with data could have been obtained if the bluntness noise contribution was eliminated for blade segments exceeding Mach numbers of 0.45 or 0.5. This is in some conflict with comparisons in section 6 for the blade section noise of Schlinker and Amiet (ref. 3), which shows apparently strong bluntness noise at $M = 0.43$ and 0.5. However, based on the rotor results, an upper limit of 0.45 for the bluntness noise contribution is recommended as a refinement to the prediction method.

Appendix D

Prediction Code

The airfoil self-noise prediction method is available as a computer code written in standard FORTRAN 5 specifically for the Digital Equipment Corp. VAX-11/780 series machine running under the VMS operating system. To the extent possible, the code has been made machine independent. There is one input file to the code and one output file. Input consists of user supplied `NAMELIST` parameters while output is a table of 1/3-octave centered frequencies with corresponding sound pressure levels for each noise mechanism followed by their total. The user selects which of the mechanisms to calculate.

The airfoil section for which a prediction is desired is assumed to be composed of a number of segments, each having its own chord, span, angle of attack, free-stream velocity, trailing-edge bluntness, and angle parameter, as well as observer directivity angles and distance. This permits a variety of configurations such as taper, twist, spanwise-varying free-stream velocity (for rotor blades), etc. The user may specify as many or few segments as desired depending on the complexity of the geometry. Characteristics for each segment are specified in the input file, which contains the FORTRAN variables given in table D1.

Table D1. Segment Characteristics Specified in Input File

FORTRAN name	Symbol	Description
`NSEG`		Number of segments
`C`	c	Chord length, m
`L`	L	Span, m
`R`	r_e	Observer distance, m
`THETA`	Θ_e	Observer angle from x-axis, deg
`PHI`	Φ_e	Observer angle from y-axis, deg
`ALPSTAR`	α_*	Aerodynamic angle of attack, deg
`ALPHTIP`	α'_{TIP}	Tip flow angle, deg
`H`	h	Trailing-edge bluntness, m
`PSI`	Ψ	Trailing-edge angle, deg
`U`	U	Free-stream velocity, m/sec
`ITRIP`		0—Use untripped BL condition 1—Use tripped BL condition 2—Use lightly tripped BL condition
`ILAM`		1—Compute LBL-VS noise 0—Do not compute LBL-VS noise
`ITURB`		1—Compute turbulent TBL-TE noise 0—Do not compute TBL-TE noise
`IBLUNT`		1—Compute TE bluntness noise 0—Do not compute TE bluntness noise
`ITIP`		1—Compute tip noise 0—Do not compute tip noise
`IROUND`		`.TRUE.`—Use rounded tip in tip calculation `.FALSE.`—Use square tip in tip calculation
`VISC`	ν	Kinematic viscosity, m^2/sec
`CO`	c_o	Speed of sound, m/sec

The prediction shown in figure 45(a) was obtained using the following input:

```
$INDATA
  NSEG     =  1,
  C        =  .3048,
  L        =  .4572,
  R        =  1.22,
  THETA    =  90.,
  PHI      =  90.,
  ALPSTAR  =  1.516,
  U        =  71.3,
  ITRIP    =  0,
  ILAM     =  1,
  ITURB    =  1,
$END
```

Note that all parameters need not be included in the input if their default values are desired (see program listing for default values). In this example, only the laminar and turbulent mechanisms are computed and the untripped boundary layer condition is used in both mechanisms. The airfoil consists of one segment of constant chord and the observer is 122 cm directly beneath the trailing edge at the midspan. The free-stream velocity has a constant value of 71.3 m/sec across the span. For this example, the output file is given in table D2.

Similarly, the prediction shown in figure 91, was obtained using the following input:

```
$INDATA
  NSEG     =  10.,
  C        =  10*.1524
  L        =  10*.0305
  R        =  10* 1.22,
  THETA    =  10* 90.,
  PHI      =  10* 90.,
  ALPSTAR  =  10* 5.4,
  ALPHTIP  =  7.7,
  U        =  10* 71.3,
  ITRIP    =  1,
  ILAM     =  0,
  ITURB    =  1,
  ITIP     =  1,
  ROUND    =  .TRUE.,
$END
```

This is an example of a multisegmented case where each segment has the same geometry and inflow conditions. Turbulent-boundary-layer noise and tip noise are calculated where the tip is rounded and at an effective angle of attack of 7.7°. All segments are summed to yield a total prediction for each mechanism as shown in table D3.

For the VAX-11/780 machine running under VMS, the following commands will compile, link, and execute the code (assumed to reside on `PREDICT.FOR`), read input from a file `EXAMPLE.IN`, and write results to a file `EXAMPLE.OUT`:

```
$ FOR PREDICT
$ LINK PREDICT
$ ASSIGN EXAMPLE.IN FOR004
$ ASSIGN EXAMPLE.OUT FOR006
$ RUN PREDICT
```

The details of execution for other machines or operating systems may vary. A listing of the code follows.

Table D2. Output File From Prediction Code for Test Case of Figure 45(a)

```
                                          ONE-THIRD OCTAVE
                                        SOUND PRESSURE LEVELS


                    PRESSURE        SUCTION        SEPARATION
FREQUENCY(HZ)       SIDE TBL        SIDE TBL        SIDE TBL         LAMINAR        BLUNTNESS          TIP            TOTAL
--------------  --------------  --------------  --------------  --------------  --------------  --------------  --------------

    100.000         20.654          28.704        -100.000         -17.142           0.000           0.000          29.336
    125.000         24.461          31.965        -100.000         -13.285           0.000           0.000          32.676
    160.000         28.291          35.244         -75.254          -9.018           0.000           0.000          36.042
    200.000         31.437          37.937         -49.243          -5.161           0.000           0.000          38.815
    250.000         34.309          40.400         -27.506          -1.304           0.000           0.000          41.356

    315.000         37.023          42.736          -9.030           2.690           0.000           0.000          43.760
    400.000         39.577          44.949           6.266           6.820           0.000           0.000          46.057
    500.000         41.761          46.859          17.532          10.677           0.000           0.000          48.034
    630.000         43.845          48.706          26.603          14.671           0.000           0.000          49.954
    800.000         45.839          50.503          33.718          18.801           0.000           0.000          51.849

   1000.000         47.581          52.106          38.756          22.658           0.000           0.000          53.568
   1250.000         49.233          53.664          42.692          26.515           0.000           0.000          55.255
   1600.000         50.987          55.368          46.294          30.782           0.000           0.000          57.106
   2000.000         52.533          56.987          49.334          37.725           0.000           0.000          58.817
   2500.000         54.074          57.750          51.298          47.262           0.000           0.000          60.167

   3150.000         55.570          57.500          50.766          48.959           0.000           0.000          60.496
   4000.000         56.044          56.082          47.711          41.796           0.000           0.000          59.455
   5000.000         55.399          54.541          44.617          32.428           0.000           0.000          58.208
   6300.000         53.840          52.942          40.974          28.433           0.000           0.000          56.553
   8000.000         52.190          51.253          36.227          24.304           0.000           0.000          54.021

  10000.000         50.638          49.614          30.419          20.447           0.000           0.000          53.192
  12500.000         49.044          47.890          22.834          16.590           0.000           0.000          51.523
  16000.000         47.202          45.051          11.842          12.323           0.000           0.000          49.591
  20000.000         45.436          43.863          -0.924           8.466           0.000           0.000          47.731
  25000.000         43.549          41.710         -16.833           4.609           0.000           0.000          45.737

  31500.000         41.440          39.279         -37.092           0.614           0.000           0.000          43.503
  40000.000         39.065          36.522         -62.593          -3.515           0.000           0.000          40.987
```

Table D3. Output File From Prediction Code for Test Case of Figure 91

```
                                          ONE-THIRD OCTAVE
                                        SOUND PRESSURE LEVELS


                    PRESSURE        SUCTION        SEPARATION
FREQUENCY(HZ)       SIDE TBL        SIDE TBL        SIDE TBL         LAMINAR        BLUNTNESS          TIP            TOTAL
--------------  --------------  --------------  --------------  --------------  --------------  --------------  --------------

    100.000         19.913          43.083         -19.003           0.000           0.000         -34.005          43.900
    125.000         23.788          46.159          -0.396           0.000           0.000         -24.312          46.184
    160.000         27.673          48.459          16.851           0.000           0.000         -14.255          48.498
    200.000         30.853          50.372          29.124           0.000           0.000          -5.769          50.452
    250.000         33.746          52.155          38.723           0.000           0.000           2.145          52.407

    315.000         36.470          53.894          46.334           0.000           0.000           9.738          54.662
    400.000         39.024          55.609          52.245           0.000           0.000          16.940          57.320
    500.000         41.202          57.165          56.460           0.000           0.000          23.074          59.897
    630.000         43.274          58.766          59.996           0.000           0.000          28.824          62.409
    800.000         45.252          60.360          63.297           0.000           0.000          34.121          65.130

   1000.000         46.980          60.940          65.719           0.000           0.000          38.475          67.016
   1250.000         48.620          60.473          65.697           0.000           0.000          42.257          66.917
   1600.000         50.364          58.874          62.909           0.000           0.000          45.774          64.582
   2000.000         51.911          57.328          59.818           0.000           0.000          48.349          62.363
   2500.000         53.456          55.775          56.383           0.000           0.000          50.351          60.580

   3150.000         54.709          54.122          51.975           0.000           0.000          51.821          59.364
   4000.000         54.799          52.336          45.974           0.000           0.000          52.694          58.443
   5000.000         53.761          50.565          38.550           0.000           0.000          52.917          57.439
   6300.000         52.162          48.597          28.510           0.000           0.000          52.544          56.204
   8000.000         50.507          46.387          15.081           0.000           0.000          51.512          54.736

  10000.000         48.936          44.132          -0.755           0.000           0.000          49.955          53.078
  12500.000         47.311          41.665         -20.241           0.000           0.000          47.826          51.110
  16000.000         45.415          38.655         -46.603           0.000           0.000          44.802          48.594
  20000.000         43.583          35.650         -75.275           0.000           0.000          41.466          46.075
  25000.000         41.611          32.347         -90.000           0.000           0.000          37.557          43.405

  31500.000         39.390          28.582         -90.000           0.000           0.000          32.904          40.555
  40000.000         36.873          24.291         -90.000           0.000           0.000          27.449          37.552
```

```
      PROGRAM PREDICT


C                    --------------------------------
C                    ***** VARIABLE DEFINITIONS *****
C                    --------------------------------

C       VARIABLE NAME           DEFINITION                        UNITS
C       -------------           ----------                        -----

C       ALPHTIP            TIP ANGLE OF ATTACK                    DEGREES
C       ALPSTAR            SEGMENT ANGLE OF ATTACK                DEGREES
C       ALPRAT             TIP LIFT CURVE SLOPE                   ---
C       C                  SEGMENT CHORDLENGTH                    METERS
C       C0                 SPEED OF SOUND                         METERS/SEC
C       FRCEN              1/3 OCTAVE CENTERED FREQUENCIES        HERTZ
C       H                  SEGMENT TRAILING EDGE THICKNESS        METERS
C       IBLUNT             FLAG TO COMPUTE BLUNTNESS NOISE        ---
C       ILAM               FLAG TO COMPUTE LBL NOISE              ---
C       ITIP               FLAG TO COMPUTE TIP NOISE              ---
C       ITRIP              FLAG TO TRIP BOUNDARY LAYER            ---
C       ITURB              FLAG TO COMPUTE TBLTE NOISE            ---
C       L                  SEGMENT SPAN LENGTH                    METERS
C       MAXFREQ            MAXIMUM NUMBER OF FREQUENCIES          ---
C       MAXSEG             MAXIMUM NUMBER OF SEGMENTS             ---
C       NFREQ              NUMBER OF 1/3 OCTAVE FREQUENCIES       ---
C       NSEG               NUMBER OF SEGMENTS                     ---
C       P1                 PRESSURE ASSOCIATED WITH
C                            TBLTE PREDICTION                     NT/M2
C       P2                 PRESSURE ASSOCIATED WITH
C                            TBLTE PREDICTION                     NT/M2
C       P3                 PRESSURE ASSOCIATED WITH
C                            TBLTE PREDICTION                     NT/M2
C       P4                 PRESSURE ASSOCIATED WITH
C                            TOTAL PREDICTION                     NT/M2
C       P5                 PRESSURE ASSOCIATED WITH
C                            LBLVS PREDICTION                     NT/M2
C       P6                 PRESSURE ASSOCIATED WITH
C                            BLUNTNESS PREDICTION                 NT/M2
C       P7                 PRESSURE ASSOCIATED WITH
C                            TIP NOISE PREDICTION                 NT/M2
C       PHI                DIRECTIVITY ANGLE                      DEGREES
C       PSI                BLUNTNESS ANGLE                        DEGREES
C       R                  SEGMENT TO OBSERVER DISTANCE           METERS
C       ROUND              LOGICAL INDICATING ROUNDED TIP         ---
C       SPL                TOTAL SOUND PRESSURE LEVEL             DB
C       SPLALPH            SOUND PRESSURE LEVEL ASSOCIATED
C                            WITH TBLTE PREDICTION                DB
C       SPLBLNT            SOUND PRESSURE LEVEL ASSOCIATED
C                            WITH BLUNTNESS PREDICTION            DB
C       SPLLBL             SOUND PRESSURE LEVEL ASSOCIATED
C                            WITH LBL PREDICTION                  DB
C       SPLP               SOUND PRESSURE LEVEL ASSOCIATED
C                            WITH TBLTE PREDICTION                DB
C       SPLS               SOUND PRESSURE LEVEL ASSOCIATED
C                            WITH TBLTE PREDICTION                DB
C       SPLTBL             TOTAL PRESSURE LEVEL ASSOCIATED
C                            WITH TBLTE PREDICTION                DB
C       SPLTIP             SOUND PRESSURE LEVEL ASSOCIATED
C                            WITH TIP NOISE PREDICTION            DB
C       ST                 STROUHAL NUMBER                        --
C       THETA              DIRECTIVITY ANGLE                      DEGREES
C       U                  SEGMENT FREESTREAM VELOCITY            METERS/SEC
C       VISC               KINEMATIC VISCOSITY                    M2/SEC


      PARAMETER (MAXSEG = 20, MAXFREQ = 27)


      DIMENSION    FRCEN(MAXFREQ)    ,C(MAXSEG)        ,L(MAXSEG)         ,
     1             ST(MAXFREQ)       ,SPLLBL(MAXFREQ)  ,SPLTBL(MAXFREQ)   ,
     2             U(MAXSEG)         ,SPLP(MAXFREQ)    ,SPLS(MAXFREQ)     ,
     3             SPLALPH(MAXFREQ)  ,SPL(7,MAXFREQ)   ,R(MAXSEG)         ,
     5             SPLBLNT(MAXFREQ)  ,PHI(MAXSEG)      ,SPLTIP(MAXFREQ)   ,
     7             THETA(MAXSEG)     ,ALPSTAR(MAXSEG)  ,PSI(MAXSEG)       ,
     8              H(MAXSEG)       ,P1(MAXFREQ)      ,P2(MAXFREQ)     ,
     9              P3(MAXFREQ)     ,P4(MAXFREQ)      ,P5(MAXFREQ)     ,
     1              P6(MAXFREQ)     ,P7(MAXFREQ)


      REAL          L
      LOGICAL       ROUND

C     DEFINE DEFAULT VALUES FOR NAMELIST DATA
C     ---------------------------------------


      DATA C       /  MAXSEG*1.0    /
      DATA L       /  MAXSEG*.10    /
      DATA R       /  MAXSEG * 1.   /
      DATA THETA   /  MAXSEG * 90.  /
      DATA PHI     /  MAXSEG * 90.  /
      DATA ALPSTAR /  MAXSEG * 0.0  /
      DATA H       /  MAXSEG * .0005/
      DATA PSI     /  MAXSEG * 14.0 /
      DATA U       /  MAXSEG * 100. /
      DATA ITRIP   /    0       /
      DATA ILAM    /    0       /
      DATA ITURB   /    0       /
      DATA IBLUNT  /    0       /
      DATA ITIP    /    0       /
      DATA ALPHTIP /    0.0     /
      DATA NSEG    /   10       /
      DATA VISC    / 1.4529E-5  /
      DATA C0      /  340.46    /
      DATA ALPRAT  /    1.0     /
      DATA ROUND   /  .FALSE.   /

      DATA NFREQ   /    27      /

C     SET UP VALUES OF 1/3 OCTAVE CENTERED FREQUENCIES
C     ------------------------------------------------

      DATA FRCEN / 100.    ,  125.    ,  160.    ,  200.    ,  250.    ,
     1             315.    ,  400.    ,  500.    ,  630.    ,  800.    ,
     1            1000.    , 1250.    , 1600.    , 2000.    , 2500.    ,
     3            3150.    , 4000.    , 5000.    , 6300.    , 8000.    ,
     2           10000.    ,12500.    ,16000.    ,20000.    ,25000.    ,
     3           31500.    ,40000.    /


      NAMELIST /INDATA / C         ,L         ,R         ,
     1                   THETA     ,PHI       ,ALPSTAR   ,
     2                   H         ,PSI       ,U         ,
     1                   ITRIP     ,ILAM      ,ITURB     ,
     2                   IBLUNT    ,ITIP      ,ROUND     ,
     3                   ALPHTIP   ,NSEG      ,C0        ,
     4                   VISC



C      READ IN NAMELIST DATA AND ECHO INPUT TO OUTPUT FILE
C      ---------------------------------------------------

      OPEN(UNIT=4, STATUS = 'OLD')
      READ(4,INDATA)

      OPEN(UNIT=5, STATUS = 'NEW')
      WRITE(5,INDATA)


C      INITIALIZE ALL PREDICTED PRESSURES AND SOUND
C      PRESSURE LEVELS TO ZERO
C      ----------------------------------------

      DO 6001 I=1,NFREQ
        P1(I) = 0.0
        P2(I) = 0.0
        P3(I) = 0.0
        P4(I) = 0.0
```

```
       P5(I) = 0.0
       P6(I) = 0.0
       P7(I) = 0.0

       DO 6002 J=1,7
         SPL(J,I) = 0.0
6002   CONTINUE
6001 CONTINUE


C    FOR EACH BLADE SEGMENT, MAKE A NOISE PREDICTION ACCORDING
C    TO THE MECHANISMS SELECTED. TIP NOISE IS PREDICTED FOR
C    THE LAST SEGMENT ONLY.
C    -------------------------------------------------------

      DO 6000 III=1,NSEG

       IF (ILAM .EQ. 1)
     1   CALL LBLVS(ALPSTAR(III),C(III),U(III),FRCEN,SPLLBL,
     2           THETA(III),PHI(III),L(III),R(III),NFREQ,
     3           VISC,C0)

       IF (ITURB .EQ. 1)
     1  CALL TBLTE(ALPSTAR(III),C(III),U(III),FRCEN,ITRIP,SPLP,
     1          SPLS,SPLALPH,SPLTBL,THETA(III),PHI(III),L(III),R(III),
     2          NFREQ,VISC,C0)

       IF (IBLUNT .EQ. 1)
     1   CALL BLUNT(ALPSTAR(III),C(III),U(III),FRCEN,ITRIP,SPLBLNT,
     1            THETA(III),PHI(III),L(III),R(III),H(III),PSI(III),
     2            NFREQ,VISC,C0)

       IF ((ITIP .EQ. 1) .AND. (III .EQ. NSEG))
     1   CALL TIPNOIS(ALPHTIP,ALPRAT,C(III),U(III),FRCEN,SPLTIP,
     2                THETA,PHI,R(III),NFREQ,VISC,C0,ROUND)


C     ADD IN THIS SEGMENT'S CONTRIBUTION ON A MEAN-SQUARE
C     PRESSURE BASIS
C     ----------------------------------------------

       DO 989 I=1,NFREQ

         IF (ILAM .EQ. 1) THEN
           P5(I) = P5(I) + 10.**(SPLLBL(I)/10.)
         ENDIF

         IF (ITURB .EQ. 1) THEN
           P1(I) = P1(I) + 10.**(SPLP(I)/10.)
           P2(I) = P2(I) + 10.**(SPLS(I)/10.)
           P3(I) = P3(I) + 10.**(SPLALPH(I)/10.)
         ENDIF

         IF (IBLUNT .EQ. 1) THEN
           P6(I) = P6(I) + 10.**(SPLBLNT(I)/10.)
         ENDIF

         IF ((ITIP .EQ. 1) .AND. (III .EQ. NSEG)) THEN
           P7(I) = P7(I) + 10.**(SPLTIP(I)/10.)
         ENDIF


C     COMPUTE TOTAL PRESSURE FOR THE SEGMENT FOR ALL MECHANISMS
C     -----------------------------------------------------

         P4(I) = P1(I) + P2(I) + P3(I) + P5(I) + P6(I) + P7(I)

 989   CONTINUE
6000 CONTINUE

C     CONTRIBUTIONS FROM ALL SEGMENTS ARE NOW ACCOUNTED FOR.
C     COMPUTE SOUND PRESSURE LEVELS FOR EACH MECHANISM AND
C     FOR THE TOTAL
C     -----------------------------------------------

```

```
      DO 6003 I=1,NFREQ
        IF (P1(I) .NE. 0.) SPL(1,I) = 10.*ALOG10(P1(I))
        IF (P2(I) .NE. 0.) SPL(2,I) = 10.*ALOG10(P2(I))
        IF (P3(I) .NE. 0.) SPL(3,I) = 10.*ALOG10(P3(I))
        IF (P4(I) .NE. 0.) SPL(4,I) = 10.*ALOG10(P4(I))
        IF (P5(I) .NE. 0.) SPL(5,I) = 10.*ALOG10(P5(I))
        IF (P6(I) .NE. 0.) SPL(6,I) = 10.*ALOG10(P6(I))
        IF (P7(I) .NE. 0.) SPL(7,I) = 10.*ALOG10(P7(I))
 6003 CONTINUE


C      WRITE OUTPUT FILE
C      -----------------

      WRITE(5,7000)

      DO 6005 I=1,NFREQ

        WRITE(5,7100) FRCEN(I),(SPL(J,I),J=1,3),(SPL(J,I),J=5,7),
     1                           SPL(4,I)
        IF (MOD(I,5) .EQ. 0) WRITE(5,7200)
 6005 CONTINUE

 7000 FORMAT(1H1,52X,'ONE-THIRD OCTAVE',/,50X,'SOUND PRESSURE LEVELS'
     1       ////,5X,'               ','    PRESSURE     ',
     2                 '     SUCTION    ','   SEPARATION    '/,
     3              5X,' FREQUENCY(HZ) ','     SIDE TBL     ',
     4                 '    SIDE TBL    ','     SIDE TBL     ',
     5                 '     LAMINAR    ','   BLUNTNESS     ',
     6                 '       TIP      ','      TOTAL      ',
     7                 /,5X,8('--------------- '),/)

 7100 FORMAT(8F15.3)
 7200 FORMAT(' ')
 8000 FORMAT(I3)
 8002 FORMAT(4I10)


      STOP
      END
      SUBROUTINE LBLVS(ALPSTAR,C,U ,FRCEN,SPLLAM,THETA,PHI,L,R,
     1                 NFREQ,VISC,C0)

      PARAMETER (MAXFREQ = 27)



C                  --------------------------------
C                  ***** VARIABLE DEFINITIONS *****
C                  --------------------------------

C       VARIABLE NAME               DEFINITION                 UNITS
C       -------------               ----------                 -----


C       ALPSTAR                     ANGLE OF ATTACK           DEGREES
C       C                          CHORD LENGTH               METERS
C       C0                         SPEED OF SOUND             METERS/SEC
C       D                          REYNOLDS NUMBER RATIO      ---
C       DBARH                      HIGH FREQUENCY DIRECTIVITY ---
C       DELTAP                     PRESSURE SIDE BOUNDARY LAYER
C                                    THICKNESS                METERS
C       DSTRP                      PRESSURE SIDE BOUNDARY LAYER
C                                    DISPLACEMENT THICKNESS   METERS
C       DSTRS                      SUCTION SIDE BOUNDARY LAYER
C                                    DISPLACEMENT THICKNESS   METERS
C       E                          STROUHAL NUMBER RATIO      ---
C       FRCEN                      1/3 OCTAVE FREQUENCIES     HERTZ
C       G1                         SOUND PRESSURE LEVEL FUNCTION DB
C       G2                         OVERALL SOUND PRESSURE LEVEL
C                                    FUNCTION                 DB
C       G3                         OVERALL SOUND PRESSURE LEVEL
C                                    FUNCTION                 DB
C       ITRIP                      FLAG TO TRIP BOUNDARY LAYER ---
C       L                          SPAN                       METERS
C       M                          MACH NUMBER                ---
C       NFREQ                      NUMBER OF FREQUENCIES      ---
C       OASPL                      OVERALL SOUND PRESSURE LEVEL DB
C       PHI                        DIRECTIVITY ANGLE          DEGREES
C       R                          OBSERVER DISTANCE FROM SEGMENT METERS
C       RC                         REYNOLDS NUMBER BASED ON CHORD ---
C       RC0                        REFERENCE REYNOLDS NUMBER  ---
C       SCALE                      GEOMETRIC SCALING TERM
C       SPLLAM                     SOUND PRESSURE LEVEL DUE TO
C                                    LAMINAR MECHANISM        DB
C       STPRIM                     STROUHAL NUMBER BASED ON PRESSURE
C                                    SIDE BOUNDARY LAYER THICKNESS ---
C       ST1PRIM                    REFERENCE STROUHAL NUMBER  ---
C       STPKPRM                    PEAK STROUHAL NUMBER       ---
C       THETA                      DIRECTIVITY ANGLE          DEGREES
C       U                          FREESTREAM VELOCITY        METERS/SEC
C       VISC                       KINEMATIC VISCOSITY        M2/SEC



      DIMENSION STPRIM(MAXFREQ)  ,SPLLAM(MAXFREQ)   ,FRCEN(MAXFREQ)

      REAL      L                  ,M


C      COMPUTE REYNOLDS NUMBER AND MACH NUMBER
C      ---------------------------------------

      M        = U  / C0
      RC       = U  * C/VISC


C      COMPUTE BOUNDARY LAYER THICKNESSES
C      ----------------------------------

      CALL THICK(C,U ,ALPSTAR,ITRIP,DELTAP,DSTRS,DSTRP,C0,VISC)



C      COMPUTE DIRECTIVITY FUNCTION
```

```
C      ----------------------------

      CALL DIRECTH(M,THETA,PHI,DBARM)



C      COMPUTE REFERENCE STROUHAL NUMBER
C      ---------------------------------

      IF (RC .LE. 1.3E+05) ST1PRIM = .18
      IF((RC .GT. 1.3E+05).AND.(RC.LE.4.0E+05))ST1PRIM=.001756*RC**.3931
      IF (RC .GT. 4.0E+05) ST1PRIM = .28

      STPKPRM  = 10.**(-.04*ALPSTAR) * ST1PRIM



C      COMPUTE REFERENCE REYNOLDS NUMBER
C      ---------------------------------

      IF (ALPSTAR .LE. 3.0) RC0=10.**(.215*ALPSTAR+4.978)
      IF (ALPSTAR .GT. 3.0) RC0=10.**(.120*ALPSTAR+5.263)




C      COMPUTE PEAK SCALED SPECTRUM LEVEL
C      ----------------------------------

      D   = RC / RC0

      IF (D .LE. .3237) G2=77.852*ALOG10(D)+15.328
      IF ((D .GT. .3237).AND.(D .LE. .5689))
     1  G2 = 65.188*ALOG10(D) + 9.125
      IF ((D .GT. .5689).AND.(D .LE. 1.7579))
     1  G2 = -114.052 * ALOG10(D)**2.
      IF ((D .GT. 1.7579).AND.(D .LE. 3.0889))
     1  G2 = -65.188*ALOG10(D)+9.125
      IF (D .GT. 3.0889) G2 =-77.852*ALOG10(D)+15.328


      G3      = 171.04 - 3.03 * ALPSTAR

      SCALE   = 10. * ALOG10(DELTAP*M**5*DBARH*L/R**2)



C      COMPUTE SCALED SOUND PRESSURE LEVELS FOR EACH STROUHAL NUMBER
C      -------------------------------------------------------------

      DO 100 I=1,NFREQ

         STPRIM(I)  = FRCEN(I) * DELTAP / U

         E          = STPRIM(I) / STPKPRM

         IF (E .LT. .5974) G1=39.8*ALOG10(E)-11.12
         IF ((E .GE. .5974).AND.(E .LE. .8545))
     1     G1 = 98.409 * ALOG10(E) + 2.0
         IF ((E .GE. .8545).AND.(E .LT. 1.17))
     1     G1 = -5.076+SQRT(2.484-506.25*(ALOG10(E))**2.)
         IF ((E .GE. 1.17).AND.(E .LT. 1.674))
     1     G1 = -98.409 * ALOG10(E) + 2.0
         IF (E .GE. 1.674) G1=-39.80*ALOG10(E)-11.12

         SPLLAM(I) = G1 + G2 + G3 + SCALE

  100 CONTINUE

      RETURN
      END
      SUBROUTINE TBLTE(ALPSTAR,C,U ,FRCEN,ITRIP,SPLP,SPLS,
     1              SPLALPH,SPLTBL,THETA,PHI,L,R,NFREQ,VISC,C0)



C                  ---------------------------------
C                  ***** VARIABLE DEFINITIONS *****
C                  ---------------------------------



C       VARIABLE NAME                DEFINITION                    UNITS
C       -------------                ----------                  -----

C       A                   STROUHAL NUMBER RATIO                   ---
C       A0                  FUNCTION USED IN 'A' CALCULATION        ---
C       A02                 FUNCTION USED IN 'A' CALCULATION        ---
C       AA                  'A' SPECTRUM SHAPE EVALUATED AT
C                              STROUHAL NUMBER RATIO                 DB
C       ALPSTAR             ANGLE OF ATTACK                       DEGREES
C       AMAXA               MAXIMUM 'A' CURVE EVALUATED AT
C                             STROUHAL NUMBER RATIO                  DB
C       AMAXA0              MAXIMUM 'A' CURVE EVALUATED AT A0        DB
C       AMAXA02             MAXIMUM 'A' CURVE EVALUATED AT A02       DB
C       AMAXB               MAXIMUM 'A' CURVE EVALUATED AT B         DB
C       AMINA               MINIMUM 'A' CURVE EVALUATED AT
C                             STROUHAL NUMBER RATIO                  DB
C       AMINA0              MINIMUM 'A' CURVE EVALUATED AT A0        DB
C       AMINA02             MINIMUM 'A' CURVE EVALUATED AT A02       DB
C       AMINB               MINIMUM 'A' CURVE EVALUATED AT B         DB
C       ARA0                INTERPOLATION FACTOR                    ---
C       ARA02               INTERPOLATION FACTOR                    ---
C       B                   STROUHAL NUMBER RATIO                   ---
C       B0                  FUNCTION USED IN 'B' CALCULATION        ---
C       BB                  'B' SPECTRUM SHAPE EVALUATED AT
C                             STROUHAL NUMBER RATIO                  DB
C       BETA                USED IN 'B' COMPUTATION                 ---
C       BETA0               USED IN 'B' COMPUTATION                 ---
C       BMAXB               MAXIMUM 'B' EVALUATED AT B               DB
C       BMAXB0              MAXIMUM 'B' EVALUATED AT B0              DB
C       BMINB               MINIMUM 'B' EVALUATED AT B               DB
C       BMINB0              MINIMUM 'B' EVALUATED AT B0              DB
C       BRB0                INTERPOLATION FACTOR                     DB
C       C                   CHORD LENGTH                            METERS
C       C0                  SPEED OF SOUND                       METERS/SEC
C       DBARH               HIGH FREQUENCY DIRECTIVITY              ---
C       DBARL               LOW FREQUENCY DIRECTIVITY               ---
C       DELK1               CORRECTION TO AMPLITUDE FUNCTION         DB
C       DELTAP              PRESSURE SIDE BOUNDARY LAYER THICKNESS METERS
C       DSTRP               PRESSURE SIDE DISPLACEMENT THICKNESS    METERS
C       DSTRS               SUCTION SIDE DISPLACEMENT THICKNESS     METERS
C       FRCEN               ARRAY OF CENTERED FREQUENCIES           HERTZ
C       GAMMA               USED IN 'B' COMPUTATION                 ---
C       GAMMA0              USED IN 'B' COMPUTATION                 ---
C       ITRIP               TRIGGER TO TRIP BOUNDARY LAYER          ---
C       K1                  AMPLITUDE FUNCTION                       DB
C       K2                  AMPLITUDE FUNCTION                       DB
C       L                   SPAN                                    METERS
C       M                   MACH NUMBER                             ---
C       NFREQ               NUMBER OF CENTERED FREQUENCIES          ---
C       PHI                 DIRECTIVITY ANGLE                     DEGREES
C       P1                  PRESSURE SIDE PRESSURE                 NT/M2
C       P2                  SUCTION SIDE PRESSURE                  NT/M2
C       P4                  PRESSURE FROM ANGLE OF ATTACK
C                             CONTRIBUTION                         NT/M2
C       R                   SOURCE TO OBSERVER DISTANCE             METERS
C       RC                  REYNOLDS NUMBER BASED ON  CHORD         ---
C       RDSTRP              REYNOLDS NUMBER BASED ON PRESSURE
C                             SIDE DISPLACEMENT THICKNESS           ---
C       RDSTRS              REYNOLDS NUMBER BASED ON SUCTION
C                             SIDE DISPLACEMENT THICKNESS           ---
C       SPLALPH             SOUND PRESSURE LEVEL DUE TO ANGLE OF
C                             ATTACK CONTRIBUTION                    DB
C       SPLP                SOUND PRESSURE LEVEL DUE TO PRESSURE
C                             SIDE OF AIRFOIL                        DB
```

```
C       SPLS                SOUND PRESSURE LEVEL DUE TO SUCTION
C                             SIDE OF AIRFOIL                      DB
C       SPLTBL              TOTAL SOUND PRESSURE LEVEL DUE TO
C                             TBLTE MECHANISM                      DB
C       STP                 PRESSURE SIDE STROUHAL NUMBER          ---
C       STS                 SUCTION SIDE STROUHAL NUMBER           ---
C       ST1                 PEAK STROUHAL NUMBER                   ---
C       ST1PRIM             PEAK STROUHAL NUMBER                   ---
C       ST2                 PEAK STROUHAL NUMBER                   ---
C       STPEAK              PEAK STROUHAL NUMBER                   ---
C       SWITCH              LOGICAL FOR COMPUTATION OF ANGLE
C                             OF ATTACK CONTRIBUTION               ---
C       THETA               DIRECTIVITY ANGLE                    DEGREES
C       U                   VELOCITY                           METERS/SEC
C       VISC                KINEMATIC VISCOSITY                 M2/SEC
C       XCHECK              USED TO CHECK FOR ANGLE OF ATTACK
C                             CONTRIBUTION                         ---
C

      PARAMETER (MAXFREQ = 27)


      DIMENSION SPLTBL(MAXFREQ)   ,SPLP(MAXFREQ)     ,SPLS(MAXFREQ)   ,
     1          SPLALPH(MAXFREQ)  ,STP(MAXFREQ)      ,
     1          STS(MAXFREQ)      ,PRCEN(MAXFREQ)

      LOGICAL SWITCH
      REAL    L,M,K1,K2

      RC        = U  * C / VISC
      M         = U  / C0


C      COMPUTE BOUNDARY LAYER THICKNESSES
C      ----------------------------------

      CALL THICK(C,U ,ALPSTAR,ITRIP,DELTAP,DSTRS,DSTRP,C0,VISC)

C     COMPUTE DIRECTIVITY FUNCTION
C     ----------------------------

      CALL DIRECTL(M,THETA,PHI,DBARL)
      CALL DIRECTH(M,THETA,PHI,DBARH)


C     CALCULATE THE REYNOLDS NUMBERS BASED ON PRESSURE AND
C     SUCTION DISPLACEMENT THICKNESS
C     --------------------------------------------------

      RDSTRS = DSTRS * U  / VISC
      RDSTRP = DSTRP * U  / VISC

C      DETERMINE PEAK STROUHAL NUMBERS TO BE USED FOR
C      'A' AND 'B' CURVE CALCULATIONS
C      ---------------------------------------------

      ST1    = .02 * M ** (-.6)

      IF (ALPSTAR .LE. 1.333) ST2 = ST1
      IF ((ALPSTAR .GT. 1.333).AND.(ALPSTAR .LE. 12.5))
     1   ST2 = ST1*10.**(.0054*(ALPSTAR-1.333)**2.)
      IF (ALPSTAR .GT. 12.5) ST2 = 4.72 * ST1


      ST1PRIM = (ST1+ST2)/2.


      CALL A0COMP(RC,A0)
      CALL A0COMP(3.*RC,A02)

C      EVALUATE MINIMUM AND MAXIMUM 'A' CURVES AT A0
C      ---------------------------------------------

      CALL AMIN(A0,AMINA0)
      CALL AMAX(A0,AMAXA0)
      CALL AMIN(A02,AMINA02)
      CALL AMAX(A02,AMAXA02)

C      COMPUTE 'A' MAX/MIN RATIO
C      -------------------------

      ARA0  = (20. + AMINA0) / (AMINA0 - AMAXA0)
      ARA02 = (20. + AMINA02)/ (AMINA02- AMAXA02)

C      COMPUTE B0 TO BE USED IN 'B' CURVE CALCULATIONS
C      -----------------------------------------------

      IF (RC .LT. 9.52E+04) B0 = .30
      IF ((RC .GE. 9.52E+04).AND.(RC .LT. 8.57E+05))
     1    B0 = (-4.48E-13)*(RC-8.57E+05)**2. + .56
      IF (RC .GE. 8.57E+05) B0 = .56

C      EVALUATE MINIMUM AND MAXIMUM 'B' CURVES AT B0
C      ---------------------------------------------

      CALL BMIN(B0,BMINB0)
      CALL BMAX(B0,BMAXB0)

C      COMPUTE 'B' MAX/MIN RATIO
C      -------------------------

      BRB0  = (20. + BMINB0) / (BMINB0 - BMAXB0)

C      FOR EACH CENTER FREQUENCY, COMPUTE AN
C      'A' PREDICTION FOR THE PRESSURE SIDE
C      ------------------------------------

      STPEAK = ST1

      DO 100 I=1,NFREQ
        STP(I) = FRCEN(I) * DSTRP / U
        A      = ALOG10( STP(I) / STPEAK )
        CALL AMIN(A,AMINA)
        CALL AMAX(A,AMAXA)
        AA     = AMINA + ARA0 * (AMAXA - AMINA)

        IF (RC .LT. 2.47E+05) K1 = -4.31 * ALOG10(RC) + 156.3
        IF((RC .GE. 2.47E+05).AND.(RC .LT. 8.0E+05))
     1    K1 = -9.0 * ALOG10(RC) + 181.6
        IF (RC .GT. 8.0E+05) K1 = 128.5

        IF (RDSTRP .LE. 5000.) DELK1 = -ALPSTAR*(5.29-1.43*
     1    ALOG10(RDSTRP))
        IF (RDSTRP .GT. 5000.) DELK1 = 0.0

        SPLP(I)=AA+K1-3.+10.*ALOG10(DSTRP*M**5.*DBARH*L/R**2.)+DELK1




      GAMMA   = 27.094 * M +  3.31
      BETA    = 72.650 * M + 10.74
      GAMMA0  = 23.430 * M +  4.651
      BETA0   =-34.190 * M - 13.820

      IF (ALPSTAR .LE. (GAMMA0-GAMMA)) K2 = -1000.0
      IF ((ALPSTAR.GT.(GAMMA0-GAMMA)).AND.(ALPSTAR.LE.(GAMMA0+GAMMA)))
     1 K2=SQRT(BETA**2.-(BETA/GAMMA)**2.*(ALPSTAR-GAMMA0)**2.)+BETA0
      IF (ALPSTAR .GT. (GAMMA0+GAMMA)) K2 = -12.0

      K2 = K2 + K1



      STS(I) = FRCEN(I) * DSTRS / U

C      CHECK FOR 'A' COMPUTATION FOR SUCTION SIDE
C      ------------------------------------------

```

```
      XCHECK = GAMMA0
      SWITCH = .FALSE.
      IF ((ALPSTAR .GE. XCHECK).OR.(ALPSTAR .GT. 12.5))SWITCH=.TRUE.
      IF (.NOT. SWITCH) THEN
        A      = ALOG10( STS(I) / ST1PRIM )
        CALL AMIN(A,AMINA)
        CALL AMAX(A,AMAXA)
        AA = AMINA + ARA0 * (AMAXA - AMINA)

        SPLS(I) = AA+K1-3.+10.*ALOG10(DSTRS*M**5.*DBARH*
     1            L/R**2.)

C      'B' CURVE COMPUTATION
C       --------------------

        B = ABS(ALOG10(STS(I) / ST2))
        CALL BMIN(B,BMINB)
        CALL BMAX(B,BMAXB)
        BB = BMINB + BRB0 * (BMAXB-BMINB)
        SPLALPH(I)=BB+K2+10.*ALOG10(DSTRS*M**5.*DBARH*L/R**2.)

      ELSE

C       THE 'A' COMPUTATION IS DROPPED IF 'SWITCH' IS TRUE
C       --------------------------------------------------


        SPLS(I) = 0.0 + 10.*ALOG10(DSTRS*M**5.*DBARL*
     1              L/R**2.)
        SPLP(I) = 0.0 + 10.*ALOG10(DSTRS*M**5.*DBARL*
     1              L/R**2.)
        B = ABS(ALOG10(STS(I) / ST2))
        CALL AMIN(B,AMINB)
        CALL AMAX(B,AMAXB)
        BB = AMINB + ARA02 * (AMAXB-AMINB)
        SPLALPH(I)=BB+K2+10.*ALOG10(DSTRS*M**5.*DBARL*
     1           L/R**2.)
      ENDIF


C      SUM ALL CONTRIBUTIONS FROM 'A' AND 'B' ON BOTH
C      PRESSURE AND SUCTION SIDE ON A MEAN-SQUARE PRESSURE
C      BASIS
C      ---------------------------------------------------

      IF (SPLP(I)    .LT. -100.) SPLP(I)    = -100.
      IF (SPLS(I)    .LT. -100.) SPLS(I)    = -100.
      IF (SPLALPH(I) .LT. -100.) SPLALPH(I) = -100.

      P1  = 10.**(SPLP(I) / 10.)
      P2  = 10.**(SPLS(I) / 10.)
      P4  = 10.**(SPLALPH(I) / 10.)

      SPLTBL(I) = 10. * ALOG10(P1 + P2 + P4)

  100 CONTINUE

      RETURN
      END
      SUBROUTINE AMIN(A,AMINA)

C     THIS SUBROUTINE DEFINES THE CURVE FIT CORRESPONDING
C     TO THE A-CURVE FOR THE MINIMUM ALLOWED REYNOLDS NUMBER.
C

      X1 = ABS(A)

      IF (X1 .LE. .204) AMINA=SQRT(67.552-886.788*X1**2.)-8.219
      IF((X1 .GT. .204).AND.(X1 .LE. .244))AMINA=-32.665*X1+3.981
      IF (X1 .GT. .244)AMINA=-142.795*X1**3.+103.656*X1**2.-57.757*X1+6.006

      RETURN
      END
```

```
      SUBROUTINE AMAX(A,AMAXA)

C     THIS SUBROUTINE DEFINES THE CURVE FIT CORRESPONDING
C     TO THE A-CURVE FOR THE MAXIMUM ALLOWED REYNOLDS NUMBER.

      X1 = ABS(A)

      IF (X1 .LE. .13)AMAXA=SQRT(67.552-886.788*X1**2.)-8.219
      IF((X1 .GT. .13).AND.(X1 .LE. .321))AMAXA=-15.901*X1+1.098
      IF (X1 .GT. .321)AMAXA=-4.669*X1**3.+3.491*X1**2.-16.699*X1+1.149

      RETURN
      END
```

```
      SUBROUTINE BMIN(B,BMINB)

C     THIS SUBROUTINE DEFINES THE CURVE FIT CORRESPONDING
C     TO THE B-CURVE FOR THE MINIMUM ALLOWED REYNOLDS NUMBER.

      X1 = ABS(B)

      IF (X1 .LE. .13)BMINB=SQRT(16.888-886.788*X1**2.)-4.109
      IF((X1 .GT. .13).AND.(X1 .LE. .145))BMINB=-83.607*X1+8.138
      IF (X1.GT..145)BMINB=-817.81*X1**3.+355.21*X1**2.-135.024*X1+10.619

      RETURN
      END
```

```
      SUBROUTINE BMAX(B,BMAXB)

C     THIS SUBROUTINE DEFINES THE CURVE FIT CORRESPONDING
C     TO THE B-CURVE FOR THE MAXIMUM ALLOWED REYNOLDS NUMBER.

      X1 = ABS(B)

      IF (X1 .LE. .1) BMAXB=SQRT(16.888-886.788*X1**2.)-4.109
      IF((X1 .GT. .1).AND.(X1 .LE. .187))BMAXB=-31.313*X1+1.854
      IF (X1.GT..187)BMAXB=-80.541*X1**3.+44.174*X1**2.-39.381*X1+2.344

      RETURN
      END
      SUBROUTINE A0COMP(RC,A0)

C     THIS SUBROUTINE DETERMINES WHERE THE A-CURVE
C     TAKES ON A VALUE OF -20 dB.

      IF (RC .LT. 9.52E+04) A0 = .57
      IF ((RC .GE. 9.52E+04).AND.(RC .LT. 8.57E+05))
     1   A0 = (-9.57E-13)*(RC-8.57E+05)**2. + 1.13
      IF (RC .GE. 8.57E+05) A0 = 1.13
      RETURN
      END
```

```
      SUBROUTINE DIRECTH(M,THETA,PHI,DBAR)

C     THIS SUBROUTINE COMPUTES THE HIGH FREQUENCY
C     DIRECTIVITY FUNCTION FOR THE INPUT OBSERVER LOCATION

      REAL M,MC

      DEGRAD  = .017453

      MC     = .8 * M
      THETAR = THETA * DEGRAD
      PHIR   = PHI * DEGRAD

      DBAR=2.*SIN(THETAR/2.)**2.*SIN(PHIR)**2./((1.+M*COS(THETAR))*
     1      (1.+(M-MC)*COS(THETAR))**2.)
      RETURN
      END
```

```
      SUBROUTINE DIRECTL(M,THETA,PHI,DBAR)

C     THIS SUBROUTINE COMPUTES THE LOW FREQUENCY
C     DIRECTIVITY FUNCTION FOR THE INPUT OBSERVER LOCATION

      REAL M,MC

      DEGRAD  = .017453

      MC     = .8 * M
      THETAR = THETA * DEGRAD
      PHIR   = PHI * DEGRAD

      DBAR = (SIN(THETAR)*SIN(PHIR))**2/(1.+M*COS(THETAR))**4

      RETURN
      END
      SUBROUTINE BLUNT(ALPSTAR,C,U ,FRCEN,ITRIP,SPLBLNT,THETA,PHI,
     1                 L,R,H,PSI,NFREQ,VISC,C0)


C                    -------------------------------
C                    ***** VARIABLE DEFINITIONS *****
C                    -------------------------------

C       VARIABLE NAME                 DEFINITION                  UNITS
C       -------------                 ----------                  -----

C       ALPSTAR            ANGLE OF ATTACK                       DEGREES
C       ATERM              USED TO COMPUTE PEAK STROUHAL NO.       ---
C       C                  CHORD LENGTH                          METERS
C       C0                 SPEED OF SOUND                        METERS/SEC
C       DBARH              HIGH FREQUENCY DIRECTIVITY              ---
C       DELTAP             PRESSURE SIDE BOUNDARY LAYER
C                            THICKNESS                           METERS
C       DSTARH             AVERAGE DISPLACEMENT THICKNESS
C                            OVER TRAILING EDGE BLUNTNESS          ---
C       DSTRAVG            AVERAGE DISPLACEMENT THICKNESS        METERS
C       DSTRP              PRESSURE SIDE DISPLACEMENT THICKNESS  METERS
C       DSTRS              SUCTION SIDE DISPLACEMENT THICKNESS   METERS
C       ETA                RATIO OF STROUHAL NUMBERS               ---
C       FRCEN              ARRAY OF 1/3 OCTAVE CENTERED FREQ.    HERTZ
C       F4TEMP             G5 EVALUATED AT MINIMUM HDSTARP         DB
C       G4                 SCALED SPECTRUM LEVEL                   DB
C       G5                 SPECTRUM SHAPE FUNCTION                 DB
C       G50                G5 EVALUATED AT PSI=0.0                 DB
C       G514               G5 EVALUATED AT PSI=14.0                DB
C       H                  TRAILING EDGE BLUNTNESS               METERS
C       HDSTAR             BLUNTNESS OVER AVERAGE DISPLACEMENT
C                            THICKNESS                             ---
C       HDSTARL            MINIMUM ALLOWED VALUE OF HDSTAR         ---
C       HDSTARP            MODIFIED VALUE OF HDSTAR                ---
C       ITRIP              TRIGGER FOR BOUNDARY LAYER TRIPPING     ---
C       L                  SPAN                                  METERS
C       M                  MACH NUMBER                             ---
C       NFREQ              NUMBER OF CENTERED FREQUENCIES          ---
C       PHI                DIRECTIVITY ANGLE                     DEGREES
C       PSI                TRAILING EDGE ANGLE                   DEGREES
C       R                  SOURCE TO OBSERVER DISTANCE           METERS
C       RC                 REYNOLDS NUMBER BASED ON CHORD          ---
C       SCALE              SCALING FACTOR                          ---
C       SPLBLNT            SOUND PRESSURE LEVELS DUE TO
C                            BLUNTNESS                             DB
C       STPEAK             PEAK STROUHAL NUMBER                    ---
C       STPPP              STROUHAL NUMBER                         ---
C       THETA              DIRECTIVITY ANGLE                       ---
C       U                  FREESTREAM VELOCITY                   METERS/SEC
C       VISC               KINEMATIC VISCOSITY                   M2/SEC


      PARAMETER (MAXFREQ = 27)

      DIMENSION SPLBLNT(MAXFREQ)  ,FRCEN(MAXFREQ)   ,STPPP(MAXFREQ)

      REAL M,L

C      COMPUTE NECESSARY QUANTITIES
C      ----------------------------

      M  = U /C0
      RC = U  * C / VISC


C      COMPUTE BOUNDARY LAYER THICKNESSES
C      ----------------------------------

      CALL THICK(C,U ,ALPSTAR,ITRIP,DELTAP,DSTRS,DSTRP,C0,VISC)

C      COMPUTE AVERAGE DISPLACEMENT THICKNESS
C      --------------------------------------

      DSTRAVG = (DSTRS + DSTRP) / 2.
      HDSTAR  = H / DSTRAVG

      DSTARH = 1. /HDSTAR

C      COMPUTE DIRECTIVITY FUNCTION
C      ----------------------------

      CALL DIRECTH(M,THETA,PHI,DBARH)


C      COMPUTE PEAK STROUHAL NUMBER
C      ----------------------------

      ATERM  = .212 - .0045 * PSI

      IF (HDSTAR .GE. .2)
     1   STPEAK     = ATERM / (1.+.235*DSTARH-.0132*DSTARH**2.)
      IF (HDSTAR .LT. .2)
     1   STPEAK     = .1 * HDSTAR + .095 - .00243 * PSI

C      COMPUTE SCALED SPECTRUM LEVEL
C      -----------------------------

      IF (HDSTAR .LE. 5.) G4=17.5*ALOG10(HDSTAR)+157.5-1.114*PSI
      IF (HDSTAR .GT. 5.) G4=169.7 - 1.114 * PSI


C      FOR EACH FREQUENCY, COMPUTE SPECTRUM SHAPE REFERENCED TO 0 DB
C      -------------------------------------------------------------

      DO 1000 I=1,NFREQ

        STPPP(I) = FRCEN(I) * H / U
        ETA      = ALOG10(STPPP(I)/STPEAK)

        HDSTARL = HDSTAR

        CALL G5COMP(HDSTARL,ETA,G514)

        HDSTARP = 6.724 * HDSTAR **2.-4.019*HDSTAR+1.107

        CALL G5COMP(HDSTARP,ETA,G50)


        G5 = G50 + .0714 * PSI * (G514-G50)
        IF (G5 .GT. 0.) G5 = 0.
        CALL G5COMP(.25,ETA,P4TEMP)
        IF (G5 .GT. P4TEMP) G5 = P4TEMP


        SCALE = 10. * ALOG10(M**5.5*H*DBARH*L/R**2.)

        SPLBLNT(I) = G4 + G5 + SCALE


 1000 CONTINUE

      RETURN
      END
      SUBROUTINE G5COMP(HDSTAR,ETA,G5)


      REAL M,K,MU


      IF (HDSTAR .LT. .25) MU = .1211
      IF ((HDSTAR .GT. .25).AND.(HDSTAR .LE. .62))
     1     MU=-.2175*HDSTAR + .1755
      IF ((HDSTAR .GT. .62).AND.(HDSTAR .LT. 1.15))
     1 MU = -.0308 * HDSTAR + .0596
      IF (HDSTAR .GE. 1.15)MU = .0242

      IF (HDSTAR .LE. .02) M = 0.0
      IF ((HDSTAR .GE. .02).AND.(HDSTAR .LT. .5))
     1    M=68.724*HDSTAR - 1.35
      IF ((HDSTAR .GT. .5).AND.(HDSTAR .LE. .62))
     1  M = 308.475 * HDSTAR - 121.23
      IF ((HDSTAR .GT. .62).AND.(HDSTAR .LE. 1.15))
     1  M = 224.811 * HDSTAR - 69.354
      IF ((HDSTAR .GT. 1.15) .AND. (HDSTAR .LT. 1.2))
     1  M = 1583.28 * HDSTAR - 1631.592
      IF (HDSTAR .GT. 1.2) M = 268.344
      IF (M .LT. 0.0) M = 0.0

      ETA0 = -SQRT((M*M*MU**4)/(6.25+M*M*MU*MU))

      K    = 2.5*SQRT(1.-(ETA0/MU)**2.)-2.5-M*ETA0

      IF (ETA .LE. ETA0) G5 = M * ETA + K
      IF ((ETA .GT. ETA0).AND.(ETA .LE. 0.))G5=2.5*SQRT(1.-(ETA/MU)**2.)-2.5
      IF((ETA.GT.0.).AND.(ETA.LE..03616))G5=SQRT(1.5625-1194.99*ETA**2.)-1.25
      IF (ETA .GT. .03616) G5=-155.543 * ETA + 4.375

      RETURN
      END
      SUBROUTINE TIPNOIS(ALPHTIP,ALPRAT,C,U ,FRCEN,SPLTIP,THETA,PHI,
     1                  R,NFREQ,VISC,C0,ROUND)

C                 --------------------------------
C                 ***** VARIABLE DEFINITIONS *****
C                 --------------------------------

C       VARIABLE NAME              DEFINITION                 UNITS
C       -------------              ----------                 -----

C       ALPHTIP           TIP ANGLE OF ATTACK               DEGREES
C       ALPRAT            TIP LIFT CURVE SLOPE               ---
C       ALPTIPP           CORRECTED TIP ANGLE OF ATTACK     DEGREES
C       C                 CHORD LENGTH                        METERS
C       C0                SPEED OF SOUND                   METERS/SEC
C       DBARH             DIRECTIVITY                        ---
C       FRCEN             CENTERED FREQUENCIES              HERTZ
C       L                 CHARACTERISTIC LENGTH FOR TIP       METERS
C       M                 MACH NUMBER                        ---
C       MM                MAXIMUM MACH NUMBER                ---
C       NFREQ             NUMBER OF CENTERED FREQUENCIES     ---
C       PHI               DIRECTIVITY ANGLE                 DEGREES
C       R                 SOURCE TO OBSERVER DISTANCE         METERS
C       ROUND             LOGICAL SET TRUE IF TIP IS ROUNDED ---
C       SCALE             SCALING TERM                       ---
C       SPLTIP            SOUND PRESSURE LEVEL DUE TO TIP
C                           MECHANISM                        DB
C       STPP              STROUHAL NUMBER                    ---
C       TERM              SCALING TERM                       ---
C       THETA             DIRECTIVITY ANGLE                 DEGREES
C       U                 FREESTREAM VELOCITY              METERS/SEC
C       UM                MAXIMUM VELOCITY                 METERS/SEC
C       VISC              KINEMATIC VISCOSITY              M2/SEC

      PARAMETER (MAXFREQ =27)

      DIMENSION SPLTIP(MAXFREQ),FRCEN(MAXFREQ)
      REAL L,M,MM
      LOGICAL ROUND


      ALPTIPP = ALPHTIP * ALPRAT
      M       = U  / C0

      CALL DIRECTH(M,THETA,PHI,DBARH)

      IF (ROUND) THEN
        L = .008 * ALPTIPP * C
      ELSE
        IF (ABS(ALPTIPP) .LE. 2.) THEN
          L = (.023 + .0169*ALPTIPP) * C
        ELSE
          L = (.0378 + .0095*ALPTIPP) * C
        ENDIF
      ENDIF


      MM     = (1. + .036*ALPTIPP) * M

      UM     = MM * C0

      TERM  = M*M*MM**3.*L**2.*DBARH/R**2.
      IF (TERM .NE. 0.0) THEN
        SCALE = 10.*ALOG10(TERM)
      ELSE
        SCALE = 0.0
      ENDIF

      DO 100 I=1,NFREQ
        STPP      = FRCEN(I) * L / UM
        SPLTIP(I) = 126.-30.5*(ALOG10(STPP)+.3)**2. + SCALE
 100  CONTINUE
      RETURN
      END
      SUBROUTINE THICK(C,U ,ALPSTAR,ITRIP,DELTAP,DSTRS,DSTRP,C0,VISC)

C                 ----------------------------------
C                 ***** VARIABLE DEFINITIONS *****
C                 ----------------------------------

C       VARIABLE NAME             DEFINITION                     UNITS
C       -------------             ----------                     -----

C       ALPSTAR         ANGLE OF ATTACK                        DEGREES
C       C               CHORD LENGTH                            METERS
C       C0              SPEED OF SOUND                      METERS/SEC
C       DELTA0          BOUNDARY LAYER THICKNESS AT
C                         ZERO ANGLE OF ATTACK                  METERS
C       DELTAP          PRESSURE SIDE BOUNDARY LAYER
C                         THICKNESS                             METERS
C       DSTR0           DISPLACEMENT THICKNESS AT ZERO
C                         ANGLE OF ATTACK                       METERS
C       DSTRP           PRESSURE SIDE DISPLACEMENT
C                         THICKNESS                             METERS
C       DSTRS           SUCTION SIDE DISPLACEMENT
C                         THICKNESS                             METERS
C       ITRIP           TRIGGER FOR BOUNDARY LAYER TRIPPING      ---
C       M               MACH NUMBER                              ---
C       RC              REYNOLDS NUMBER BASED ON CHORD           ---
C       U               FREESTREAM VELOCITY                  METERS/SEC
C       VISC            KINEMATIC VISCOSITY                  M2/SEC


C      COMPUTE ZERO ANGLE OF ATTACK BOUNDARY LAYER
C      THICKNESS (METERS) AND REYNOLDS NUMBER
C      ----------------------------------------

      M        = U  / C0

      RC       = U  * C/VISC

      DELTA0   = 10.**(1.6569-.9045*ALOG10(RC)+
     1            .0596*ALOG10(RC)**2.)*C
      IF (ITRIP .EQ. 2) DELTA0 = .6 * DELTA0


C      COMPUTE PRESSURE SIDE BOUNDARY LAYER THICKNESS
C      ----------------------------------------------

      DELTAP   = 10.**(-.04175*ALPSTAR+.00106*ALPSTAR**2.)*DELTA0


C      COMPUTE ZERO ANGLE OF ATTACK DISPLACEMENT THICKNESS
C      ---------------------------------------------------

      IF ((ITRIP .EQ. 1) .OR. (ITRIP .EQ. 2)) THEN
        IF (RC .LE. .3E+06) DSTR0 = .0601 * RC **(-.114)*C
        IF (RC .GT. .3E+06)
     1    DSTR0=10.**(3.411-1.5397*ALOG10(RC)+.1059*ALOG10(RC)**2.)*C
        IF (ITRIP .EQ. 2) DSTR0 = DSTR0 * .6
      ELSE
        DSTR0=10.**(3.0187-1.5397*ALOG10(RC)+.1059*ALOG10(RC)**2.)*C
      ENDIF

C      PRESSURE SIDE DISPLACEMENT THICKNESS
C      ------------------------------------

      DSTRP    = 10.**(-.0432*ALPSTAR+.00113*ALPSTAR**2.)*DSTR0
      IF (ITRIP .EQ. 3) DSTRP = DSTRP * 1.48

C      SUCTION SIDE DISPLACEMENT THICKNESS
C      -----------------------------------

      IF (ITRIP .EQ. 1) THEN
        IF (ALPSTAR .LE. 5.) DSTRS=10.**(.0679*ALPSTAR)*DSTR0
        IF((ALPSTAR .GT. 5.).AND.(ALPSTAR .LE. 12.5))
     1   DSTRS = .381*10.**(.1516*ALPSTAR)*DSTR0
        IF (ALPSTAR .GT. 12.5)DSTRS=14.296*10.**(.0258*ALPSTAR)*DSTR0
      ELSE
      IF (ALPSTAR .LE. 7.5)DSTRS =10.**(.0679*ALPSTAR)*DSTRO
      IF((ALPSTAR .GT. 7.5).AND.(ALPSTAR .LE. 12.5))
   1   DSTRS = .0162*10.**(.3066*ALPSTAR)*DSTRO
      IF (ALPSTAR .GT. 12.5) DSTRS = 52.42*10.**(.0258*ALPSTAR)*DSTRO
     ENDIF

     RETURN
     END
```

References

1. Brooks, Thomas F.; and Schlinker, Robert H.: Progress in Rotor Broadband Noise Research. *Vertica*, vol. 7, no. 4, 1983, pp. 287–307.
2. Brooks, T. F.; and Hodgson, T. H.: Trailing Edge Noise Prediction From Measured Surface Pressures. *J. Sound & Vibration*, vol. 78, no. 1, Sept. 8, 1981, pp. 69–117.
3. Schlinker, Robert H.; and Amiet, Roy K.: *Helicopter Rotor Trailing Edge Noise.* NASA CR-3470, 1981. (See also AIAA Paper 81-2001.)
4. Liu, N. S.; and Shamroth, S. J.: *On the Application of a Hairpin Vortex Model of Wall Turbulence to Trailing Edge Noise Prediction.* NASA CR-177938, 1985.
5. Ffowcs Williams, J. E.; and Hall, L. H.: Aerodynamic Sound Generation by Turbulent Flow in the Vicinity of a Scattering Half Plane. *J. Fluid Mech.*, vol. 40, pt. 4, Mar. 1970, pp. 657–670.
6. Brooks, Thomas F.; and Marcolini, Michael A.: Scaling of Airfoil Self-Noise Using Measured Flow Parameters. *AIAA J.*, vol. 23, no. 2, Feb. 1985, pp. 207–213.
7. Chou, S.-T.; and George, A. R.: Effect of Angle of Attack on Rotor Trailing-Edge Noise. *AIAA J.*, vol. 22, no. 12, Dec. 1984, pp. 1821–1823.
8. George, Albert R.; and Chou, Shau-Tak: *Broadband Rotor Noise Analyses.* NASA CR-3797, 1984.
9. Grosveld, Ferdinand W.: Prediction of Broadband Noise From Horizontal Axis Wind Turbines. *AIAA J. Propuls. & Power*, vol. 1, no. 4, July–Aug. 1985, pp. 292–299.
10. Glegg, S. A. L.; Baxter, S. M.; and Glendinning, A. G.: The Prediction of Broadband Noise From Wind Turbines. *J. Sound & Vibration*, vol. 118, no. 2, Oct. 22, 1987, pp. 217–239.
11. Fink, M. R.; and Bailey, D. A.: *Airframe Noise Reduction Studies and Clean-Airframe Noise Investigation.* NASA CR-159311, 1980.
12. Paterson, Robert W.; Amiet, Roy K.; and Munch, C. Lee: Isolated Airfoil-Tip Vortex Interaction Noise. AIAA Paper No. 74-194, Jan.–Feb. 1974.
13. Tam, Christopher K. W.: Discrete Tones of Isolated Airfoils. *J. Acoust. Soc. America*, vol. 55, no. 6, June 1974, pp. 1173–1177.
14. Wright, S. E.: The Acoustic Spectrum of Axial Flow Machines. *J. Sound & Vibration*, vol. 45, no. 2, Mar. 22, 1976, pp. 165–223.
15. Fink, M. R.: *Fine Structure of Airfoil Tone Frequency.* UTRC78-10, United Technologies Research Center, Jan. 1978.
16. Paterson, Robert W.; Vogt, Paul G.; Fink, Martin R.; and Munch, C. Lee: Vortex Noise of Isolated Airfoils. *J. Aircr.*, vol. 10, no. 5, May 1973, pp. 296–302.
17. George, A. R.; Najjar, F. E.; and Kim, Y. N.: Noise Due to Tip Vortex Formation on Lifting Rotors. AIAA-80-1010, June 1980.
18. Brooks, Thomas F.; and Marcolini, Michael A.: Airfoil Tip Vortex Formation Noise. *AIAA J.*, vol. 24, no. 2, Feb. 1986, pp. 246–252.
19. Blake, William K.: *Aero-Hydroacoustics for Ships, Volume II.* Rep. No. DTNSRDC-84/010, U.S. Navy, June 1984.
20. Chou, S.-T.; and George, A. R.: Effect of Blunt Trailing Edge on Rotor Broadband Noise. *AIAA J.*, vol. 24, no. 8, Aug. 1986, pp. 1380–1382.
21. Brooks, Thomas F.; Marcolini, Michael A.; and Pope, Dennis S.: Airfoil Trailing-Edge Flow Measurements. *AIAA J.*, vol. 24, no. 8, Aug. 1986, pp. 1245–1251.
22. Amiet, R. K.: Refraction of Sound by a Shear Layer. *J. Sound & Vibration*, vol. 58, no. 4, June 1978, pp. 467–482.
23. Schlinker, R. H.; and Amiet, R. K.: Refraction of Sound by a Shear Layer—Experimental Assessment. AIAA Paper 79-0628, Mar. 1979.
24. Paterson, Robert W.; and Amiet, Roy K.: *Acoustic Radiation and Surface Pressure Characteristics of an Airfoil Due to Incident Turbulence.* NASA CR-2733, 1976. (See also AIAA Paper 76-571.)
25. Fink, Martin R.: Noise Component Method for Airframe Noise. AIAA Paper 77-1271, Oct. 1977.
26. Schlinker, R. H.: Airfoil Trailing Edge Noise Measurements With a Directional Microphone. AIAA Paper 77-1269, Oct. 1977.
27. Fink, M. R.; Schlinker, R. H.; and Amiet, R. K.: *Prediction of Rotating-Blade Vortex Noise From Noise of Nonrotating Blades.* NASA CR-2611, 1976.
28. Bendat, Julius S.; and Piersol, Allan G.: *Random Data: Analysis and Measurement Procedures.* John Wiley & Sons, Inc., c.1971.
29. Dowling, A. P.; and Ffowcs Williams, J. E.: *Sound and Sources of Sound.* John Wiley & Sons, c.1983.
30. Brooks, Thomas F.; Marcolini, Michael A.; and Pope, D. Stuart: Main Rotor Broadband Noise Study in the DNW. J. American Helicopter Soc., vol. 34, no. 2, Apr. 1989, pp. 3–12.
31. Golub, R. A.; Weir, D. S.; and Tracy, M. B.: Application of the Baseline Rotonet System to the Prediction of Helicopter Tone Noise. AIAA-86-1904, July 1986.

Table 1. Test and Data Processing Conditions for Tripped Boundary-Layer Airfoil Cases of Figures 11 to 43

Fig. no.	Run no.	Chord, c, cm	Tunnel angle, α_t, deg	Effective angle, α_*, deg	Tunnel velocity, U, m/s	Reynolds number, $R_c \times 10^{-6}$	Calculated ratio, δ_s^*/c	Peak Strouhal no., St_{peak} (fig. 76)	TBL-TE peak scaled $L_{1/3}$, dB (fig. 77)	Data processing (app. A) Microphones		No. avg.	Field
11(a)	101	30.48	0.0	0.0	71.3	1.497	0.0087	0.046	128.5	[illegible]	[illegible]	0	[illegible]
11(b)	102	30.48	0.0	0.0	55.5	1.164	0.0093	[illegible]	[illegible]	[illegible]	[illegible]	0	[illegible]
11(c)	103	30.48	0.0	0.0	39.6	0.831	0.0102	0.065	[illegible]	[illegible]	[illegible]	0	[illegible]
11(d)	104	30.48	0.0	0.0	31.7	0.665	0.0109	[illegible]	[illegible]	[illegible]	[illegible]	0	[illegible]
12(a)	105	30.48	5.4	1.5	71.3	1.497	0.0111	0.050	[illegible]	[illegible]	[illegible]	0	[illegible]
12(b)	106	30.48	5.4	1.5	39.6	0.831	0.0129	0.076	[illegible]	[illegible]	[illegible]	0	[illegible]
13(a)	107	30.48	10.8	3.0	71.3	1.497	0.0140	0.050	[illegible]	[illegible]	[illegible]	0	[illegible]
13(b)	108	30.48	10.8	3.0	55.5	1.164	0.0149	0.059	[illegible]	[illegible]	[illegible]	0	[illegible]
13(c)	109	30.48	10.8	3.0	39.6	0.831	0.0163	0.101	[illegible]	[illegible]	[illegible]	0	[illegible]
13(d)	110	30.48	10.8	3.0	31.7	0.665	0.0174	0.125	[illegible]	[illegible]	[illegible]	0	[illegible]
14(a)	111	30.48	14.4	4.0	71.3	1.497	0.0164	0.057	[illegible]	[illegible]	[illegible]	0	[illegible]
14(b)	112	30.48	14.4	4.0	39.6	0.831	0.0191	0.103	[illegible]	[illegible]	[illegible]	0	[illegible]
15(a)	251	22.86	0.0	0.0	71.3	1.122	0.0094	0.061	[illegible]	[illegible]	[illegible]	0	[illegible]
15(b)	252	22.86	0.0	0.0	55.5	0.873	0.0100	0.059	[illegible]	[illegible]	[illegible]	0	[illegible]
15(c)	253	22.86	0.0	0.0	39.6	0.624	0.0111	0.075	[illegible]	[illegible]	[illegible]	0	[illegible]
15(d)	254	22.86	0.0	0.0	31.7	0.499	0.0119	[illegible]	[illegible]	[illegible]	[illegible]	0	[illegible]
16(a)	255	22.86	5.4	2.0	71.3	1.122	0.0128	0.057	[illegible]	[illegible]	[illegible]	0	[illegible]
16(b)	256	22.86	5.4	2.0	55.5	0.873	0.0137	0.061	[illegible]	[illegible]	[illegible]	0	[illegible]
16(c)	257	22.86	5.4	2.0	39.6	0.624	[illegible]	[illegible]	[illegible]	[illegible]	[illegible]	0	[illegible]
16(d)	258	22.86	5.4	2.0	31.7	0.499	0.0163	0.110	[illegible]	[illegible]	[illegible]	0	[illegible]
17(a)	259	22.86	10.8	4.0	71.3	1.122	0.0175	[illegible]	[illegible]	[illegible]	[illegible]	0	[illegible]
17(b)	260	22.86	10.8	4.0	55.5	0.873	0.0187	0.075	[illegible]	[illegible]	[illegible]	0	[illegible]
17(c)	261	22.86	10.8	4.0	39.6	0.624	0.0207	[illegible]	[illegible]	[illegible]	[illegible]	0	[illegible]
17(d)	262	22.86	10.8	4.0	31.7	0.499	0.0223	0.130	[illegible]	[illegible]	[illegible]	0	[illegible]
18(a)	263	22.86	14.4	5.3	71.3	1.122	0.0229	0.061	[illegible]	[illegible]	[illegible]	0	[illegible]
18(b)	264	22.86	14.4	5.3	39.6	0.624	0.0271	[illegible]	[illegible]	[illegible]	[illegible]	0	[illegible]
19(a)	265	22.86	19.8	7.3	71.3	1.122	0.0461	0.050	[illegible]	[illegible]	[illegible]	0	[illegible]
19(b)	266	22.86	19.8	7.3	55.5	0.873	0.0493	0.074	[illegible]	[illegible]	[illegible]	0	[illegible]
19(c)	267	22.86	19.8	7.3	39.6	0.624	[illegible]	[illegible]	[illegible]	[illegible]	[illegible]	0	[illegible]
19(d)	268	22.86	19.8	7.3	31.7	0.499	[illegible]	0.157	[illegible]	[illegible]	[illegible]	0	[illegible]
20(a)	133	15.24	0.0	0.0	71.3	0.748	0.0105	[illegible]	[illegible]	[illegible]	[illegible]	0	[illegible]
20(b)	134	15.24	0.0	0.0	55.5	0.582	0.0113	0.055	[illegible]	[illegible]	[illegible]	0	[illegible]
20(c)	135	15.24	0.0	0.0	39.6	0.416	0.0127	0.070	[illegible]	[illegible]	[illegible]	0	[illegible]
20(d)	136	15.24	0.0	0.0	31.7	0.333	0.0137	0.087	[illegible]	[illegible]	[illegible]	0	[illegible]
21(a)	137	15.24	5.4	2.7	71.3	0.748	0.0150	0.057	[illegible]	[illegible]	[illegible]	0	[illegible]
21(b)	138	15.24	5.4	2.7	39.6	0.416	0.0193	[illegible]	[illegible]	[illegible]	[illegible]	0	[illegible]
22(a)	139	15.24	10.8	5.4	71.3	0.748	[illegible]	0.075	[illegible]	[illegible]	[illegible]	0	[illegible]
22(b)	140	15.24	10.8	5.4	55.5	0.582	[illegible]	[illegible]	[illegible]	[illegible]	[illegible]	0	[illegible]
22(c)	141	15.24	10.8	5.4	39.6	0.416	[illegible]	[illegible]	[illegible]	[illegible]	[illegible]	0	[illegible]
22(d)	142	15.24	10.8	5.4	31.7	0.333	[illegible]	0.105	[illegible]	[illegible]	[illegible]	0	[illegible]
23(a)	143	15.24	14.4	7.2	71.3	0.748	[illegible]	[illegible]	[illegible]	[illegible]	[illegible]	0	[illegible]
23(b)	144	15.24	14.4	7.2	39.6	0.416	[illegible]	[illegible]	[illegible]	[illegible]	[illegible]	0	[illegible]
24(a)	145	15.24	19.8	9.9	71.3	0.748	[illegible]	[illegible]	[illegible]	[illegible]	[illegible]	0	[illegible]
24(b)	146	15.24	19.8	9.9	55.5	0.582	[illegible]	[illegible]	[illegible]	[illegible]	[illegible]	0	[illegible]
24(c)	147	15.24	19.8	9.9	39.6	0.416	[illegible]	[illegible]	[illegible]	[illegible]	[illegible]	0	[illegible]
24(d)	148	15.24	19.8	9.9	31.7	0.333	[illegible]	[illegible]	[illegible]	[illegible]	[illegible]	0	[illegible]
25(a)	149	15.24	25.2	12.6	71.3	0.748	[illegible]	0.170	[illegible]	[illegible]	[illegible]	0	[illegible]
25(b)	150	15.24	25.2	12.6	39.6	0.416	[illegible]	[illegible]	[illegible]	[illegible]	[illegible]	0	[illegible]
26(a)	293	10.16	0.0	0.0	71.3	0.499	0.0119	[illegible]	[illegible]	[illegible]	[illegible]	0	[illegible]
26(b)	294	10.16	0.0	0.0	55.5	0.388	[illegible]	0.057	[illegible]	[illegible]	[illegible]	0	[illegible]
26(c)	295	10.16	0.0	0.0	39.6	0.277	[illegible]	0.072	[illegible]	[illegible]	[illegible]	0	[illegible]
26(d)	296	10.16	0.0	0.0	31.7	0.222	[illegible]	0.077	[illegible]	[illegible]	[illegible]	0	[illegible]
27(a)	297	10.16	5.4	3.3	71.3	0.499	[illegible]	[illegible]	[illegible]	[illegible]	[illegible]	0	[illegible]
27(b)	298	10.16	5.4	3.3	55.5	0.388	[illegible]	0.074	[illegible]	[illegible]	[illegible]	0	[illegible]
27(c)	299	10.16	5.4	3.3	39.6	0.277	[illegible]	[illegible]	[illegible]	[illegible]	[illegible]	0	[illegible]
27(d)	300	10.16	5.4	3.3	31.7	0.222	[illegible]	0.120	[illegible]	[illegible]	[illegible]	0	[illegible]
28(a)	301	10.16	10.8	6.7	71.3	0.499	0.0470	[illegible]	136.5	[illegible]	[illegible]	0	[illegible]

Table 1. Concluded

Fig. no.	Run no.	Chord, c, cm	Tunnel angle, α_t, deg	Effective angle, α_*, deg	Tunnel velocity, U, m/s	Reynolds number, $R_c \times 10^{-6}$	Calculated ratio, δ_s^*/c	Peak Strouhal no., St_{peak} (fig. 76)	TBL-TE peak scaled $SPL_{1/3}$, dB (fig. 77)	Data processing (app. A) Microphones		No. avg.	Fold
28(b)	302	10.16	10.8	6.7	55.5	0.388	0.0513	0.102	136.0	[illegible]	[illegible]	0	F
28(c)	303	10.16	10.8	6.7	39.6	0.277	0.0528	0.125	133.5	[illegible]	[illegible]	0	F
28(d)	304	10.16	10.8	6.7	31.7	0.222	0.0543	0.156	131.5	[illegible]	[illegible]	0	F
29(a)	305	10.16	14.4	8.9	71.3	0.499	0.1024	0.085	130.0	[illegible]	[illegible]	0	[illegible]
29(b)	306	10.16	14.4	8.9	39.6	0.277	0.1238	0.130	132.5	[illegible]	[illegible]	0	[illegible]
30(a)	307	10.16	19.8	12.3	71.3	0.499	[illegible]	0.209	132.5	[illegible]	[illegible]	0	[illegible]
30(b)	309	10.16	19.8	12.3	55.5	0.388	[illegible]	0.220	135.0	[illegible]	[illegible]	0	[illegible]
30(c)	308	10.16	19.8	12.3	39.6	0.277	[illegible]	0.265	129.0	[illegible]	[illegible]	0	[illegible]
30(d)	310	10.16	19.8	12.3	31.7	0.222	0.4067	0.341	125.0	[illegible]	[illegible]	0	[illegible]
31(a)	311	10.16	25.2	15.6	71.3	0.499	0.4309	0.192	127.5	[illegible]	[illegible]	0	[illegible]
31(b)	312	10.16	25.2	15.6	39.6	0.277	0.5209	0.330	123.5	[illegible]	[illegible]	0	[illegible]
32(a)	179	5.08	0.0	0.0	71.3	0.249	0.0146	0.044	133.5	[illegible]	[illegible]	0	F
32(b)	180	5.08	0.0	0.0	55.5	0.194	0.0150	0.057	134.0	[illegible]	[illegible]	2	F
32(c)	181	5.08	0.0	0.0	39.6	0.139	0.0156	0.068	134.5	[illegible]	[illegible]	2	F
32(d)	182	5.08	0.0	0.0	31.7	0.111	0.0160	0.077	134.5	[illegible]	[illegible]	2	F
33(a)	183	5.08	5.4	4.2	71.3	0.249	0.0282	0.076	133.0	[illegible]	[illegible]	0	F
33(b)	184	5.08	5.4	4.2	39.6	0.139	0.0301	0.109	133.0	[illegible]	[illegible]	0	F
34(a)	185	5.08	10.8	8.4	71.3	0.249	0.1051	0.156	134.0	[illegible]	[illegible]	0	F
34(b)	186	5.08	10.8	8.4	55.5	0.194	0.1082	0.164	132.0	[illegible]	[illegible]	0	F
34(c)	187	5.08	10.8	8.4	39.6	0.139	0.1124	0.205	130.0	[illegible]	[illegible]	0	F
34(d)	188	5.08	10.8	8.4	31.7	0.111	0.1153	0.236	128.5	[illegible]	[illegible]	0	F
35(a)	189	5.08	14.4	11.2	71.3	0.249	0.2801	0.220	135.5	[illegible]	[illegible]	0	F
35(b)	190	5.08	14.4	11.2	39.6	0.139	0.2995	0.303	132.0	[illegible]	[illegible]	0	F
36(a)	191	5.08	19.8	15.4	71.3	0.249	0.5215	0.412	131.5	[illegible]	[illegible]	0	F
36(b)	192	5.08	19.8	15.4	55.5	0.194	0.5367	0.483	129.5	[illegible]	[illegible]	0	F
36(c)	193	5.08	19.8	15.4	39.6	0.139	0.5577	0.621	128.0	[illegible]	[illegible]	0	F
36(d)	194	5.08	19.8	15.4	31.7	0.111	0.5721	0.741	125.0	[illegible]	[illegible]	0	F
37(a)	195	5.08	25.2	19.7	71.3	0.249	0.6698	0.294	127.0	[illegible]	[illegible]	0	F
37(b)	196	5.08	25.2	19.7	39.6	0.139	0.7162	0.318	129.5	[illegible]	[illegible]	0	[illegible]
38(a)	213	2.54	0.0	0.0	71.3	0.125	0.0158			[illegible]	[illegible]	0	[illegible]
38(b)	214	2.54	0.0	0.0	55.5	0.097	0.0162	0.051	133.0	[illegible]	[illegible]	2	F
38(c)	215	2.54	0.0	0.0	39.6	0.069	0.0169	0.072	135.5	[illegible]	[illegible]	2	F
38(d)	216	2.54	0.0	0.0	31.7	0.055	0.0173	0.083	137.5	[illegible]	[illegible]	2	F
39(a)	217	2.54	5.4	4.8	71.3	0.125	0.0332	0.060	134.0	[illegible]	[illegible]	0	F
39(b)	218	2.54	5.4	4.8	55.5	0.097	0.0341	0.087	134.5	[illegible]	[illegible]	0	F
39(c)	219	2.54	5.4	4.8	39.6	0.069	0.0355	0.116	134.0	[illegible]	[illegible]	0	F
39(d)	220	2.54	5.4	4.8	31.7	0.055	0.0364	0.131	134.5	[illegible]	[illegible]	0	F
40(a)	221	2.54	10.8	9.5	71.3	0.125	0.1658	0.164	135.0	[illegible]	[illegible]	0	F
40(b)	222	2.54	10.8	9.5	55.5	0.097	0.1707	0.190	133.5	[illegible]	[illegible]	0	F
40(c)	223	2.54	10.8	9.5	39.6	0.069	0.1773	0.218	130.5	[illegible]	[illegible]	0	F
40(d)	224	2.54	10.8	9.5	31.7	0.055	0.1819	0.209	130.5	[illegible]	[illegible]	0	F
41(a)	225	2.54	14.4	12.7	71.3	0.125	0.4787	0.356	133.5	[illegible]	[illegible]	0	F
41(b)	226	2.54	14.4	12.7	39.6	0.069	0.5119	0.501	129.0	[illegible]	[illegible]	0	F
42(a)	227	2.54	19.8	17.4	71.3	0.125	0.6349	0.493	128.0	[illegible]	[illegible]	0	F
42(b)	228	2.54	19.8	17.4	55.5	0.097	0.6533	0.518	128.5	[illegible]	[illegible]	0	[illegible]
42(c)	229	2.54	19.8	17.4	39.6	0.069	0.6799	0.413	135.0	[illegible]	[illegible]	0	F
42(d)	230	2.54	19.8	17.4	31.7	0.055	0.6964	0.402	135.5	[illegible]	[illegible]	0	F
43(a)	231	2.54	25.2	22.2	71.3	0.125	0.8420	0.356	133.0	[illegible]	[illegible]	0	F
43(b)	232	2.54	25.2	22.2	39.6	0.069	0.9003	0.413	135.0	[illegible]	[illegible]	0	F

Table 2. Test and Data Processing Conditions for Untripped Boundary-Layer Airfoil Cases of Figures 44 to 74

Fig. no.	Run no.	Chord, c, cm	Tunnel angle, α_t, deg	Effective angle, α_*, deg	Tunnel velocity, U, m/s	Reynolds number, $R_c \times 10^{-6}$	Calculated ratio, δ_p/c	Peak Strouhal no., St'_{peak} (fig. 86)	[illegible] Peak scaled level, dB (fig. 88)	Data processing (app. A) Microphones		No. sep.	Fold
44(a)	113	30.48	0.0	0.0	71.3	1.497	0.0221			4,5	4,6	0	F
44(b)	114	30.48	0.0	0.0	55.5	1.164	0.0231			4,5	4,6	0	F
44(c)	115	30.48	0.0	0.0	39.6	0.831	0.0246			4,5	4,6	0	F
44(d)	116	30.48	0.0	0.0	31.7	0.665	0.0258			4,5	4,6	0	F
45(a)	117	30.48	5.4	1.5	71.3	1.497	0.0192			4,5	4,6	0	NF
45(b)	118	30.48	5.4	1.5	39.6	0.831	0.0214	0.235	136.5	4,5	4,6	0	NF
46(a)	119	30.48	10.8	3.0	71.3	1.497	0.0169	0.225	138.0	4,5	4,6	0	NF
46(b)	120	30.48	10.8	3.0	55.5	1.164	0.0176	0.210	147.5	4,5	4,6	0	NF
46(c)	121	30.48	10.8	3.0	39.6	0.831	0.0188	0.210	152.0	4,5	4,6	0	NF
46(d)	122	30.48	10.8	3.0	31.7	0.665	0.0197	0.205	154.5	4,5	4,6	0	NF
47(a)	123	30.48	14.4	4.0	71.3	1.497	0.0156	0.210	148.0	4,5	4,6	0	NF
47(b)	124	30.48	14.4	4.0	39.6	0.831	0.0174	0.200	154.0	4,5	4,6	0	NF
48(a)	269	22.86	0.0	0.0	71.3	1.122	0.0232			4,5	4,6	0	F
48(b)	270	22.86	0.0	0.0	55.5	0.873	0.0244			4,5	4,6	0	NF
48(c)	271	22.86	0.0	0.0	39.6	0.624	0.0261			4,5	4,6	0	NF
48(d)	272	22.86	0.0	0.0	31.7	0.499	0.0274	0.310	126.5	4,5	4,6	0	NF
49(a)	273	22.86	5.4	2.0	71.3	1.122	0.0194			4,5	4,6	0	NF
49(b)	274	22.86	5.4	2.0	55.5	0.873	0.0203	0.220	135.0	4,5	4,6	0	NF
49(c)	275	22.86	5.4	2.0	39.6	0.624	0.0218	0.205	145.5	4,5	4,6	0	NF
49(d)	276	22.86	5.4	2.0	31.7	0.499	0.0229	0.215	150.5	4,5	4,6	0	NF
50(a)	277	22.86	10.8	4.0	71.3	1.122	0.0165	0.185	148.5	4,5	4,6	0	NF
50(b)	278	22.86	10.8	4.0	55.5	0.873	0.0173	0.200	152.0	4,5	4,6	0	NF
50(c)	279	22.86	10.8	4.0	39.6	0.624	0.0185	0.190	152.5	4,5	4,6	0	NF
50(d)	280	22.86	10.8	4.0	31.7	0.499	0.0194	0.200	154.5	4,5	4,6	0	NF
51(a)	281	22.86	14.4	5.3	71.3	1.122	0.0149	0.165	154.5	4,5	4,6	0	NF
51(b)	282	22.86	14.4	5.3	39.6	0.624	0.0168	0.185	150.5	4,5	4,6	0	NF
52(a)	283	22.86	19.8	7.3	71.3	1.122	0.0131			4,5	4,6	0	NF
52(b)	284	22.86	19.8	7.3	39.6	0.624	0.0147			4,5	4,6	0	NF
53(a)	151	15.24	0.0	0.0	71.3	0.748	0.0251			4,5	4,6	0	F
53(b)	152	15.24	0.0	0.0	55.5	0.582	0.0265			4,5	4,6	0	F
53(c)	153	15.24	0.0	0.0	39.6	0.416	0.0286	0.265	136.0	4,5	4,6	0	F
53(d)	154	15.24	0.0	0.0	31.7	0.333	0.0302	0.265	144.0	4,5	4,6	0	F
54(a)	155	15.24	5.4	2.7	71.3	0.748	0.0197	0.205	147.0	4,5	4,6	0	F
54(b)	156	15.24	5.4	2.7	39.6	0.416	0.0225	0.190	159.0	4,5	4,6	0	F
55(a)	157	15.24	10.8	5.4	71.3	0.748	0.0161	0.160	155.0	4,5	4,6	0	NF
55(b)	158	15.24	10.8	5.4	55.5	0.582	0.0169	0.170	153.0	4,5	4,6	0	F
55(c)	159	15.24	10.8	5.4	39.6	0.416	0.0183	0.180	142.5	4,5	4,6	0	F
55(d)	160	15.24	10.8	5.4	31.7	0.333	0.0193			4,5	4,6	0	F
56(a)	161	15.24	14.4	7.2	71.3	0.748	0.0143			4,5	4,6	0	F
56(b)	162	15.24	14.4	7.2	39.6	0.416	0.0162			4,5	4,6	0	F
57(a)	163	15.24	19.8	9.9	71.3	0.748	0.0123			4,5	4,6	0	NF
57(b)	164	15.24	19.8	9.9	39.6	0.416	0.0140			4,5	4,6	0	NF
58(a)	165	15.24	25.2	12.6	71.3	0.748	0.0110			4,5	4,6	0	NF
58(b)	166	15.24	25.2	12.6	39.6	0.416	0.0125			4,5	4,6	0	NF
59(a)	313	10.16	0.0	0.0	71.3	0.499	0.0274	0.290	132.0	4,5	4,6	0	F
59(b)	314	10.16	0.0	0.0	55.5	0.388	0.0291	0.300	138.5	4,5	4,6	0	F
59(c)	315	10.16	0.0	0.0	39.6	0.277	0.0316	0.240	151.0	4,5	4,6	0	F
59(d)	316	10.16	0.0	0.0	31.7	0.222	0.0335	0.210	159.5	4,5	4,6	0	F
60(a)	317	10.16	5.4	3.3	71.3	0.499	0.0204	0.180	161.5	4,5	4,6	0	NF
60(b)	318	10.16	5.4	3.3	55.5	0.388	0.0217	0.185	159.5	4,5	4,6	0	NF
60(c)	319	10.16	5.4	3.3	39.6	0.277	0.0235	0.190	157.0	4,5	4,6	2	F
60(d)	320	10.16	5.4	3.3	31.7	0.222	0.0249	0.220	147.0	4,5	4,6	2	F
61(a)	321	10.16	10.8	6.7	71.3	0.499	0.0161			4,5	4,6	2	NF
61(b)	322	10.16	10.8	6.7	55.5	0.388	0.0170			4,5	4,6	2	F
61(c)	323	10.16	10.8	6.7	39.6	0.277	0.0185			4,5	4,6	2	F
61(d)	324	10.16	10.8	6.7	31.7	0.222	0.0196			4,5	4,6	2	F
62(a)	325	10.16	14.4	8.9	71.3	0.499	0.0141			4,5	4,2	2	F

Table 2. Concluded

Fig. no.	Run no.	Chord, c, cm	Tunnel angle, α_t, deg	Effective angle, α_*, deg	Tunnel velocity, U, m/s	Reynolds number, $R_c \times 10^{-6}$	Calculated ratio, δ_p/c	Peak Strouhal no., St'_{peak} (fig. 86)	LBL-VS peak scaled level, dB (fig. 88)	Data processing (app. A) Microphones		No. sep.	Fold
62(b)	326	10.16	14.4	8.9	39.6	0.277	0.0163			4x5	4x2	2	F
63(a)	327	10.16	19.8	12.3	71.3	0.499	0.0122			4x5	4x2	0	NF
63(b)	328	10.16	19.8	12.3	39.6	0.277	0.0140			4x5	4x2	0	NF
64(a)	329	10.16	25.2	15.6	71.3	0.499	0.0111			4x5	4x2	0	NF
64(b)	330	10.16	25.2	15.6	39.6	0.277	0.0128			4x5	4x2	0	NF
65(a)	197	5.08	0.0	0.0	71.3	0.249	0.0325	0.230	153.0	4x5	4x2	0	F
65(b)	198	5.08	0.0	0.0	55.5	0.194	0.0347	0.210	160.5	4x5	4x2	0	NF
65(c)	199	5.08	0.0	0.0	39.6	0.139	0.0382	0.210	166.0	4x5	4x2	0	NF
65(d)	200	5.08	0.0	0.0	31.7	0.111	0.0408	0.190	172.5	4x5	4x2	0	NF
66(a)	201	5.08	5.4	4.2	71.3	0.249	0.0226	0.157	164.0	4x5	4x2	0	NF
66(b)	202	5.08	5.4	4.2	39.6	0.139	0.0266	0.190	148.0	4x5	4x2	0	NF
67(a)	203	5.08	10.8	8.4	71.3	0.249	0.0172			4x5	4x2	2	F
67(b)	204	5.08	10.8	8.4	55.5	0.194	0.0184			4x5	4x2	2	F
67(c)	205	5.08	10.8	8.4	39.6	0.139	0.0202			4x5	4x2	2	F
67(d)	206	5.08	10.8	8.4	31.7	0.111	0.0216			4x5	4x2	2	F
68(a)	207	5.08	14.4	11.2	71.3	0.249	0.0150			4x5	4x2	0	F
68(b)	208	5.08	14.4	11.2	39.6	0.139	0.0176			4x5	4x2	0	F
69(a)	209	5.08	19.8	15.4	71.3	0.249	0.0132			4x5	4x2	0	F
69(b)	210	5.08	19.8	15.4	39.6	0.139	0.0155			4x5	4x2	0	F
70(a)	211	5.08	25.2	19.7	71.3	0.249	0.0126			4x5	4x2	0	NF
70(b)	212	5.08	25.2	19.7	39.6	0.139	0.0148			4x5	4x2	0	NF
71(a)	233	2.54	0.0	0.0	71.3	0.125	0.0394	0.170	169.0	4x5	4x2	0	NF
71(b)	234	2.54	0.0	0.0	55.5	0.097	0.0425	0.180	170.0	4x5	4x2	0	NF
71(c)	235	2.54	0.0	0.0	39.6	0.069	0.0473	0.180	170.0	4x5	4x2	0	NF
71(d)	236	2.54	0.0	0.0	31.7	0.055	0.0510	0.210	164.5	4x5	4x2	0	NF
72(a)	237	2.54	5.4	4.8	71.3	0.125	0.0264			4x5	4x2	0	F
72(b)	238	2.54	5.4	4.8	55.5	0.097	0.0284			4x5	4x2	0	F
72(c)	239	2.54	5.4	4.8	39.6	0.069	0.0317			4x5	4x2	0	F
72(d)	240	2.54	5.4	4.8	31.7	0.055	0.0341			4x5	4x2	0	F
73(a)	241	2.54	10.8	9.5	71.3	0.125	0.0197			4x5	4x2	0	F
73(b)	242	2.54	10.8	9.5	55.5	0.097	0.0213			4x5	4x2	0	F
73(c)	243	2.54	10.8	9.5	39.6	0.069	0.0237			4x5	4x2	0	F
73(d)	244	2.54	10.8	9.5	31.7	0.055	0.0255			4x5	4x2	0	F
74(a)	245	2.54	14.4	12.7	71.3	0.125	0.0172			4x5	4x2	0	F
74(b)	246	2.54	14.4	12.7	39.6	0.069	0.0207			4x5	4x2	0	F

Report Documentation Page

1. Report No.
NASA RP-1218

2. Government Accession No.

3. Recipient's Catalog No.

4. Title and Subtitle
Airfoil Self-Noise and Prediction

5. Report Date
July 1989

6. Performing Organization Code

7. Author(s)
Thomas F. Brooks, D. Stuart Pope, and Michael A. Marcolini

8. Performing Organization Report No.
L-16528

9. Performing Organization Name and Address
NASA Langley Research Center
Hampton, VA 23665-5225

10. Work Unit No.
505-63-51-06

11. Contract or Grant No.

12. Sponsoring Agency Name and Address
National Aeronautics and Space Administration
Washington, DC 20546-0001

13. Type of Report and Period Covered
Reference Publication

14. Sponsoring Agency Code

15. Supplementary Notes
Thomas F. Brooks and Michael A. Marcolini: Langley Research Center, Hampton, Virginia.
D. Stuart Pope: PRC Kentron, Inc., Aerospace Technologies Division, Hampton, Virginia.

16. Abstract
A prediction method is developed for the self-generated noise of an airfoil blade encountering smooth flow. The prediction methods for the individual self-noise mechanisms are semiempirical and are based on previous theoretical studies and data obtained from tests of two- and three-dimensional airfoil blade sections. The self-noise mechanisms are due to specific boundary-layer phenomena, that is, the boundary-layer turbulence passing the trailing edge, separated-boundary-layer and stalled flow over an airfoil, vortex shedding due to laminar-boundary-layer instabilities, vortex shedding from blunt trailing edges, and the turbulent vortex flow existing near the tip of lifting blades. The predictions are compared successfully with published data from three self-noise studies of different airfoil shapes. An application of the prediction method is reported for a large-scale-model helicopter rotor, and the predictions compared well with experimental broadband noise measurements. A computer code of the method is given.

17. Key Words (Suggested by Authors(s))
Airframe noise
Helicopter rotor acoustics
Rotor broadband noise
Propeller noise
Wind turbine noise
Trailing-edge noise
Vortex-shedding noise

18. Distribution Statement
Unclassified—Unlimited

Subject Category 71

19. Security Classif. (of this report)
Unclassified

20. Security Classif. (of this page)
Unclassified

21. No. of Pages
142

22. Price
A07

NASA FORM 1626 OCT 86

NASA-Langley, 1989

For sale by the National Technical Information Service, Springfield, Virginia 22161-2171

END

DATE

FILMED

SEP 98